Model-based Graded Electrode Design for Lithium-ion Batteries

Yanbo Qi

A dissertation
submitted in partial fulfillment of the
requirements for the degree of

Doctor of Philosophy

University of Washington

2019

Reading Committee:

Venkat R. Subramanian, Chair
Daniel T. Schwartz, Chair
Jihui Yang

Program Authorized to Offer Degree:
Chemical Engineering

University of Washington

Abstract

Model-based Graded Electrode Design for Lithium-ion Batteries

Yanbo Qi

Chair of the Supervisory Committee:

Prof. Venkat R. Subramanian
Prof. Daniel T. Schwartz

Department of Chemical Engineering

Lithium-ion battery, due to its high power and energy densities and long life, has been identified as a preferred candidate for various applications, ranging from small-scaled consumer electronics to large-scaled energy storage systems for electric vehicles and grid applications. However, the performance of lithium-ion batteries today still needs to be improved to fully meet the requirements of these applications. There are two ways to achieve better performance, either by modifying the chemistry to reach a revolutionary breakthrough or by optimizing the cell design to realize a series of gradual and continuous improvement. This work focuses on the latter approach. Whatever material we end up using, it is always necessary to optimize the cell design to fully utilize that material.

This dissertation is focused on model-based graded electrode design using electro-chemical models, and the implementation of optimization and simulation methods necessary to achieve the optimal design profiles. Design with constraints and multi-objective optimization have also been explored to provide a framework that works for a wide range of applications.

TABLE OF CONTENTS

List of Figures

List of Tables

ACKNOWLEDGEMENTS

First and foremost, I would like to thank my advisors, Prof. Venkat Subramanian and Prof. Dan Schwartz for their support and mentorship. In addition to their technical guidance, their work ethic and career passion have set a perfect example for me to follow. Venkat's enduring enthusiasm for mathematics and Dan's intellectual inquisitiveness have inspired me to seek my passion and to be motivated to work hard. I am especially grateful for how much they genuinely care about their students. During my PhD, I had the chance to explore my interests in data science and entrepreneurship by taking classes and participating in competitions beyond my curriculum. I could not have had a better graduate school experience or personal development opportunity.

I would also like to thank my committee members Prof. Jihui Yang, Prof. Corie Cobb, and Prof. Don MacKenzie for taking the time to provide critical feedback for my doctoral work. I want to thank the people that I collaborated with during my PhD. This includes students and PIs in the Battery500 project, among them Prof. Jihui Yang, Dr. Vish Viswanathan, Prof. Ping Liu, and Dr. Eric Dufek. I have truly enjoyed the fruitful discussion and learned an enormous amount from the community, both about battery technology and about work principles.

I am grateful to all the past and present members of the MAPLE lab: Dr. Venkat Ramadesigan, Dr. Kishalay Mitra, Dr. Dayaram Sonawane, Dr. Suryanarayana Kolluri, Dr. Bharat Suthar, Dr. Matt Lawder, Chintan Pathak, Dr. Manan Pathak, Dr. Seongbeom Lee, Neal, Jerry, Caitlin, Tae-Jin, Akshay, Linnette, and Maitri; and the EMI lab: Dr. Trevor Braun, Dr. Matt Murbach, Victor, and Erica for making my research more productive and my life more fun.

I would like the acknowledge the financial support from the Assistant Secretary for Energy Efficiency and Renewable Energy, Office of Vehicle Technologies of the U. S. Department of

Energy through the Advanced Battery Materials Research (BMR) Program (Battery500 Consortium) as well as the Clean Energy Institute at UW.

Finally, I wish to give a special thanks to my friends and family who supported me through all the ups and downs in the course of grad school. To my parents, who have believed in me at all times; and to Fei, who has always been on my side and constantly cheers me up with food and love.

DEDICATION

To My Family

Chapter I. Introduction

I.1 Design of Lithium-ion Batteries

Thanks to its relatively high energy density and specific energy, the lithium-ion battery has been widely used in a variety of applications ranging from consumer electronics to electric vehicles, and aerospace and military applications. However, there are still deficiencies of current lithium-ion batteries, attracting researchers in academia and in industry to continue developing better and cheaper batteries. There are generally two ways to improve battery performances, implementation of new materials/new material concepts and implementation of superior cell designs[1]. The development of new materials has the potential to improve battery performance drastically, while optimizing the battery design enables us to realize the full potential of certain cell chemistry. Though battery design usually offers moderate improvement in battery performance, it is a necessary step in building the batteries regardless of the chemistry.

In a perfect world, we want to have a battery that has high energy density, high power density, low cost, long life and extremely safe under all conditions. However, there always exists trade-offs in the real world, and we need to prioritize our requirements. Because of the wide range of battery applications, the design specifications differ from one system to another. High-priced electronic devices are less sensitive to the cost but are more sensitive to the volumetric and gravimetric energy density of the batteries. While for the grid energy storage systems, the size and weight are less a problem compared to the cost. For electric vehicles, cost, volumetric and gravimetric energy densities, as well as volumetric and gravimetric power densities all play an important role in making electric vehicles competitive with the conventional gasoline-powered vehicles, thus we need to find a balance between the metrics. As a result, battery design needs to be tailored according to its application.

Traditionally, battery cell design is done by trial-and-error experimentally, which is time and money consuming, especially if it needs to be done for different applications separately. A lot of times, the design is only done for a general purpose, thus not highly efficient for the specific application. Modeling and mathematical optimization can significantly improve the efficiency of battery design, helping to meet the growing demands for various applications with ever-shorter design cycles.

I.2 Battery Modeling

At the materials level, modeling is mostly referred to as first-principles calculations that involve quantum and statistical mechanics.[2] This modeling approach is mostly used to guide materials development and understand reaction mechanisms. At the system level, full-cell behavior like charge/discharge is modeled. Since cell-level design is the focus of this dissertation, the system-level models will be used here.

There are two main categories of system level models: empirical/data-based models and electrochemical/physics-based models.[3] The empirical models fit experimental data to mathematical expressions with limited understanding of the underlying physical process. A data science approach establishing correlations between cell inputs and outputs is a representative example of a data-based model. Data-based models are simple to solve and easy to implement but suffer from high inaccuracies sometimes as high as 20%. They also require a decent-sized dataset from excessive experiments. A popular subcategory of empirical model that overcomes some of its drawback is the equivalent circuit model (ECM) that fits physical processes to electric circuit components. These models are still computationally efficient, but due to the strong physical relationship between the electric circuit components and the underlying physical processes, model accuracies can be improved with lower requirement on the size of the model-generating dataset.[4]

On the other hand, electrochemical/physics-based models are built on the kinetic, transport, and thermodynamic processes in a battery cell. Since they model the electrochemical and physical processes in all cell regions including current collectors, positive and negative electrodes, and the separator, they are also referred to as sandwich models, macroscopic models, or continuum models.[5] Compared with empirical models, physics-based models are usually more computationally intense and have higher predictability because of their complexity. Electrochemical models for batteries usually fall into two categories, the single particle model (SPM) or the pseudo-2-dimentional (P2D) model.

SPM was introduced into lithium-ion battery modeling later by the White group6 in the 2000s. The SPM is simpler compared to the P2D model but still captures the main physical processes in battery cells, including diffusion in the solid phase, reaction kinetics at the solid-electrolyte interphase, and material and charge balance. SPM uses two particles with the averaged properties to represent the positive and negative electrode. The equations are listed in Table *II-9*.

The P2D model, also known as the Doyle-Fuller-Newman (DFN) model or porous electrode model, was developed by the Newman group in the 1990s[7], which takes into account the porous electrode theory, concentrated electrolyte theory, Ohm's law, charge and material balance, and reaction kinetics. Since the P2D model include many internal variables like the location-dependent lithium-ion concentration, solid and electrolyte potential, it has the best predictive capability among system-level models, though at a greater computational cost. Since the introduction of the P2D model, it has become the most popular physics-based model in literature. The equations for a P2D model will be detailed in Chapter IV.

Building upon the basic electrochemical models, researchers have been trying to include more physics to account for more processes in the system. Thermal effect has been included for

both the single particle model[8,9] and the P2D model[10,11] to account for the temperature change during battery operation. Capacity fade/degradation is another direction for model extension. Many factors contribute to capacity loss, including intercalation/de-intercalation induced mechanical cracking in particles, separation of electrodes from the current collector, solid-electrolyte interphase (SEI) growth, lithium plating, electrolyte decomposition at high voltage/temperature.[12] Electrochemical-mechanical interactions are usually modeled by adding equations to capture the interation of spherical particles within a matrix host.[13] Other degradation mechanisms are mostly described by incorporating side reactions in addition to the main electrochemical reaction.[14–20]

Commonly used battery simulation and modeling programming languages include MATLAB/SIMULINK, Maple, C/C++, FORTRAN, ANSYS Fluent, Battery Design Studio, and COMSOL.

I.3 Model-based Battery Design

The idea of using modeling for battery design was first introduced by W. Tiedemann and J. Newman in 1975.[21] They used an ohmically limited porous electrode model to maximize the cell effective capacity by changing the electrode thickness and porosity. Newman later applied the reaction-zone model to maximize the specific energy of the system, taking mass into consideration as well.[22] For these two models, the objective function can be directly related to the design variables, thus the optimum can be obtained by simply observing the plot or from the analytical solution. They further optimized the thickness and porosity of lithium iron phosphate electrode, where they maximized the specific energy using the Ragone plots.[23] V. Ramadesigan et al.[24] went one step further by including the linear electrode kinetics to minimize the internal resistance of the electrode. They used control vector parameterization to minimize the ohmic resistance in the

positive electrode by varying porosity. They also introduced the graded electrode design using a layered approach and reported up to 33% decrease in resistance,

With the development of battery modeling, more physical processes have been included, and one of the most popular models is the pseudo-2D (P2D) model developed by the Newman group.[7] The P2D model involves a set of nonlinear partial differential equations (PDEs) that can only be solved numerically. Therefore, a numerical optimization approach is required to perform optimization on the system. W. Du et al. proposed a surrogate-model-based approach,[25] and later developed a sophisticated framework based on this approach with a gradient-based sequential quadratic programming optimization method.[26] They applied the framework to a lithium manganese oxide electrode and investigated the effect of discharge rate, electrode thickness, porosity, particle size, and solid-state diffusivity and conductivity on the specific energy and power density of the battery cell. S. Golmon et al.[27] extended the P2D model by incorporating the mechanical stress-strain relationship to account for the degradation due to cracks on the electrode particles. Thereafter, they developed a systematic framework to formulate the multi-objective and multi-design-parameter optimization problem with adjoint sensitivity analysis to reduce the computational cost.[28] They found that porosity and particle size distribution profiles can improve discharge capacity for both half and full cells with controlled mechanical stress. Another attempt along the line of faster optimization was done by S. De and his coworkers.[29] They used a reformulated model developed by P. Northrop et al.,[30] which greatly improved the computational efficiency, and performed simultaneous optimization of multiple design parameters including the thickness and porosity of the positive and negative electrodes to maximize the specific energy of the cell. N. Xue et al. used an alternative way to do the optimization more efficiently by using an effective optimizer.[31] They applied the gradient-based algorithm framework to optimize the cell

design to maximize the energy density with specific power density requirements for a spinel manganese dioxide cathode and meso-carbon micro beads anode system.

More recently, Y. Dai and V. Srinivasan revisited the idea of using graded electrodes to achieve better performance.[32] They used a gradient-free direct search method to maximize the specific energy under a certain discharge time by varying the design parameters such as electrode porosities and thicknesses, and compared the cases of uniform porosity and the graded electrode. They concluded that no significant improvement was observed by using the graded electrode design from their simulation. Later, Z. Du et al. examined the effects of several design parameters, including graded porosity, on the performance of thick electrodes by simulation. They proposed several continuously changing porosity profile in opposed to the more practical layered approach, and confirmed Dai and Srinivasan's conclusion that graded electrode design can only increase the performance slightly.[33]

Attempts to include multi-objective optimization in electrode design has also been made. C. Liu et al. developed a multi-objective optimization framework to optimize for minimizing degradation, maximizing specific energy and power at the same time by varying the conductivity, particle sizes, electrode thickness, and porosity for both electrodes.[34] They also considered the degradation mechanism and the long-term performance for design.

I.4 Thesis Outline

This thesis is focused on model-based battery design using electrochemical models, and the implementation of optimization and simulation methods necessary to achieve the graded electrode design profile.

Chapter I summarizes the necessary background information for the work, covering the motivation for battery design, current status and research directions for battery modeling and

model-based battery design. Following that, Chapter II introduces the electrode model based on the secondary current distribution and analyzed different cases of the model based on different sets of parameters. Chapter III focuses on the implementation of the simultaneous optimization approach for graded electrode design. This chapter details the simultaneous approach and presents the results of optimal graded electrode design with constraints. The pros and cons of the simultaneous optimization approach is also reported in comparison to the sequential approach, laying out the foundation for design optimization using a more complicated model.

Chapter IV takes the simultaneous optimization approach to the full cell P2D model. First, the time collocation discretization method is introduced to enable efficient full discretization on the partial differential equation system. Then the time collocation method is validated using a standard time collocation scheme. Last, the simultaneous optimization is performed with collocation in time and space to demonstrate the ability to control internal and transient variables.

Afterwards, Chapter V briefly discusses some ideas for future work on graded electrode design. Degradation mechanisms can be included for better life prediction. Specific user profiles can be used for designs tailored to specific applications. Techno-economic analysis is also necessary to determine whether graded electrode design is economically feasible.

Chapter II. Understanding Model-based Design with the Resistance Model

II.1 The Electrode Model

Generally, there are two purposes of using models to simulate the battery system; one is to develop a better understanding of the system, and the other is to use the models as guidance to achieve better performance. For the latter purpose, a model with fewer assumptions and more equations capturing as many processes as possible is desired to simulate the system better, and this is the direction that most of the researches reviewed above are moving towards. However, for a better understanding of the system, it may be worth taking a step back, and exam a simpler model where the effects of different processes can be observed clearly, even though more detailed physical models with much less assumptions would be used to guide the actual design. This is the purpose and idea behind this study.

For a typical intercalation-based lithium-ion battery cell sandwich, the positive electrode is usually made of lithium transition metal oxide while the negative electrode is composed of lithiated graphite. During charging, lithium de-intercalates from the positive active material, travels through the separator, and intercalates into the graphite; the electrons travel in the opposite direction through the external circuit. During discharging, the reverse process takes place. In this paper, the mass transport process described above is considered to be fast and the intercalation/de-intercalation process is determined by the electrochemical reaction kinetics.

The positive electrode, as depicted in Figure II-1, is the main focus in this work. The x-direction is the direction of interest, which is along the thickness of the positive electrode, with $x=0$ being the interface between the positive electrode and the separator and $x=l_p$ being the electrode-current collector interface. The model used is a one-dimensional porous electrode model developed by Newman and Tobias.[35]The following assumptions are made:

1) All variables such as potentials, current densities vary only along the thickness of the electrode, not in other directions (1-D).
2) There are no concentration gradients in the electrode. This assumption holds when charge/discharge process has just started from the equilibrium state, thus the concentration gradient has not had enough time to build up. Under this assumption, the model has no time dependency.
3) The double layer charging/discharging can be ignored.
4) The open-circuit potential of the positive electrode is assumed to be 0.

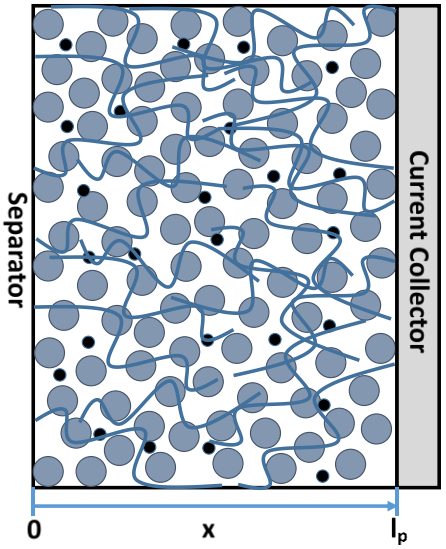

Figure II-1 Schematic of the cathode being modeled. x=0(X=0 after nondimensionalization) represents the boundary between the separator and the cathode, and x=lp (X=1) refers to the interface between the cathode and the current collector.

The 1-dimentional secondary current distribution model for a porous electrode was used to derive the dimensionless groups. Details about the model equations and simplification can be found in our recent paper.[36] Since it is a secondary current distribution model, the effect of mass transport is ignored, and the variables have no time dependency. This is true when the battery is operated under low rates or at the very beginning of charge or discharge.

The final equation set for the positive electrode is listed below for clarity.

$$
\begin{cases}
\dfrac{d\Phi_1(x)}{dx} = -\dfrac{i_1(x)}{\sigma} \\
\dfrac{d\Phi_2(x)}{dx} = -\dfrac{i_{app} - i_1(x)}{\kappa} \\
-\dfrac{di_1(x)}{dx} = ai_0 \left\{ \exp\left[\dfrac{\alpha_a F}{RT}\left(\Phi_1(x) - \Phi_2(x) - E_{eq}\right)\right] - \exp\left[\dfrac{-\alpha_c F}{RT}\left(\Phi_1(x) - \Phi_2(x) - E_{eq}\right)\right]\right\} \\
(\textit{nonlinear kinetics}) \\
-\dfrac{di_1(x)}{dx} = ai_0 \dfrac{(\alpha_a + \alpha_c)F}{RT}\left(\Phi_1(x) - \Phi_2(x) - E_{eq}\right) \\
(\textit{linear kinetics}) \\
\textit{with boundary conditions}: \\
i_1(0) = 0; \qquad i_1(l_p) = i_{app}; \\
\Phi_2(0) = 0.
\end{cases}
\tag{II-1}
$$

where the solid phase conductivity, liquid phase conductivity, active surface area can be expressed as:

$$
\begin{cases}
\sigma = \sigma_0 \left(1 - \varepsilon_{f+p} - \varepsilon\right)^{1.5} \\
\kappa = \kappa_0 \varepsilon^{1.5} \\
a = \dfrac{3\left(1 - \varepsilon_{f+p} - \varepsilon\right)}{R_p}
\end{cases}
\tag{II-2}
$$

The variables $\Phi_1(x)$, $i_1(x)$, and $\Phi_2(x)$ are potential in the solid matrix, current density in the solid matrix, and potential in the electrolyte respectively. A list of the nomenclature used in the equations is provided in Table 1.

II.2 Nondimensionalization Analysis

To gain a better understanding of the electrode model and evaluate the relative importance of ohmic resistance versus reaction kinetics, the original equation set was scaled to make all the variables dimensionless.

Set the equilibrium potential between the solid and electrolyte (E_{eq}) to be 0 and the overpotential $\Phi_1(x)$ - $\Phi_2(x)$ can be defined as $\eta(x)$. Subtract the second equation from the first one

in equation set (II-1) and then take the derivative with respective to x assuming the conductivities of the solid and the electrolyte (σ and κ) are constants, we can get

$$\frac{d^2\eta(x)}{dx^2} = -\left(\frac{1}{\sigma}+\frac{1}{\kappa}\right)\frac{di_1(x)}{dx} \tag{II-3}$$

Substitute equation (II-3) to the third and fourth equation in equation set (II-1) and also substitute i(x) from the first equation into the third and fourth ones, the system can be further simplified as

$$\begin{cases} \dfrac{d^2\eta(x)}{dx^2} = ai_0\left(\dfrac{1}{\sigma}+\dfrac{1}{\kappa}\right)\dfrac{(\alpha_a+\alpha_c)F}{RT}\eta(x) \\ \dfrac{d^2\phi_1(x)}{dx^2} = \dfrac{ai_0}{\sigma}\dfrac{(\alpha_a+\alpha_c)F}{RT}\eta(x) \end{cases} \tag{II-4}$$

for linear kinetics and

$$\begin{cases} \dfrac{d^2\eta(x)}{dx^2} = ai_0\left(\dfrac{1}{\sigma}+\dfrac{1}{\kappa}\right)\left\{\exp\left[\dfrac{\alpha_a F}{RT}\eta(x)\right]-\exp\left[\dfrac{-\alpha_c F}{RT}\eta(x)\right]\right\} \\ \dfrac{d^2\phi_1(x)}{dx^2} = \dfrac{ai_0}{\sigma}\left\{\exp\left[\dfrac{\alpha_a F}{RT}\eta(x)\right]-\exp\left[\dfrac{-\alpha_c F}{RT}\eta(x)\right]\right\} \end{cases} \tag{II-5}$$

for nonlinear kinetics.

The independent special variable *x* can be scaled by the thickness of the positive electrode to make the dimensionless thickness *X* vary from 0 to 1. For the potentials, a common way to scale is to use the thermal potential $\frac{RT}{F}$. The dimensionless variables after scaling are

$$\begin{cases} X = \dfrac{x}{l_p} \\ \eta^* = \dfrac{\eta F}{RT} \\ \phi_1^* = \dfrac{\phi_1 F}{RT} \end{cases} \tag{II-6}$$

Substitute the expressions (3) into the equation set (2), the equations with linear kinetics become

$$\begin{cases} \dfrac{d^2\eta^*(X)}{dX^2} = \upsilon^2 \eta^*(X) \\ \dfrac{d^2\Phi_1^*(X)}{dX^2} = \upsilon^2 \dfrac{1}{1+\dfrac{1}{\beta}} \eta^*(X) \end{cases} \tag{II-7}$$

And the equations with the nonlinear kinetics become

$$\begin{cases} \dfrac{d^2\eta^*(X)}{dX^2} = \upsilon^2 [e^{\frac{1}{1+\frac{1}{\sigma}}\eta^*(X)} - e^{-\frac{1}{1+\alpha}\eta^*(X)}] \\ \dfrac{d^2\Phi_1^*(X)}{dX^2} = \upsilon^2 \dfrac{1}{1+\dfrac{1}{\beta}} [e^{\frac{1}{1+\frac{1}{\alpha}}\eta^*(X)} - e^{-\frac{1}{1+\alpha}\eta^*(X)}] \end{cases} \tag{II-8}$$

With the boundary conditions

$$\begin{cases} \left.\dfrac{d\eta^*(X)}{dX}\right|_{X=0} = \dfrac{q\upsilon^2}{1+\beta} \\ \Phi_1^*(0) = \eta^* \\ \left.\dfrac{d\eta^*(X)}{dX}\right|_{X=1} = -\dfrac{q\upsilon^2}{1+\dfrac{1}{\beta}} \\ \left.\dfrac{d\Phi_1^*(X)}{dX}\right|_{X=1} = -\dfrac{q\upsilon^2}{1+\dfrac{1}{\beta}} \end{cases} \tag{II-9}$$

The dimensionless parameters appeared during the nondimensionalization analysis and their respective physical meaning are listed in the table below:

Table II-1 Dimensionless Parameters for the Electrode Model

Dimensionless Parameter	Physical Meaning
$q = \frac{i_{app}}{ai_0lp}$	Kinetic Linearity
$\upsilon^2 = \frac{(\alpha_a + \alpha_c)Fai_0lp^2}{RT}(\frac{1}{\kappa} + \frac{1}{\sigma})$	Dimensionless exchange current
$\beta = \frac{\kappa}{\sigma}$	Conductivity Ratio
$\alpha = \frac{\alpha_a}{\alpha_c}$	Reaction Direction

In order to understand the effects of each dimensionless parameter on the optimal design profile, 16 high-low combinations of the dimensionless parameters with linear and nonlinear kinetics were simulated to cover the possible design space of the problem. The plots for internal variables are as following. Through these plots, we wanted to separate the influence of different processes and generalize the problem with different parameter sets.

Table II-2 High and Low Value Case Studies of the Dimensionless Parameters

High	Low
10	0.1
10	0.1
10	0.1
9	1/9

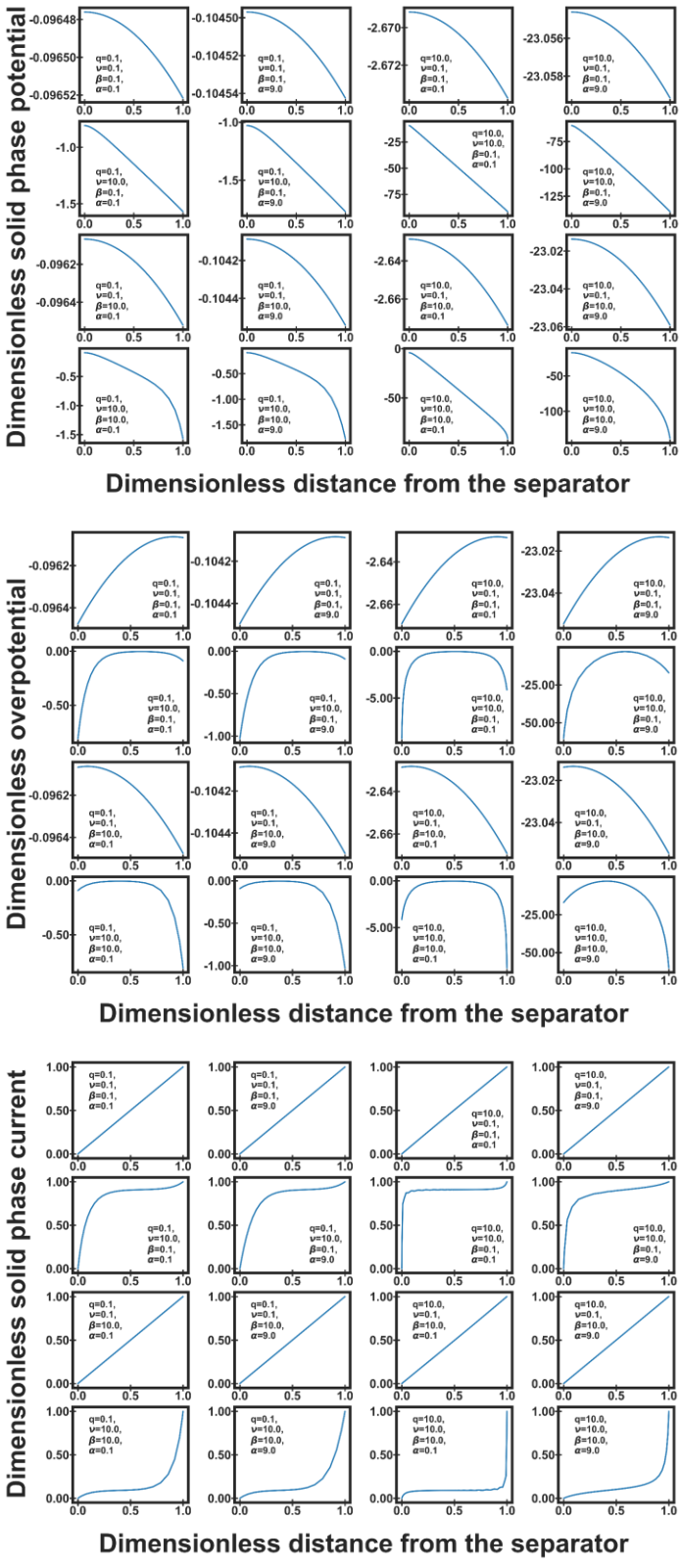

Figure II-2 State variable profiles for different parameter combinations

The first dimensionless parameter q is the ratio of the applied current density to the exchange current density. When this value is high, the system deviates significantly from the equilibrium, thus the nonlinear kinetics is a more accurate description and the difference between the linear and nonlinear kinetics will be bigger. This change in difference can be observed by comparing the first two columns of Figure II-2 with the last two columns.

The penetration depth L/υ represents the thickness of the reaction zone. When υ is larger, the reaction zone is thinner, thus the variation in the state variables is bigger. The influence of the penetration depth can be seen by comparing the first, third rows with the second and fourth rows in Figure II-2.

The conductivity ratio β basically shows the difference in conductivity in two phases. For the same current

distribution between the two phases, when β is reversed, the potential values in the two phases also changed. This explains why there exists a symmetry between the overpotential profiles between the first and the third and the second and the fourth rows of Figure II-2.

The reaction direction constant α represents whether a reduction or an oxidation reaction is favored. It is a measure of how easily a certain reaction can happen. Switched from 9 to 1/9, the favored reaction changed from an anodic reduction reaction to a catholic oxidation reaction, which accounts for the difference between the first and third and the second and the fourth columns, as shown in Figure II-2.

For graded electrodes, there exists four dimensionless parameters for each layer. To simplify the problem, α was set to 1, which means $\alpha_a = \alpha_c = 0.5$, in each layer. The simplest case is a graded electrode with 2 layers. Similarly, the high low parameter cases were simulated, with values listed in the table below where subscript 1 represents the layer near the separator and 2 is the layer near the current collector.

Table II-3 High and Low Values of the Dimensionless Parameters for the 2-layer Graded Electrode Simulation

Dimensionless Parameter	**Physical Meaning**	**High**	**Low**
$q_1,\ q_2$	Kinetic Linearity	10	0.1
$\upsilon_1^2,\ \upsilon_2^2$	Dimensionless Exchange Current	10	0.1
$\beta_1,\ \beta_2$	Conductivity Ratio	10	0.1

When a second layer is included, the situation is much more complicated. There are 6 parameters, and each parameter can take 2 possible values, constituting 64 (2^6) cases. The internal profile for all variables can be plot for the 2-layer graded electrode in a similar way as the uniform electrode, shown in Figure II-3.

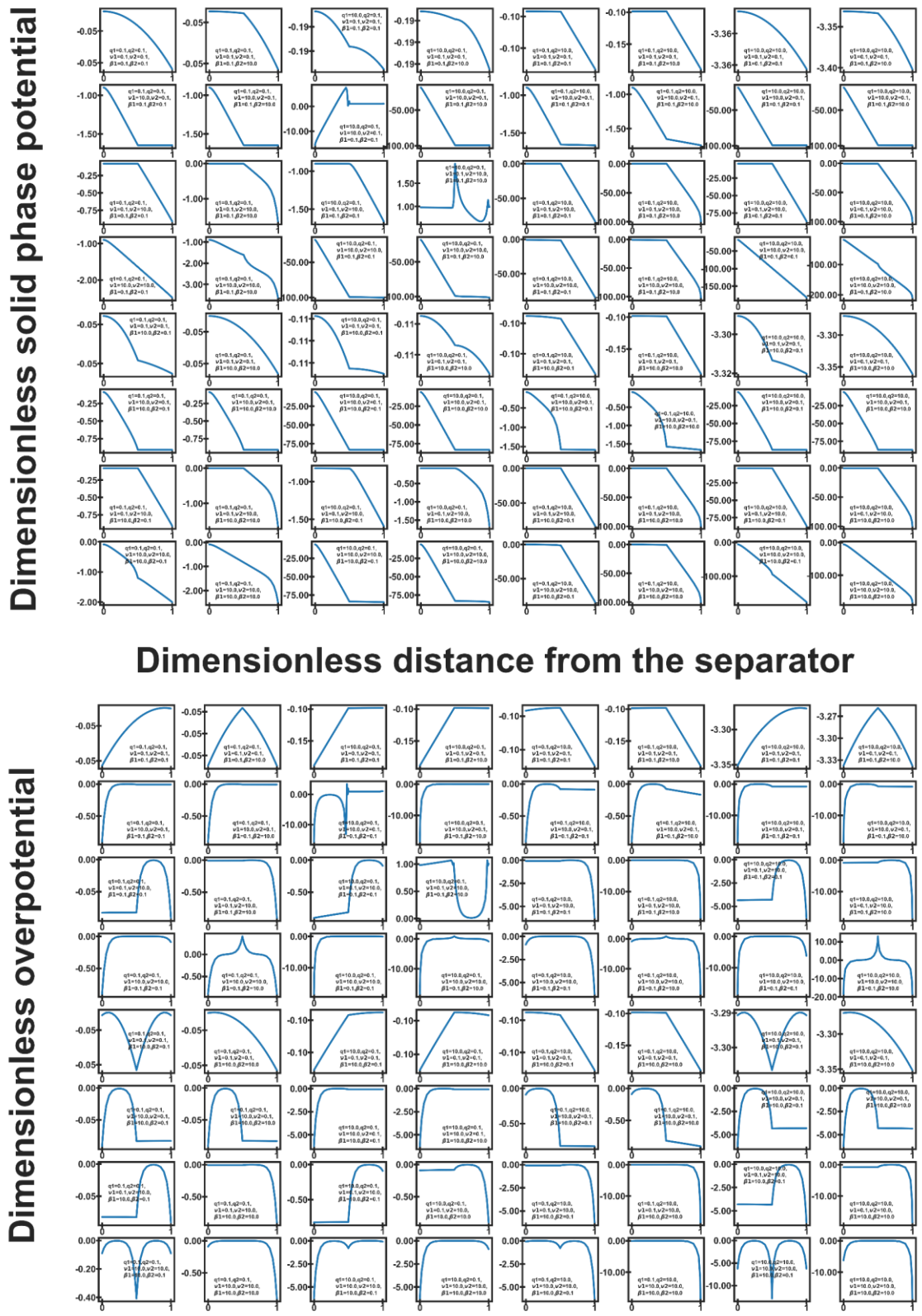
Dimensionless solid phase potential
Dimensionless distance from the separator
Dimensionless overpotential
Dimensionless distance from the separator

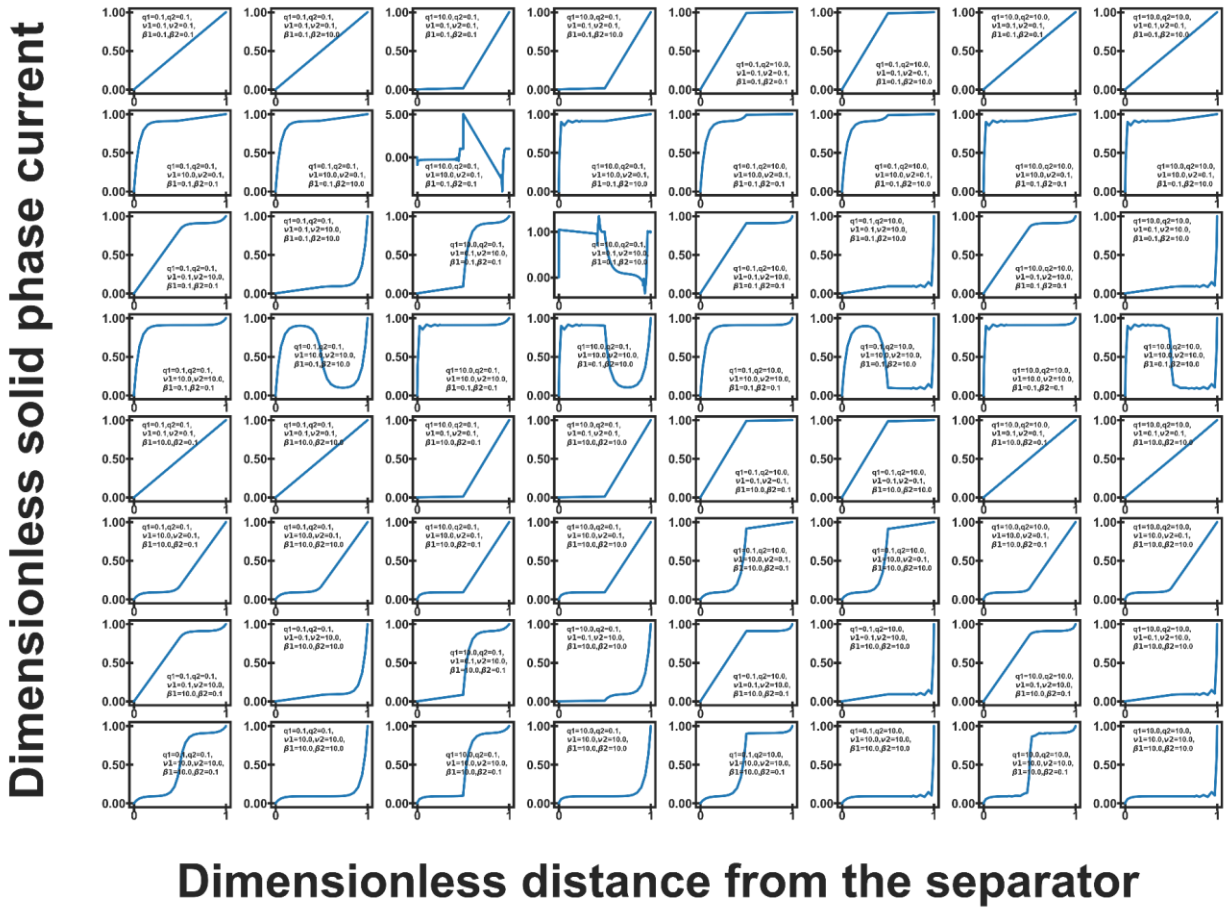

Figure II-3 Internal variable profiles of a 2-layer graded electrode with high-low parameter values

As can be observed from the plots above, there are many possible cases for a 2-layer graded electrode depending on the system parameters. To better understand the effect of other parameters on the optimal electrode design, 6 different positive electrode materials were selected to calculate the common ranges of dimensionless parameters and to analyze the corresponding optimal designs.

II.3 The Effect of Parameters on Optimal Design

6 common positive electrode materials with modeling parameters were chosen from literature to investigate the effect of other model parameters on optimal deign of the electrode porosity. Base case parameters for lithium iron phosphate ($LiFePO_4$, LFP), lithium cobalt oxide ($LiCoO_2$, LCO), lithium manganese oxide ($LiMn_2O_4$, LMO), lithium nickel cobalt aluminum oxide

($LiNi_{0.8}Co_{0.15}Al_{0.05}O_2$, NCA), lithium nickel manganese cobalt ($LiNi_{0.6}Mn_{0.2}Co_{0.2}O_2$, NMC), and titanium disulfide (TiS_2) are listed in Table II-4 below.

4 case studies were performed on theses 6 chemistries to compare the effect of parameters when designing porosity profiles. For all the case studies, the values provided in Table II-4 were used as base cases. All design optimization was done keeping the total amount of active material the same as the base cases for each chemistry respectively and varying porosity values. Since the total amount of the active material is a constant, the applied current to discharge the battery in 1 hour (1C) or 6 minutes (10C) will also be the same for each chemistry across designs. Because the total amount of active material is kept constant, the electrode thickness will change as the porosity changes according to the following equation:

$$\sum_{i=1}^{Nc} l_{p,i}(1-\varepsilon_i-\varepsilon_{fp,i}) = \text{constant} \qquad \text{(II-10)}$$

Where Nc is the total number of graded layers (1 for the uniform electrode).

Case study 1: minimizing total resistance under 1C discharge (Table II-5, Figure II-4)

Case study 1: minimizing total resistance under 10C discharge (Table II-6, Figure II-5)

Case study 1: minimizing overpotential variance under 1C discharge while the total resistance does not exceed the base case (Table II-7, Figure II-6)

Case study 1: minimizing overpotential variance under 10C discharge while the total resistance does not exceed the base case (Table II-8, Figure II-7)

Table II-4 Parameters of the Positive Electrode for Different Chemistries

Parameter[1]	Symbol	Unit	LFP[37]	LCO[38]	LMO[39]	NCA[40,41]	NMC622[42]	TiS_2[7]
Reaction Rate[1]	k	A/m^2	0.011	1.833	4.160	7.428	3.520	4.581
Solid Phase Conductivity[1]	σ	S/m	11.8	100	3.8	10	10	10000
Electrolyte Conductivity[1]	κ	S/m	1.105	0.205	0.980	0.828	0.826	0.1[43]
Maximum Solid Phase Concentration[1]	c_{max}	mol/m^3	20950[23]	51554	22860	49459.2	59493	29000
DoD[1]	Θ	-	0.8	0.6	0.6	0.6	0.6	0.6
1C current density	iapp	A/m^2	28.048	39.131	19.641	18.995	90.071	26.938
Porosity[1]	ε	-	0.31	0.385	0.416	0.4	0.25	0.3
Filler Fraction[2]	ε_f	-	0.12236	0.025	0.214	0.12236	0.12236	0.12236
Bruggeman Constant[1]	Brugg	-	1.5	4	5.2	2.2	1.8	1.5
Thickness[1]	L	um	110	80	144.4	50	150	100
Particle Radius[1]	Rp	um	0.15	2	8.5	2.5	4.5	1

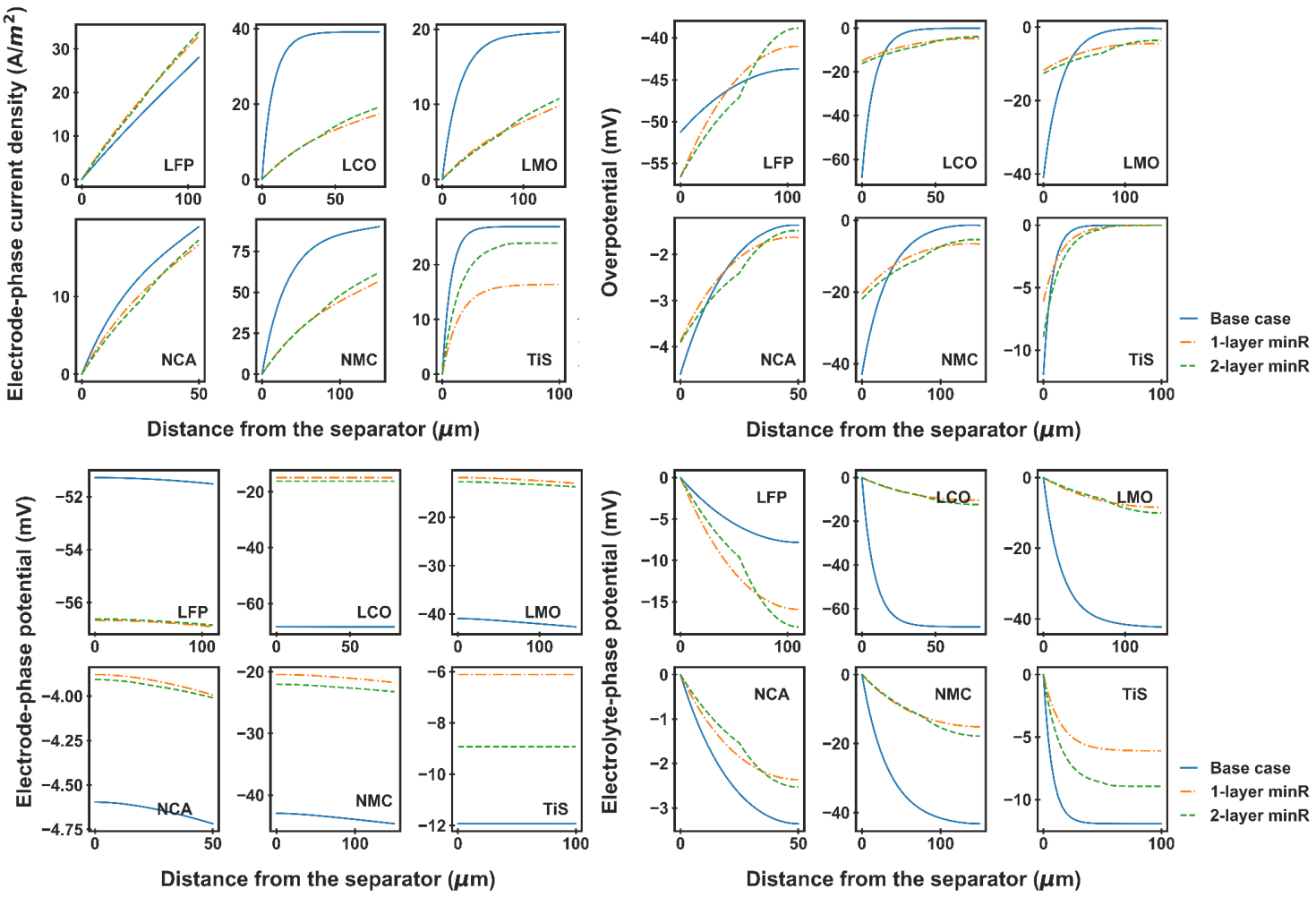

Figure II-4 Optimal Design with Minimal Total Resistance of a Uniform (orange) and a 2-layer Graded Electrode (green) Under 1C Discharge

The blue solid lines are for the base case using parameters in Table II-4, the orange dashed lines are profiles for the uniform electrode and the green dashed lines are for a 2-layer graded electrode

Table II-5 Optimal Design for Resistance Minimization Under 1C

	LFP		LCO		LMO		NCA		NMC		TiS	
1 layer	Optimal	Base	Optimal	Base	Optimal	Base	Optimal	Base	Optimal	Base	Optimal	Base
ep	0.491	0.310	0.774	0.385	0.594	0.416	0.561	0.400	0.494	0.250	0.526	0.300
lp (um)	161.416	110.000	234.640	80.000	277.848	144.400	75.463	50.000	245.120	150.00	164.50	100.00
R (Ohm cm^2)	17.957	18.367	7.916	17.459	13.985	21.716	2.233	2.483	3.825	4.956	3.726	4.427
1C (A/m^2)	28.048	28.048	39.131	39.131	19.641	19.641	18.995	18.995	90.071	90.071	26.938	26.938
eta_std (mV)	1.763	2.486	9.249	19.680	6.306	12.311	0.766	1.048	8.441	13.001	2.836	3.282
q	2.049	2.049	0.302	0.302	0.250	0.250	0.089	0.089	0.408	0.388	0.034	0.034
ν	0.495	0.562	4.026	9.480	3.767	6.586	1.700	1.961	3.107	4.489	11.538	13.717
β	8.32E-02	2.85E-02	3.65E-03	7.62E-05	8.91E-02	7.29E-03	7.34E-02	2.31E-02	6.03E-02	1.08E-02	1.09E-05	2.84E-06
δ	0.251	0.324	2.444	13.551	1.777	5.430	0.129	0.172	1.968	3.905	2.259	3.192
2 layers												
ep	0.519	0.422	0.778	0.707	0.637	0.487	0.593	0.482	0.542	0.347	0.524	0.321
lp (um)	153.402		203.259		238.392		70.197		217.487		126.928	
R (Ohm cm^2)	17.933		7.898		12.841		2.207		3.698		3.726	
1C (A/m^2)	28.048		39.131		19.641		18.995		90.071		26.938	
eta_std (mV)	1.806		9.337		6.620		0.789		8.753		2.939	
q	4.652	3.662	0.712	0.523	0.751	0.376	0.213	0.153	1.053	0.665	0.087	0.055
ν	0.219	0.282	1.706	2.405	1.229	3.261	0.712	1.029	1.195	2.185	4.481	8.124
β	9.76E-02	5.64E-02	3.81E-03	1.92E-03	1.65E-01	2.05E-02	9.20E-02	4.20E-02	8.19E-02	2.32E-02	1.07E-05	3.27E-06
δ	0.111	0.146	1.035	1.513	0.567	1.997	0.054	0.081	0.751	1.588	0.877	1.831
R deduction	-0.132%		-0.236%		-8.180%		-1.162%		-3.315%		-0.001%	

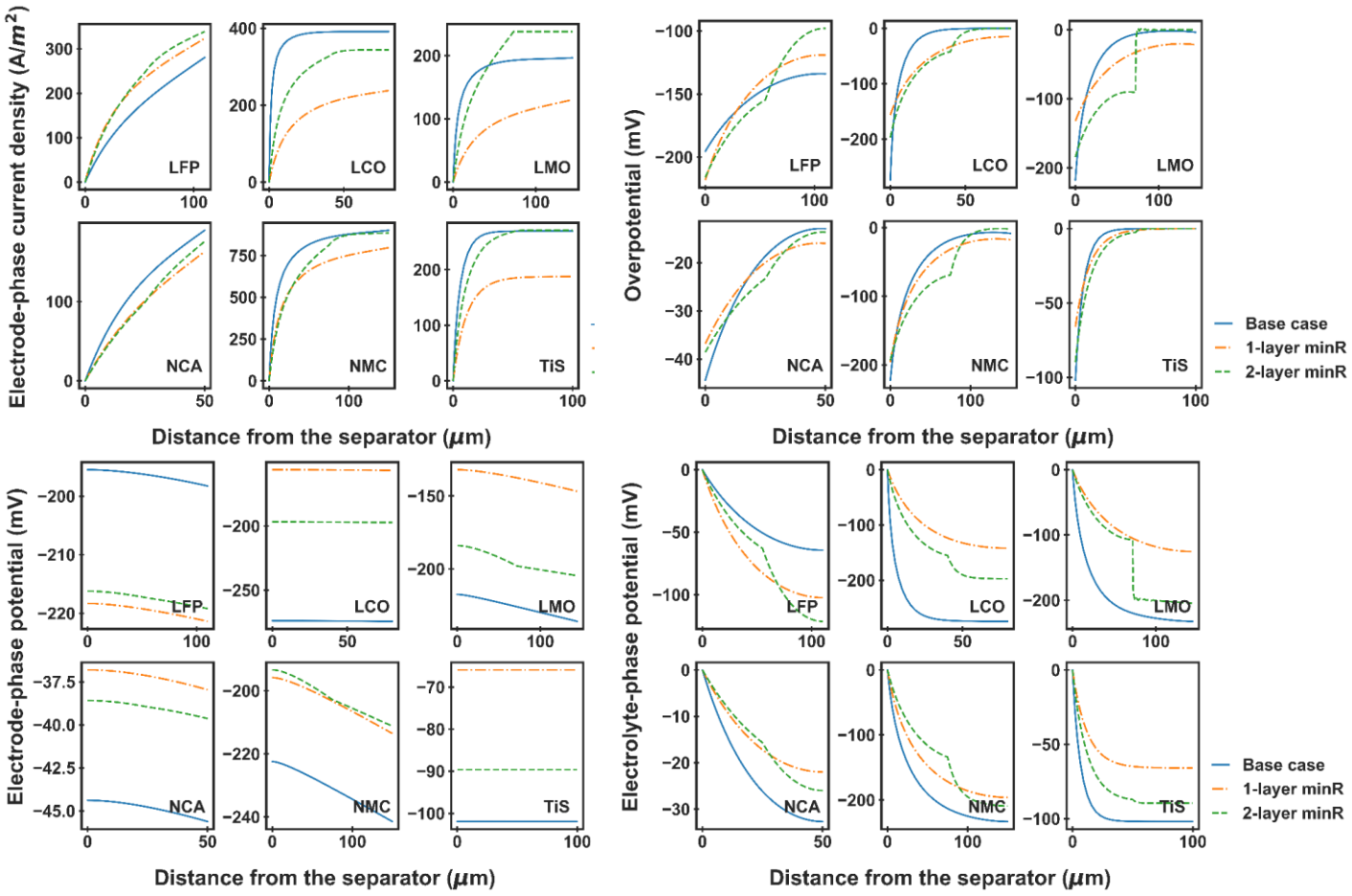

Figure II-5 Optimal Design with Minimal Total Resistance of a Uniform (orange) and a 2-layer Graded Electrode (green) Under 10C Discharge

Table II-6 Optimal Design for Resistance Minimization Under 10C

	LFP		LCO		LMO		NCA		NMC		TiS	
1 layer	Optimal	Base	Optimal	Base	Optimal	Base	Optimal	Base	Optimal	Base	Optimal	Base
ep	0.471	0.310	0.760	0.385	0.545	0.416	0.543	0.400	0.409	0.250	0.526	0.300
lp (um)	153.684	110.000	219.478	80.000	221.658	144.400	71.431	50.000	200.736	150.000	164.482	100.000
R (Ohm cm^2)	6.834	7.069	4.888	7.008	10.530	12.011	2.176	2.402	2.508	2.681	3.303	3.784
1C (A/m^2)	28.048	28.048	39.131	39.131	19.641	19.641	18.995	18.995	90.071	90.071	26.938	26.938
eta_std (mV)	15.117	19.973	54.620	71.592	47.568	61.127	7.657	10.177	53.426	63.283	24.814	27.582
q	20.492	20.492	3.016	3.016	2.504	2.504	0.892	0.892	4.077	3.875	0.339	0.339
ν	0.496	0.562	4.036	9.480	4.120	6.586	1.707	1.961	3.293	4.489	11.538	13.717
β	7.46E-02	2.85E-02	3.18E-03	7.62E-05	4.55E-02	7.29E-03	6.47E-02	2.31E-02	3.52E-02	1.08E-02	1.09E-05	2.84E-06
δ	2.523	3.241	24.566	135.513	21.246	54.298	1.300	1.715	22.100	39.053	22.588	31.923
2 layers												
ep	0.512	0.370	0.774	0.577	0.609	0.264	0.592	0.475	0.498	0.100	0.527	0.213
lp (um)	142.959		157.629		152.878		69.312		162.700		113.777	
R (Ohm cm^2)	6.797		4.849		9.248		2.146		2.344		3.303	
1C (A/m^2)	28.048		39.131		19.641		18.995		90.071		26.938	
eta_std (mV)	15.708		56.693		56.769		7.762		61.060		26.098	
q	48.891	35.279	8.986	4.540	9.877	3.354	2.150	1.525	12.427	6.067	0.982	0.519
ν	0.208	0.304	1.351	3.414	0.941	13.429	0.706	1.043	1.018	6.000	3.988	10.813
β	9.35E-02	4.16E-02	3.66E-03	5.71E-04	1.10E-01	4.88E-04	9.13E-02	3.99E-02	6.20E-02	1.68E-03	1.09E-05	1.48E-06
δ	1.057	1.634	8.202	26.454	4.373	302.435	0.536	0.830	6.437	109.207	7.807	30.314
R deduction	-0.534%		-0.811%		-12.177%		-1.357%		-6.547%		0.000%	

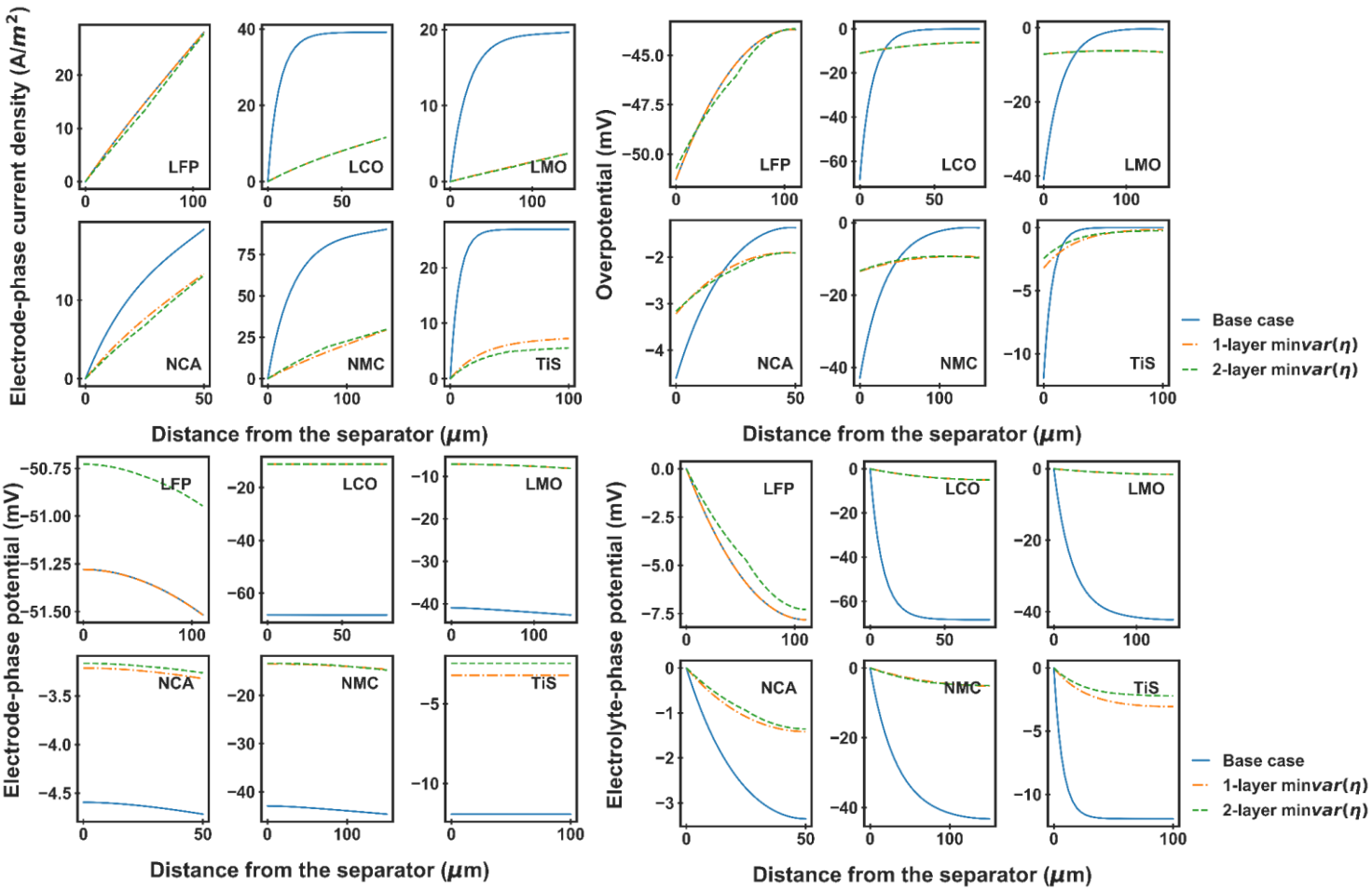

Figure II-6 Optimal Design with Minimal Overpotential Variance and Base-case Resistance of a Uniform (orange) and a 2-layer Graded Electrode (green) Under 1C Discharge

Table II-7 Optimal Design for Overpotential Variance Minimization Under 1C with Base-case Resistance

	LFP		LCO		LMO		NCA		NMC		TiS	
1 layer	Optimal	Base	Optimal	Base	Optimal	Base	Optimal	Base	Optimal	Base	Optimal	Base
ep	0.579	0.310	0.782	0.385	0.701	0.416	0.672	0.400	0.657	0.250	0.527	0.300
lp (um)	209.144	110.000	245.009	80.000	627.777	144.400	116.075	50.000	426.948	150.000	164.549	100.000
R (Ohm cm^2)	18.055	18.367	7.921	17.459	21.160	21.716	2.396	2.483	4.575	4.956	3.726	4.427
1C (A/m^2)	28.048	28.048	39.131	39.131	19.641	19.641	18.995	18.995	90.071	90.071	26.938	26.938
eta_std (mV)	1.697	2.486	9.243	19.680	4.763	12.311	0.720	1.048	7.766	13.001	2.836	3.282
q	2.049	2.049	0.302	0.302	0.250	0.250	0.089	0.089	0.408	0.388	0.034	0.034
ν	0.511	0.562	4.025	9.480	4.284	6.586	1.804	1.961	3.338	4.489	11.538	13.717
β	1.38E-01	2.85E-02	3.98E-03	7.62E-05	4.77E-01	7.29E-03	1.68E-01	2.31E-02	1.76E-01	1.08E-02	1.09E-05	2.84E-06
δ	0.267	0.324	2.443	13.551	2.298	5.430	0.145	0.172	2.271	3.905	2.259	3.192
2 layers												
ep	0.553	0.713	0.776	0.800	0.727	0.687	0.632	0.727	0.619	0.721	0.512	0.800
lp (um)	254.996		252.221		677.785		120.730		454.266		260.678	
R (Ohm cm^2)	18.367		7.932		21.716		2.483		4.956		3.731	
1C (A/m^2)	28.048		39.131		19.641		18.995		90.071		26.938	
eta_std (mV)	1.596		9.221		4.505		0.693		7.573		2.619	
q	3.088	6.092	0.566	0.645	0.674	0.398	0.144	0.235	0.654	1.082	0.041	0.194
ν	0.333	0.215	2.143	1.889	1.944	2.532	1.074	0.767	1.991	1.441	9.524	3.141
β	1.18E-01	3.42E-01	3.72E-03	4.79E-03	8.42E-01	3.69E-01	1.23E-01	2.74E-01	1.35E-01	2.94E-01	1.00E-05	9.22E-05
δ	0.172	0.141	1.301	1.151	1.275	1.277	0.083	0.069	1.297	1.123	1.866	0.956
η Variance deduction	-5.964%		-0.240%		-5.426%		-3.689%		-2.496%		-7.657%	

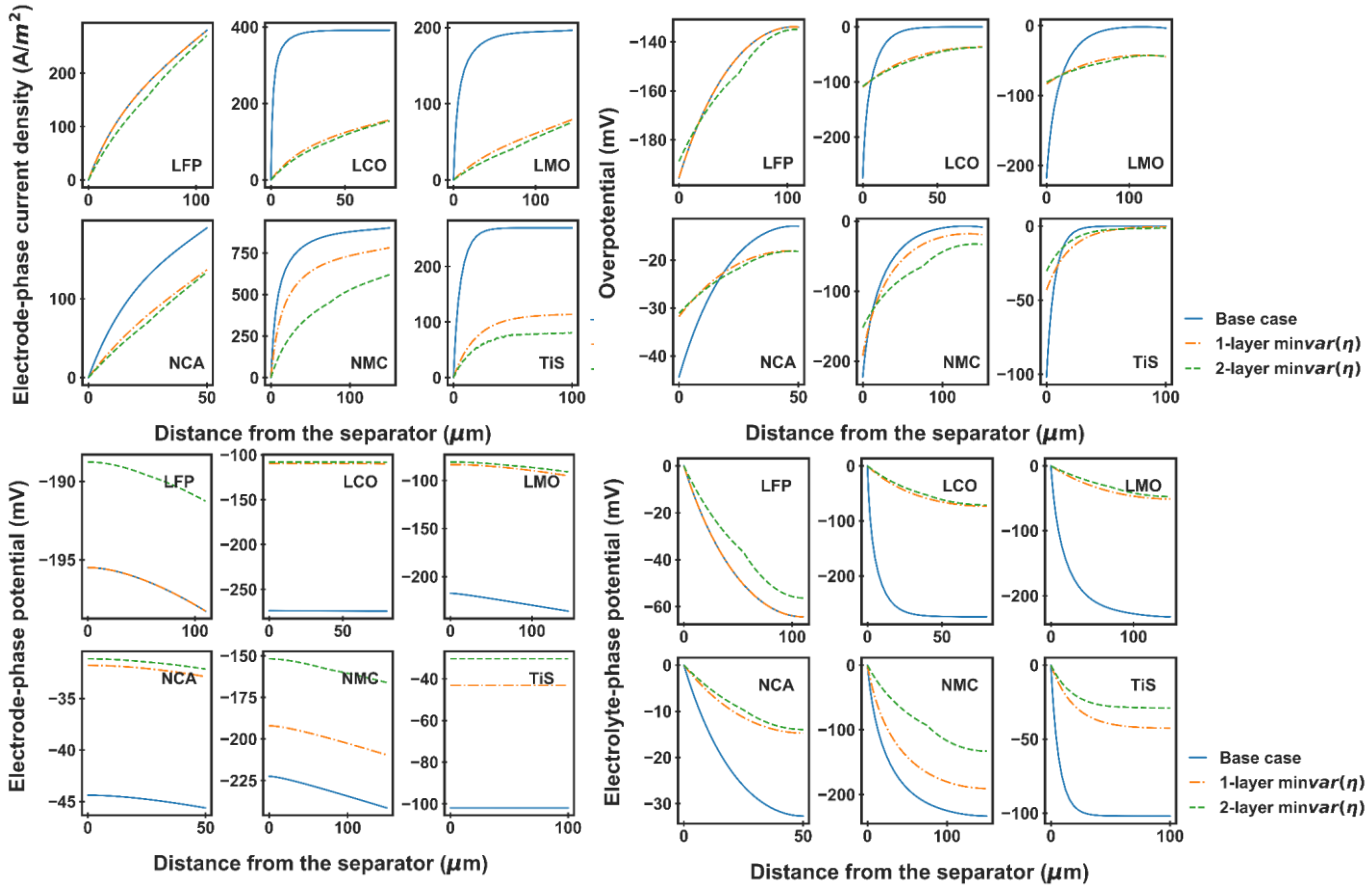

Figure II-7 Optimal Design with Minimal Overpotential Variance and Base-case Resistance of a Uniform (orange) and a 2-layer Graded Electrode (green) Under 10C Discharge

Table II-8 Optimal Design for Overpotential Variance Minimization Under 10C with Base-case Resistance

	LFP		LCO		LMO		NCA		NMC		TiS	
1 layer	Optimal	Base	Optimal	Base	Optimal	Base	Optimal	Base	Optimal	Base	Optimal	Base
ep	0.604	0.310	0.786	0.385	0.634	0.416	0.676	0.400	0.538	0.250	0.527	0.300
lp (um)	228.592	110.000	249.192	80.000	350.431	144.400	118.297	50.000	277.360	150.000	164.533	100.000
R (Ohm cm^2)	7.026	7.069	4.905	7.008	12.011	12.011	2.354	2.402	2.681	2.681	3.303	3.784
1C (A/m^2)	28.048	28.048	39.131	39.131	19.641	19.641	18.995	18.995	90.071	90.071	26.938	26.938
eta_std (mV)	14.176	19.973	54.477	71.592	38.616	61.127	7.038	10.177	48.013	63.283	24.814	27.582
q	20.492	20.492	3.016	3.016	2.504	2.504	0.892	0.892	4.077	3.875	0.339	0.339
ν	0.522	0.562	4.026	9.480	3.684	6.586	1.814	1.961	3.085	4.489	11.538	13.717
β	1.61E-01	2.85E-02	4.12E-03	7.62E-05	1.58E-01	7.29E-03	1.73E-01	2.31E-02	7.98E-02	1.08E-02	1.09E-05	2.84E-06
δ	2.792	3.241	24.448	135.513	16.994	54.298	1.468	1.715	19.401	39.053	22.588	31.923
2 layers												
ep	0.556	0.652	0.767	0.800	0.674	0.611	0.632	0.720	0.577	0.515	0.542	0.200
lp (um)	227.994		246.359		372.872		118.342		284.007		113.991	
R (Ohm cm^2)	7.069		4.910		12.011		2.402		2.681		3.432	
1C (A/m^2)	28.048		39.131		19.641		18.995		90.071		26.938	
eta_std (mV)	13.831		54.263		36.840		6.819		47.701		32.334	
q	34.854	49.730	5.551	6.604	6.431	4.100	1.467	2.279	8.985	7.462	1.024	0.507
ν	0.296	0.229	2.189	1.845	1.509	2.263	1.054	0.775	1.411	1.688	3.827	11.477
β	1.20E-01	2.18E-01	3.40E-03	4.79E-03	2.98E-01	1.14E-01	1.23E-01	2.54E-01	1.02E-01	6.92E-02	1.19E-05	1.32E-06
δ	1.525	1.305	13.303	11.245	7.324	10.501	0.814	0.684	8.948	10.631	7.497	33.425
R deduction	-2.429%		-0.392%		-4.600%		-3.117%		-0.649%		30.307%	

II.4 Parameter Estimation

The results in the previous session showed the importance of parameters in model-based design. The parameters are generally not known, as battery manufacturers treat them as trade secrets. Some parameters like the electrode thickness and particle size are not difficult to measure after opening up the cell, while some parameters are almost impossible to measure experimentally even with time-consuming destructive methods. For example, Bruggeman coefficient and tortuosity cannot be measured directly, therefore usually require fitting the simulation results from the experimental data. The kinetic data on the insertion reactions are not available, because of the fast charge transfer and slow mass transfer in the system, thus is usually estimated. Furthermore, some parameters are function of battery configuration and usage, hence may vary from cell to cell and change during the battery's lifetime. The fact that battery parameters change with use, makes direct measuring almost impossible, when updating the 'instantaneous' battery parameters over time is required for more accurate battery monitoring and control. The ability to get real-time parameters without opening up the cell is also important as greater proliferation of Lithium-ion batteries creates huge secondary usage market, which can only aim to use the batteries effectively and safely if the 'instantaneous' battery parameters are known.

Many efforts have been made for parameter estimation in the past. Commonly used methods include Electrochemical Impedance Spectroscopy (EIS), equivalent circuit model-based prediction with various Kalman filter methods, least squares method, machine learning etc. A detailed review of aforementioned methods can be found in Fleischer et al.[44]

Realizing the importance of parameter estimation in electrochemical models, many researchers have been actively working on this topic. Santhanagopalan and coworkers[45] applied the Levenberg-Marquardt method, a nonlinear least squares regression technique to both SPM and

P2D models, and estimated diffusivity in positive electrode, reaction rate constants and initial SOCs in both electrodes from both charge and discharge curve. Ramadesigan et al.[46] included capacity fade mechanism in their reformulated P2D model, and estimated the values of diffusivities in positive electrode and electrolyte and reaction rate constants in both electrodes over cycles using least squares estimation with Markov Chain Monte Carlo method for uncertainty quantification. Joel C. Forman and coworkers[47] used genetic algorithm (GA) for P2D model together with Fisher identification and successfully optimized 88 parameters at the same time for the lithium iron phosphate cell. Using a modified GA method NSGAII with TOPSIS, Zhang et al.[48] performed multi-objective parameter identification on both lithium-cobalt-oxide and lithium-iron-phosphate cells with thermal effects. More recently, Jun Li and coworkers used a heuristic algorithm to reduce the computational time during GA to estimate all parameters of a P2D model[49].

However, in literature no one has reported successful estimation of thermodynamics parameters, the OCP of a single electrode (Up). In this work, we proposed the estimation of Up, as well as other parameters for a single particle model. Up was approximated as a piecewise linear model without any knowledge of the electrode chemistry. The values of the piecewise linear Up points were treated as additional parameters of the single particle model and were estimated to match a constant rate (1C) discharge curve obtained experimentally. Different case studies are presented to estimate Up along with different types of parameters of the battery model.

In this work, we proposed a methodology and initial results for estimating battery parameters, including the thermodynamic parameters of a single electrode based on just discharge curves. With further attempts to reduce the computational time, the proposed methodology can be deployed on-site in field systems to estimate the battery parameters on the fly. This opens up the door for system integrators to pick any cell on the market and use it in the most efficient way, with just the

information provided in the battery datasheet. Since this method has the potential of real-time parameter estimation during operation, the parameters can be updated every few cycles to reflect the change in the cell. It can also facilitate the usage of second-hand batteries, even when operating history was unavailable.

We used the single particle model in this work, because it is less computationally expensive while still gives good results compared to experimental data in lower rates. SP model uses two particles with the averaged properties to represent the positive and negative electrode as shown in Figure II-8. The equations are listed in Table II-9. For the negative electrode, we assumed it is graphite, and used a regression model to represent the Un-SOC relationship.

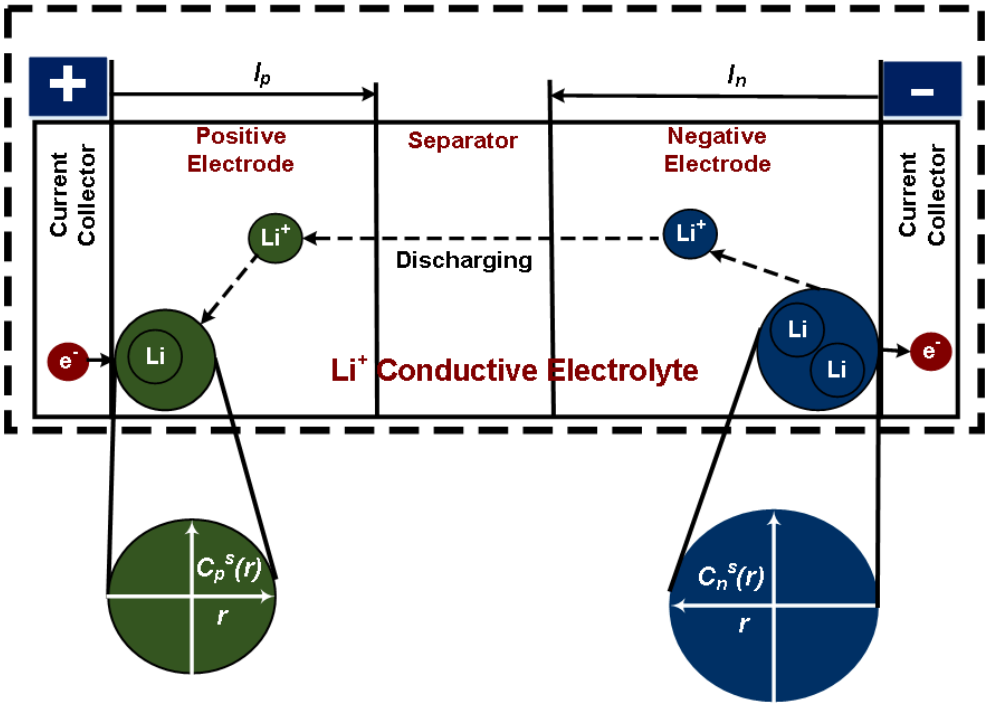

Figure II-8 Schematic of the Single Particle Model

Table II-9 SPM Equations

Governing Equations and Boundary Conditions of an Isothermal Model. $(i = p, n)$

	Governing Equations	Boundary Conditions	
Solid phase concentration (cathode): $c_p^s(r,t)$	$\frac{\partial c_p^s}{\partial t} = \frac{1}{r^2}\frac{\partial}{\partial r}\left[r^2 D_p^s \frac{\partial c_p^s}{\partial r} \right]$	$\left.\frac{\partial c_p^s}{\partial t}\right\|_{r=0} = 0, -D_p^s \left.\frac{\partial c_p^s}{\partial r}\right\|_{R_p} = \frac{I_{overall}}{A_{cross} l_i a_p F}$	(II-11)
Solid phase concentration (anode): $c_n^s(r,t)$	$\frac{\partial c_n^s}{\partial t} = \frac{1}{r^2}\frac{\partial}{\partial r}\left[r^2 D_n^s \frac{\partial c_n^s}{\partial r} \right]$	$\left.\frac{\partial c_n^s}{\partial r}\right\|_{r=0} = 0, -D_n^s \left.\frac{\partial c_n^s}{\partial r}\right\|_{R_n} = \frac{-I_{overall}}{A_{cross} l_i a_n F}$	(II-12)
Voltage: $V(t)$	$V(t) = \phi_p^s(t) - \phi_n^s(t) - I_{overall} R_c$		(II-13)

Additional equations used in the SPM

Butler-Volmer kinetics:	$\frac{I_{overall}}{A_{cross} l_i a_p F} = k_p \sqrt{c_e c_{p,surf}^s \left(1 - c_{p,surf}^s\right)} \sinh\left(\frac{F\left(f_p^s - f_{e,p} - U_p\right)}{2RT} \right)$	(II-14)
	$\frac{-I_{overall}}{A_{cross} l_i a_n F} = k_n \sqrt{c_e c_{n,surf}^s \left(1 - c_{n,surf}^s\right)} \sinh\left(\frac{F\left(f_n^s - f_{e,n} - U_n\right)}{2RT} \right)$	(II-15)
Specific Area	$a_i = \left(\frac{3}{R}\right)\left(1 - e_i - e_{f,i}\right)$	(II-16)

For cell voltage, we included a lumped parameter R_c, mainly for contact resistance at the current collector/electrode interface and the initial solid-electrolyte interface (SEI) layer resistance. The value for R_c is left as an adjustable parameter to be estimated at the beginning, and kept the same for other cases for simplicity, since it does not change much in a couple cycles. For the battery life simulation, the resistance may be a good representation of degradation over time.

Besides Up, Un, there are 10 other parameters in the SP model, namely diffusivity of positive

and negative electrodes (D_p^s, D_n^s), reaction rate constants (k_p, k_n), electrode thicknesses (l_p , l_n), electrode porosities (ε_p , ε_n), and particle sizes (R_p, R_n). We then grouped the parameters into three groups, transport parameters (D_p^s, D_n^s), kinetic parameters (k_p, k_n), and design parameters (l_p , l_n , ε_p , ε_n , R_p , R_n). The design parameters can be measure more easily compared to the transport and kinetic parameters when destructive experiments are allowed. Therefore, we prioritize the estimation of the 10 parameters. We explored the estimation of Up with transport parameters first, then included kinetic parameters, and eventually added design parameters.

To solve the SPM efficiently, finite difference method was applied for spatial discretization. For finite difference method, the more node points used, the more accurate the solution is, but the more computational cost required. We did simulations with 5, 10, 15, and 20 node points, shown in Figure II-9. From the figure, the curve with 5 node points is slightly different from the rest near 3400s, suggesting that at least 10 points are needed for accurate simulation. We used 15 node points for rest of the work to ensure precise numerical solution for the model.

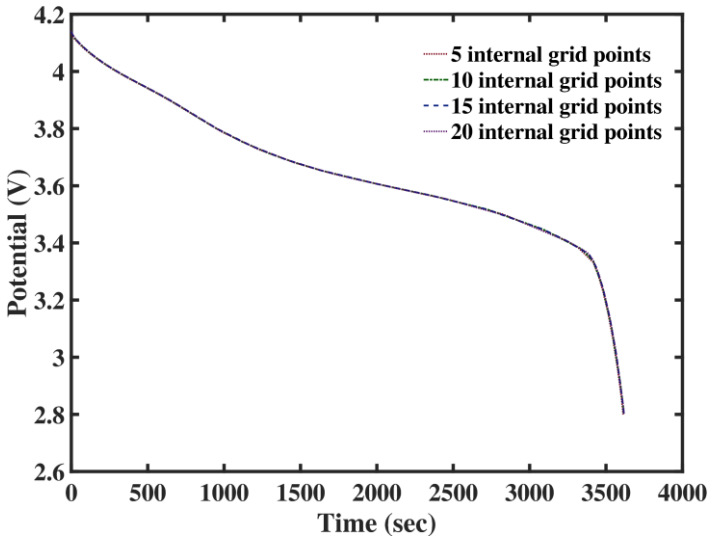

Figure II-9 Selection of number of node points for finite difference method

Estimation of Up and Other Parameters

Similar to the work done by Ramadesigan et al.[5], we used the least squares estimation approach to minimize the sum of squared differences between the experimental data and the model predictions. The objective function we used was

$$\min \sum_{t_0=0}^{t_n=tf} [V_{\exp}(t_i) - V_{model}(t_i)]^2 \qquad \text{(II-17)}$$

The experimental data was collected by discharging a fully charged Panasonic NCR18650A cell to 2.5 V at constant rates. The experimental data was recorded every second, resulting in ~3600 data points for 1C discharge. To reduce the number of data points, we used 1 point for every 10s, thus for 1C discharge, the number of data points was ~360. The typical nominal capacity of the cell is 3070mAh. The chemistry of the cell is not disclosed in its datasheet other than that it uses a nickel oxide system. It is common for commercial batteries to not disclose their chemistry, especially for positive electrode, making our work for estimation of Up relevant.

Due to the complexity and nonlinearity of the electrochemical model, and the large number of parameters involved (in this work, 21 Ups and other parameters), parameter optimization can be very challenging and computationally expensive. Genetic algorithm (GA) has been a popular approach recently for parameter estimation of electrochemical models[6]. GA is a global optimizer based on the process of natural selection and biological evolution. At every step (generation), a certain number (population) of individual solutions are randomly selected by mutation, crossover and selection from the previous generation. In this work, we used the Global Optimization Toolbox in MATLAB for GA.

Open Circuit Potential of the Positive Electrode

Owing to the existence of multi-stage intercalation voltage plateaus, the OCP-SOC relationship of a single electrode cannot be predicted by the general Nernst equation. The conventional way of getting the OCP information of a single electrode is by fitting a regression model to the experimental data measured at different state of charge (SOC)[50]. The OCP data is usually obtained by super slow discharge (at least 1/10C, sometimes as low as 1/60 C and even 1/100C) while measuring the potential vs. lithium metal as SOC changes. OCP is an intrinsic property of a certain material, thus needs to be determined every time when new electrode chemistry is used (eg. NCM[51], LCO[16]). The measurement is not only time consuming, but also destructive, as measurements need to be done for positive and negative electrode separately. Sometimes the experimental measurement can be spared if the chemistry of both electrodes is known and has been characterized, though the OCP-SOC relationship is not exactly the same for each individual cell even for the same materials fabricated with the same structures[52]. This relationship also changes as battery ages, resulting in bigger discrepancy in battery simulation. Furthermore, there are times when detailed material information is inaccessible, especially for commercial cells. As an alternative way to obtain single electrode OCP, estimation based on model-experimental comparison can be useful in practice.

In this study, we proposed a methodology to estimate Up based on a single discharge curve. It can be used during the first several cycles, to calibrate the initial status of an individual cell. This method can also be used anytime during the lifetime of a battery to help track and account for the degradation over cycles.

The most common electrode OCP-SOC relationship is of certain polynomial form. As a first attempt, we used a third-order polynomial fit for the Up-SOC relationship, shown in (II-18).

$$Up = a\theta^3 + b\theta^2 + c\theta + d \tag{II-18}$$

Where a, b, c, and d are parameters to be estimated. We assumed that all the other parameters needed for the model are known, and used some guess values (listed as base case in Table 2.2) to estimate a, b, c, and d only. The best fit was plotted in **Figure II-10**, together with the corresponding experimental data. As can been seen from the figure, the fit is far from reasonable. One can argue that by increasing the order of the polynomial function, the fit will be better and better. However, increasing the order of the Up-SOC function will dramatically increase the computational difficulty of the optimization problem. As a result, it is not favorable to pursuit the polynomial fit function.

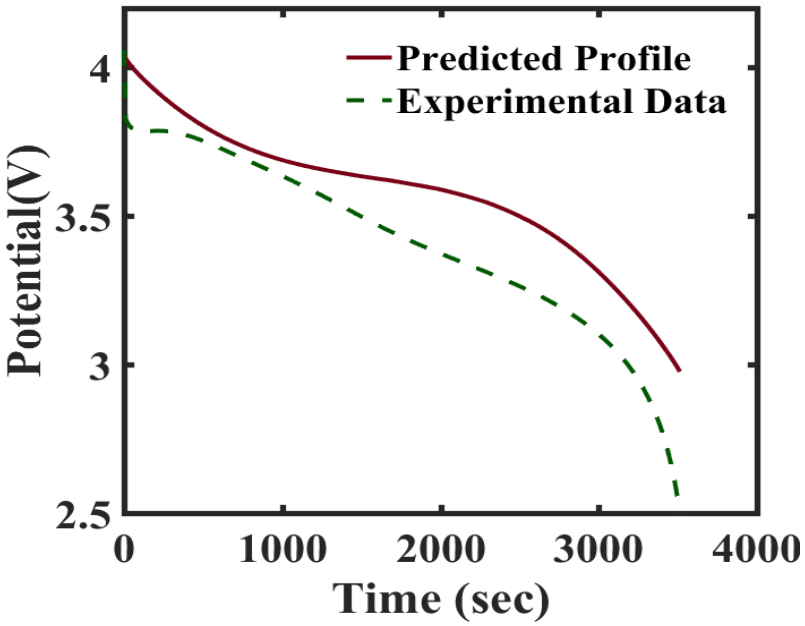

Figure II-10 Estimation of Up using a polynomial function

A piecewise linear approximated model for Up was used in this study. We picked a certain number of Up values at equally spaced SOCs, and used a linear relationship for the SOCs between two values we picked, as expressed in Equation 2.

$$U_{p,i+1} = U_{p,i} + (U_{p,i+1} - U_{p,i}) \times \frac{q_p^s - q_{p,i}^s}{q_{p,i+1}^s - q_{p,i}^s}, \quad i = 1 \ldots \tag{II-19}$$

In this work, we mainly focused on estimating the Up. We chose positive electrode because the lithium-ion batteries commercially available now mainly use graphite based negative electrode, but the positive electrode material varies from a group of lithium metal oxides and the combination

of them. The exact material formula and properties of positive electrode are generally not known, causing extra difficulty in battery management.

Case Studies

In this section, the results from several case studies estimating Up and other parameters in the model will be presented to demonstrate our idea. All the case studies were performed based on a single discharge curve at 3000mA at room temperature, roughly 1C. For the parameters not estimated in a certain case, we are using +-1% of the respective values in the 7th column of Table 2.2 as bounds, and estimating at the same time, thus the total numbers of parameter to be estimated are the same (31) for all cases.

Case Study 1: Estimation of Up and Resistance

Our first attempt was to try out the idea of using linear model to approximate Up. We estimated Up for different *n* linear approximated variables, where *n* = 4, 7, 13, and 21 Up values (Figure 4). Theoretically, when *n* is getting closer to infinity, the linear model is the same as the real case, but with a bigger n, the computational cost increases. We selected *n* = 21 for all the studies in this paper, because 21 points can give us a smooth and accurate enough discharge curve without an unaffordable computational expense. In this case, 21 points of the Up and the contact resistance were estimated using GA for SP model. The upper and lower bounds for the Up values were 2.5 V to 4.4 V. We added another constraint for the Up values such that they decrease as the SOC of the positive electrode increases, demonstrated in (II-20).

$$U_{p,i+1} - U_{p,i} \pounds 0,\quad i = 1 \leftrightharpoons \yen \qquad \text{(II-20)}$$

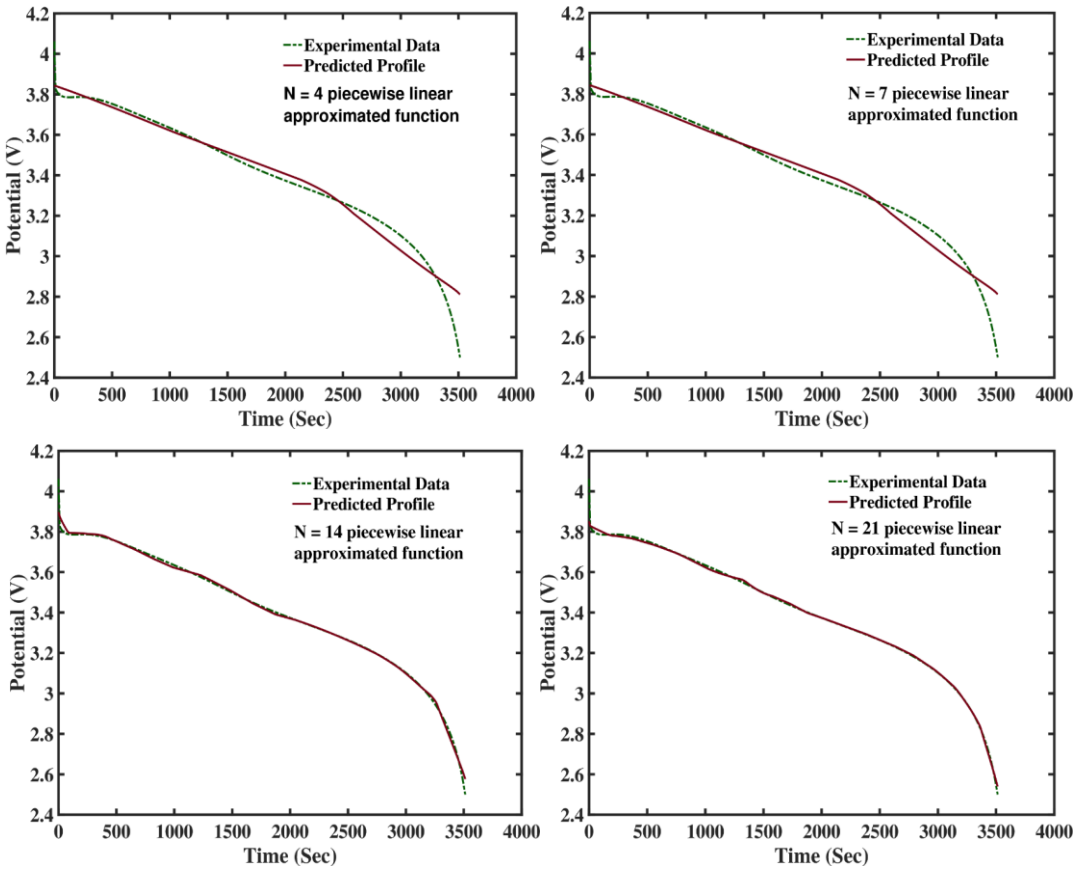

Figure II-11 Selection of number of piecewise linear approximation functions

The upper and lower bounds for K_R were 0.2Ω and 0.01 Ω. No additional information about the electrode chemistry was required for the optimization. The estimated Up values were listed in the second column of Table II-10 and plotted in Figure II-12, while the discharge curve with estimated values can be found in Figure II-13. As can be seen from Figure II-13, the estimated curve matches well with the experimental data, suggesting that our linear approximation approach is applicable to the Up.

Table II-10 Estimated Up Values

SOC	Case1	Case2	Case3	Case4
0.4	4.3464	4.3700	4.3780	4.3231
0.43	4.1450	4.1407	4.3120	4.1179
0.46	4.0884	4.0967	4.2613	4.0660
0.49	4.0687	4.0663	4.2117	4.0529
0.52	4.0359	4.0229	4.1613	4.0164
0.55	3.9966	3.9857	4.1119	3.9580
0.58	3.9445	3.9428	4.0620	3.9317
0.61	3.8890	3.8928	4.0122	3.8642
0.64	3.8676	3.8301	3.9618	3.8296
0.67	3.7959	3.7909	3.9124	3.7528
0.7	3.7594	3.7408	3.8613	3.7174
0.73	3.6984	3.6816	3.8122	3.6668
0.76	3.6613	3.6411	3.7627	3.6356
0.79	3.6311	3.6155	3.7129	3.5951
0.82	3.5805	3.5634	3.6637	3.5381
0.85	3.5373	3.5149	3.6101	3.4966
0.88	3.4841	3.4619	3.5603	3.4341
0.91	3.4139	3.3906	3.5098	3.3519
0.94	3.3173	3.2857	3.4079	3.2309
0.97	3.1506	3.0685	3.2393	2.9684
0.99	2.7847	2.6411	2.8579	2.6260

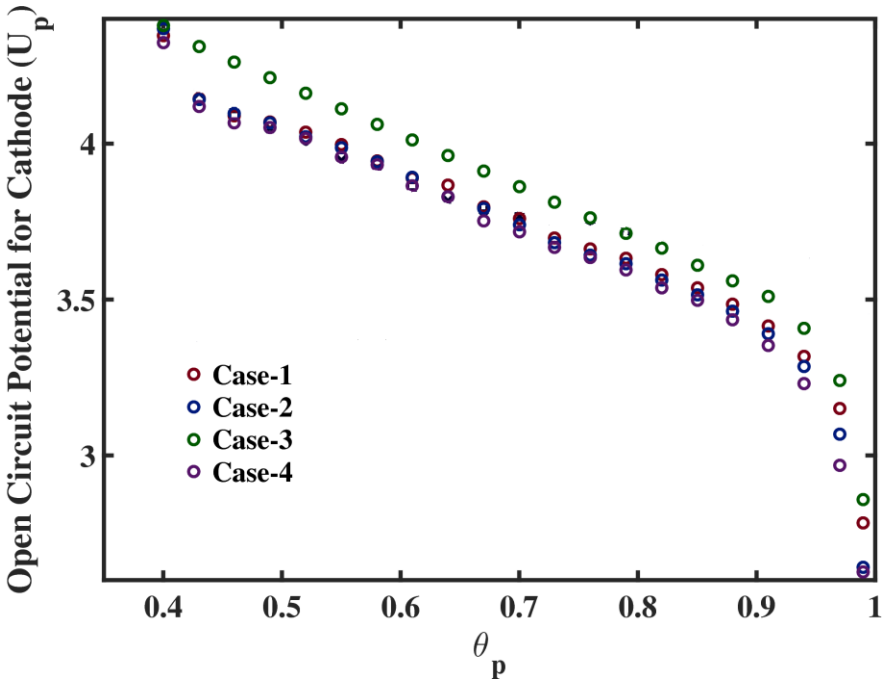

Figure II-12 Predicted profile of open circuit potential of the positive electrode using piecewise linear approximation function for each case

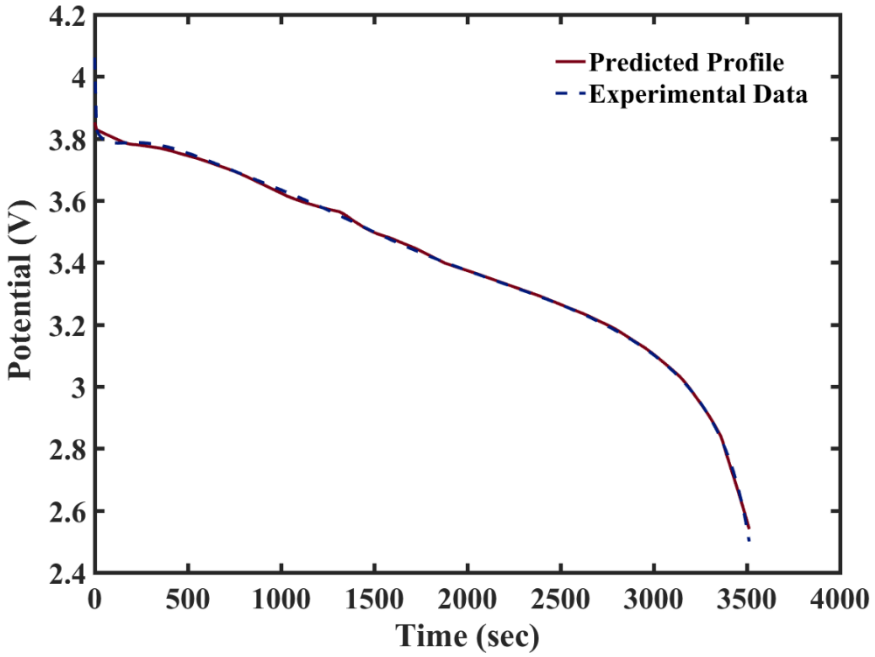

Figure II-13 Potential profile using predicted values of open circuit potential of cathode

Case Study 2: Estimation of Up and Transport Parameters

With the success of Case 1, the next step would be to increase the number of parameters actually estimated. The transport and kinetic parameters are harder to measure, thus we estimated them together with the Up first. For Case 2, we set the resistance to be 0.0615 Ω from Case 1, and estimated 21 Up values with transport parameters. The bounds for D_p^s and D_n^s were given as 3.34e-13 m^2 s^{-1} to 1e-12 m^2 s^{-1} and 1e-12 m^2 s^{-1} to 3e-12 m^2 s^{-1}. The results are shown in Figure II-12, Figure II-14, and Table II-11.

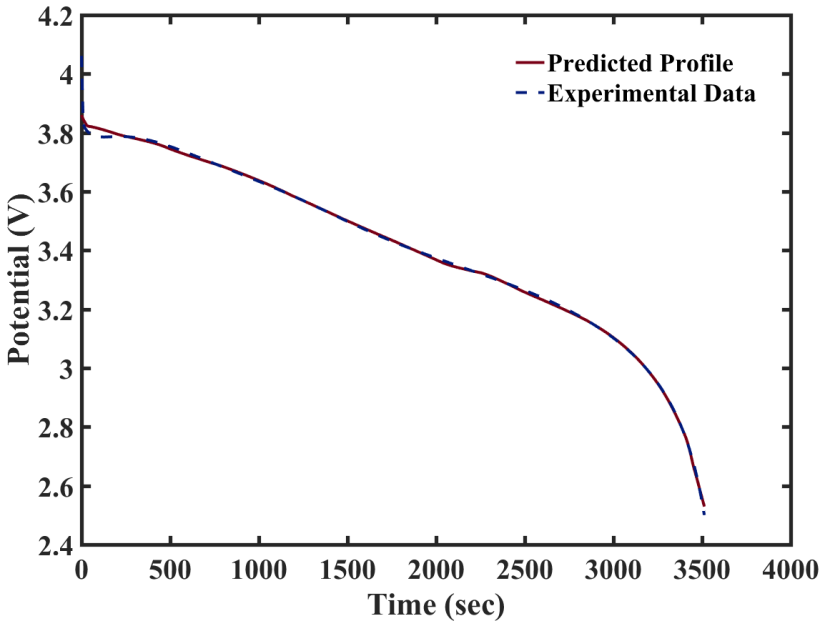

Figure II-14 Potential profile using predicted values of open circuit potential of cathode and transport parameters

Table II-11 Estimated Parameters with Up

		Unit	Case 2	Case 3	Case 4	Base Case	Reported in [42]
Transport Parameters	D_p^s	$m^2\ s^{-1}$	6.7108e-13	3.4832e-13	3.4848e-13	6.6756e-13	9.98e-13
	D_n^s	$m^2\ s^{-1}$	2.6174e-12	1.0211e-12	1.0618e-12	2.0085e-12	1.57e-14
Kinetic Parameters	k_p	$m^{2.5}mol^{-0.5}s^{-1}$	-	3.4710e-11	3.5898e-11	1.334e-10	3.94e-11
	k_n	$m^{2.5}mol^{-0.5}s^{-1}$	-	1.0046e-10	7.9500e-11	1.0307e-10	3e-11
Design Parameters	R_p	μm	-	-	2.63	8	4.5
	R_n	μm	-	-	2.0	10	10.5
	l_p	μm	-	-	42.59	43	30
	l_n	μm	-	-	46.04	46.5	54
	ε_p	-	-	-	0.421	0.423	0.2
	ε_n	-	-	-	0.409	0.413	0.37

Case Study 3: Estimation of Up, Transport and Kinetic Parameters

We included the kinetic parameters together with Up values and transport parameters in this case. The bounds for D_p^s and D_n^s were given as 3.34e-13 $m^2\ s^{-1}$ to 1e-12 $m^2\ s^{-1}$ and 1e-12 $m^2\ s^{-1}$ to 3e-12 $m^2\ s^{-1}$. The bounds for k_p and k_n were 6.67e-12 $m^{2.5}mol^{-0.5}s^{-1}$ to 3e-10 $m^{2.5}mol^{-0.5}s^{-1}$ and 5e-12 $m^{2.5}mol^{-0.5}s^{-1}$ to 2.25e-10 $m^{2.5}mol^{-0.5}s^{-1}$. The estimated discharge curve and parameter values can be found in Figure II-15, Table II-10, and Table II-11.

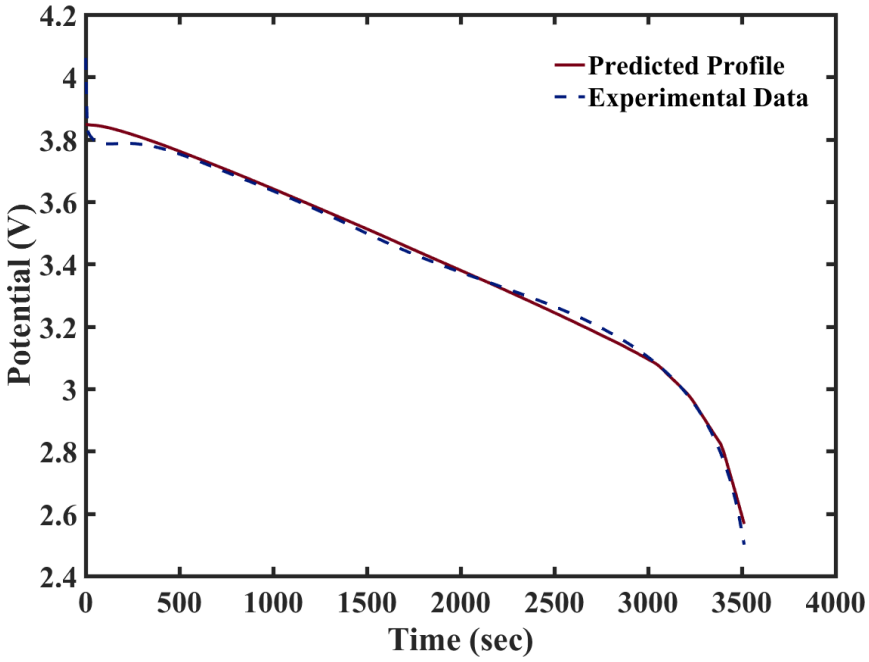

Figure II-15 Potential profile using predicted values of open circuit potential of cathode, transport and kinetic parameters

Case Study 4: Estimation of Up, Transport, Kinetic and Design Parameters

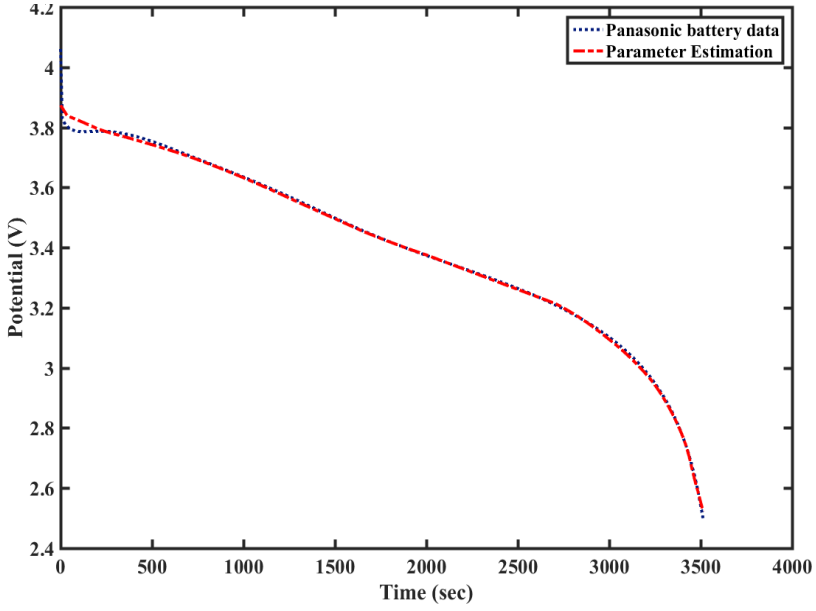

Figure II-16 Potential profile using predicted values of open circuit potential of cathode along with transport, kinetic and design parameters

In this case study, we estimated Up and all the parameters with wide bounds for SP model at the same time. The bounds for D_p^s and D_n^s were the same as in previous cases. The bounds for k_p and k_n were 3.33e-11 $m^{2.5}mol^{-0.5}s^{-1}$ to 1.67e-10 $m^{2.5}mol^{-0.5}s^{-1}$ and 2.58e-11 $m^{2.5}mol^{-0.5}s^{-1}$ to 1.29e-10 $m^{2.5}mol^{-0.5}s^{-1}$. The bounds for R_p

and R_n were 2μm to 10μm and 2.5μm to 12.5μm. While the upper and lower bounds for ε_p and ε_n were 0.3 and 0.6. The results are given in Figure II-16, Table II-10, and Table II-11.

Error Analysis

The absolute and relevant errors for each case were also calculated, listed in Table 3. The more parameters we estimate at the same time, the greater degree of freedom the solution space has, and thus the smaller error can be achieved compared to the experimental data. Since the parameter values we used in base case were just guesses based on experience, the error incorporated in the parameters, though can be cancelled by varying the parameters we are estimating under this specific condition, may show up under a different operation condition. This is probably what happened in Case 3. Even though the error under 3000mA was smaller compared to Case 1 and 2, the prediction for 600mA, 1000mA and 6000mA was further off. In general, the prediction under lower rates (C/5 and C/3) was better compared to higher rates (2C), this may result from the limitation of SP model. Since the lithium-ion concentration gradient in the electrolyte is ignored in the SP model, it is only valid under low rates.

Table II-12 Error Analysis for Various Case Studies

Case Study	Absolute Error	Relative Error
Up + R	0.0031	2.9886e-04
Up + Transport	0.0033	3.1239e-04
Up + Transport + Kinetic	4.5170e-04	3.4846e-05
Up + Transport + Kinetic + Design	2.3177e-04	2.0359e-05

Validation

To validate the estimated parameter values got from aforementioned cases, we simulated the discharge behavior at different rates, and compared with experimental data, as shown in Figure II-17 (600mA, C/5), Figure II-18 (1000mA, C/3), Figure II-19 (6000mA, 2C). As can be observed

from the plots, the general discharge performance of the battery under different discharge rates can be predicted reasonably well by our estimated parameters.

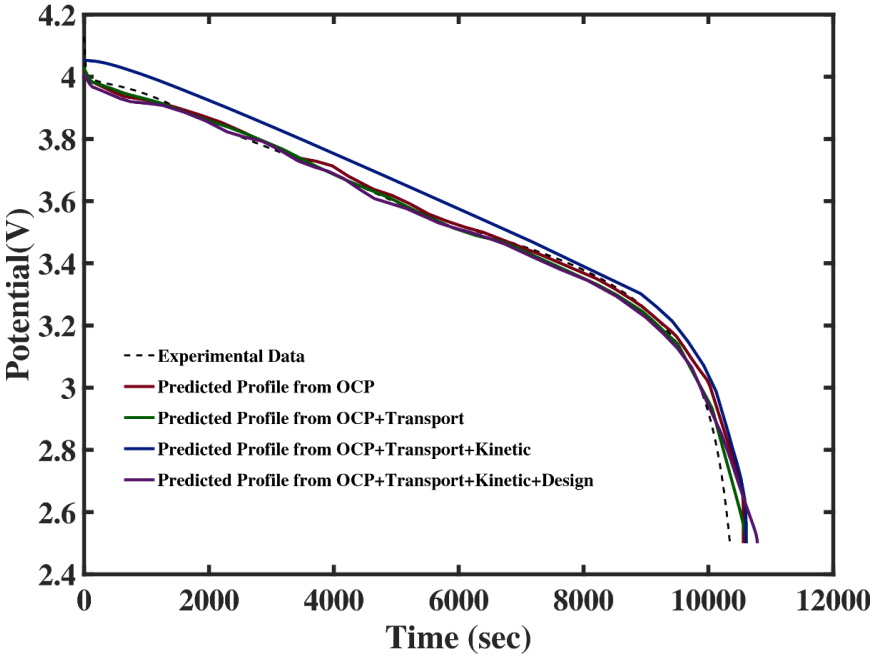

Figure II-17 Comparisons of different parameter estimation case studies with the experimental data for 1000mA

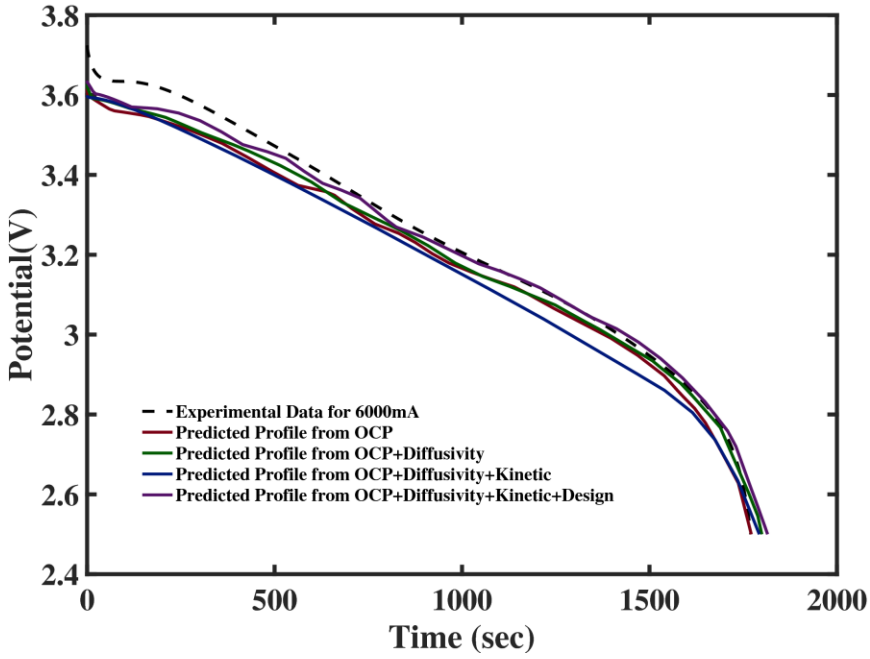

Figure II-18 Comparisons of different parameter estimation case studies with the experimental data for 600mA

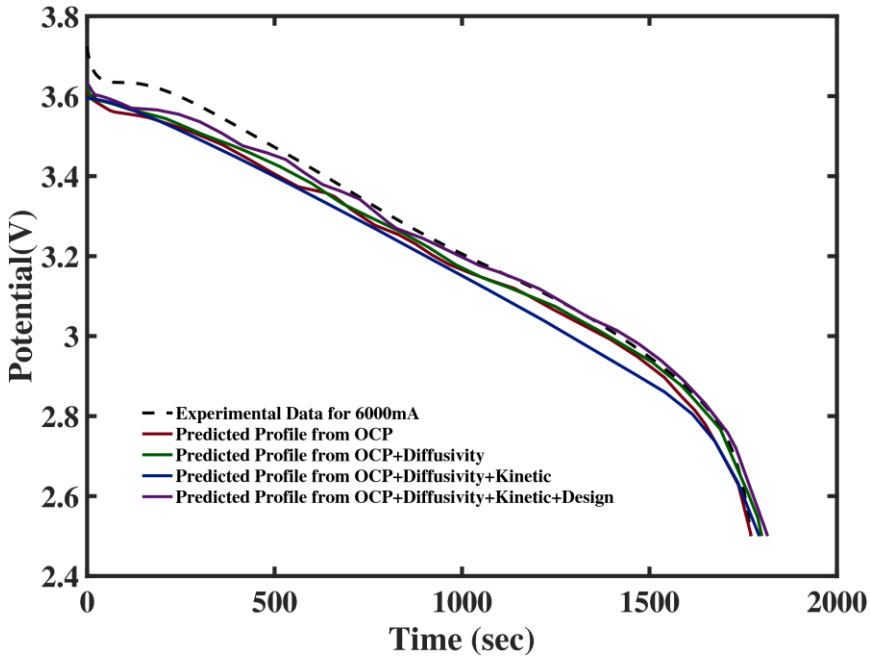

Figure II-19 Comparisons of different parameter estimation case studies with the experimental data for 6000mA

Estimation with two discharge curve at different rates might help with the predictability, but using more data means more experiments need to be conducted and more computation need to be run during estimation. Since estimation with one discharge curve can already give us reasonable results under different rate, we will not increase the time and efforts required to get and calculate additional information. However, depending on the application, if higher accuracy is desired, more data points can be easily accommodated in the current optimization framework.

Discussion

All the estimations above were run on a Dell Precision T7500 desktop with two Intel Xeon CPU W5590 3.33GHz processors and 24 GB RAM. We used the Global Optimization Toolbox in MATLAB R2015b in a Windows 7 Professional 64-bit system. The estimation time was under 10 hours for all four cases. Compared with 3 weeks for 88 parameters of P2D model needed for parameter identification on a cluster of five quad-core computers done by Forman et al.[6] and 19 hours required to identify the parameters of a thermal P2D model on a cluster with 20 cores[14], 10 hours is comparatively good. However, if we want to use the estimation as an on-line monitoring tool, then the computational cost must be reduced.

In this work, we mainly focused on Up, because the negative electrode of the common commercial cells today is based on graphite, and the OCP of lithium-ion intercalation is well studies, thus readily available when needed. People are pushing the boundary of lithium-ion batteries now, and more material including graphene and silicon is being investigated as potential next-generation battery material. If required, similar to the positive electrode, the linear approximation of negative electrode OCP can be done as well.

Chapter III. Building the Optimization Framework on the Electrode Model

In general, optimization approaches can be classified as indirect and direct approaches. The indirect approaches are also known as the variational approaches, in which the traditional necessary conditions from Pontryagin's maximum principle will be obtained for optimality.[53] Since porosity is always bounded, it is difficult to apply indirect methods for battery models. Alternatively, the direct approaches discretize the original optimization problem before solving it. There are two main subcategories of the direct methods: sequential and simultaneous approaches.

Most of the aforementioned optimization work used the gradient-based or gradient-free sequential optimization approach. The sequential approach takes the differential algebraic equation (DAE) system describing the physics, applies a certain nonlinear programming (NLP) solver to them, discretizes only the control variables (partial discretization), and solves the model. Because it discretizes only the control variable, it is also known as the control vector parameterization (CVP) method. At every iteration, a solution with a specific set of control variables is obtained. The optimal solution will be achieved over iterations. Note that as of today, global optimization cannot be guaranteed when CVP-type methods are used with P2D-based battery models.

The simultaneous approach, on the other hand, discretizes both the control variables and the design variables (full discretization) before solving the problem. When used for optimization, the DAE system will only be solved once at the optimal point, compared to the repeated numerical integration needed for the sequential optimization. By using higher order discretization scheme on both the state and the design variables, simultaneous optimization approach results in the faster determination of the optimum with fewer iterations.[54] Furthermore, this approach offers more flexibility over constraints on the state variables. Since the state variables are also discretized, it is possible to apply equality/inequality constraints on their internal values directly.

An ordinary differential equations (ODE) system (DAE system without algebraic equations) was involved due to the simplicity of the model. A general optimization framework based on a boundary value problem with ODEs can be expressed as[55]:

$$\begin{aligned} &\min_{\vec{z}(x),\vec{u}(x),\vec{p}} \varphi \\ &s.t.\, ODE\ system \\ &\frac{d\vec{z}(x)}{dx} = F(\vec{z}(x),\vec{u}(x),\vec{p}) \end{aligned} \tag{III-1}$$

with boundary conditions:

$$\vec{z}(x_{start}) = \vec{z}^{0}, \vec{z}(x_{end}) = \vec{z}^{1},$$

subject to bounds:

$$\vec{z}^{L} \le \vec{z}(x) \le \vec{z}^{U},\ \vec{u}^{L} \le \vec{u}(x) \le \vec{u}^{U},\ \vec{p}^{L} \le \vec{p} \le \vec{p}^{U},$$

Φ	Objective function
F	Differential equation constraints
$\vec{z}$	Vector of differential state variables
$\vec{u}$	Vector of control variables
$\vec{p}$	Space-independent parameters

The same electrode model as described in Objective 1 was used in this study. For the electrode model that captures the ohmic resistance in both solid phase and electrolyte, as well as the charge transfer resistance associated with the reaction kinetics, one natural optimization objective would be to minimize the overall resistance of the electrode, which can be mathematically represented as:

$$\min_{i_1(X),\Phi_1(X),\Phi_2(X),\varepsilon(X)} \varphi = \left| \frac{\Phi_1(1) - \Phi_2(0)}{i_{app}} \right| \tag{III-2}$$

III.1 The SOCOLL Method

The specific simultaneous approach we will showcase here is the simultaneous optimization and collocation (SOCOLL) method proposed by Biegler.[56] SOCOLL method uses the orthogonal collocation method to discretize both the control and state variables, before solving the problem at its optimal point. Collocation methods apply a polynomial approximation to the original differential equation. The zeros of the polynomials are called collocation points, where the differential equations should be satisfied. For a boundary value problem, the boundary conditions should also be satisfied at the end points.

The discretization of both control and state variables in scalar form can be expressed as:

$$\begin{cases} z(x) = \sum_{n=0}^{k} z_n P_n(x), \\ y(x) = \sum_{n=0}^{k} y_n P_n(x), \\ u(x) = \sum_{n=0}^{k} u_n P_n(x) \end{cases} \tag{III-3}$$

where z_n, y_n, and u_n are the values of $z(x)$, $y(x)$, and $u(x)$ at the n^{th} collocation point and P_n is a nth-degree polynomial.

Various kinds of orthogonal polynomials can be used with the SOCOLL method. In this study, we mainly used the interpolation polynomials in the Lagrange form, which can be written as:

$$P_n(x) = \prod_{\substack{0 \le i \le n \\ i \ne j}} \frac{x - x_i}{x_j - x_i} \tag{III-4}$$

Use of the Lagrange form facilitates solving only for the dependent variables at the collocation points as opposed to arbitrary constants in the polynomial representation.

All simulations and optimizations were performed using the Maple software classic worksheet 18 in the 64-bit Windows 7 Professional environment on a Dell Precision T7500 work station with two 3.33 GHz Intel Xeon CPU and 24 GB RAM. The BVP solver used in this study is the “dsolve”

function and the NLP solver is the "NLPSolve" function in the Maple program for the sequential approach. Similar solvers and optimizers are available in other programs, e.g. the "bvp4c" and "fmincon" functions in Matlab. For the simultaneous approach, collocation approach was used.

For clarity, the variables and parameters of the electrode model (equation set (1)) are listed in Table III-1. The +/- sign for the current density implies its direction. A negative applied current density was used to represent the charging process. The value of the applied current density is at 1C to represent a typical one-hour charge.

Table III-1 List of Variables and Parameters in the Optimization Problem

φ	Objective function	$\min_{i_1(X),\Phi_1(X),\Phi_2(X),\varepsilon(X)} \varphi = \frac{\Phi_1(1)-\Phi_2(0)}{i_{app}}$
F	Differential equation constraints	$\frac{d\Phi_1(X)}{dX} = -\frac{l_p i_1(X)}{\sigma_0\left(1-\varepsilon_{f+p}-\varepsilon(X)\right)^{1.5}}$ $\frac{d\Phi_2(X)}{dX} = -\frac{l_p(i_{app}-i_1(X))}{\kappa_0\varepsilon(X)^{1.5}}$ $-\frac{di_1(X)}{dX} = \frac{6i_0 l_p\left(1-\varepsilon_{f+p}-\varepsilon(X)\right)}{R_p}\sinh\{\frac{0.5F}{RT}[\Phi_1(X)-\Phi_2(X)]\}$ $BCs:\ i_1(0)=0;\quad i_1(1)=i_{app};$ $\Phi_2(0)=0.$
z	Vector of differential state variables	$[\,i_1(X),\Phi_1(X),\Phi_2(X)\,]$
u	Vector of control variables	$\varepsilon(X)$
u^L, u^U	Bounds	$u^L = 0.1,\ u^U = 0.7$

p	Space-independent parameters	Parameter[39]	Symbol	Parameter values
		Electronic conductivity of the solid matrix	σ_0	3.8 S/m
		Ionic conductivity of the electrolyte	κ_0	0.98 S/m
		Particle radius of the active material	R_p	8.5×10^{-6} m
		Thickness of the electrode	l_p	144.4×10^{-6} m
		Inert material total volume fraction	ε_{f+p}	0.214
		Faraday's constant	F	96,487 C/mol
		Ideal gas constant	R	8.314 J/(mol·K)
		Temperature	T	298.15 K
		Applied current density	i_{app}	-23.12 A/m^2
		Exchange current density	i_0	4.16 A/m^2

III.2 Uniform Porosity Optimization

The conventional battery electrode is designed to have a uniform structure without property variation. The uniform electrode is easier to manufacture, and also easier to simulate and optimize. To optimize a uniform electrode without porosity distribution, ε can be treated as a constant variable independent of X, instead of the $\varepsilon(X)$ in the equation set 1. Since porosity is now a constant variable, there is no need to discretize ε. The results from the simultaneous and the sequential

approaches are listed in Table 2. The bounds for the design variable ε are $0.1 \leq \varepsilon \leq 0.7$ for both cases. An initial guess of 0.4 was given to the optimizer.

Table III-2 Uniform Porosity Optimization Using the Simultaneous (SOCOLL) and the Sequential (CVP) Approaches

Approach	Number of collocation points	Optimization time (s)	Objective function φ (Ω-cm^2)	Optimal porosity
Simultaneous (SOCOLL)	2	0.031	4.6199	0.3052
	3	0.046	5.3414	0.3413
	4	0.047	5.3503	0.3433
	5	0.063	5.3510	0.3435
	10	0.109	5.3510	0.3435
Sequential (CVP)	N.A.	0.250	5.3510	0.3435

From Table III-2, it can be observed that for this problem, the SOCOLL method converges for $k = 5$ internal collocation points. Both approaches returned the optimal porosity of 0.3435 and minimum resistance of 5.3510 Ω-cm^2. When using $k = 5$ for the SOCOLL method, it is 4 times faster than the CVP method. Since BVP method involves solving the equations at every iteration, it is expected to be slower compared to the SOCOLL method, where the equations are solved only once at the optimum.

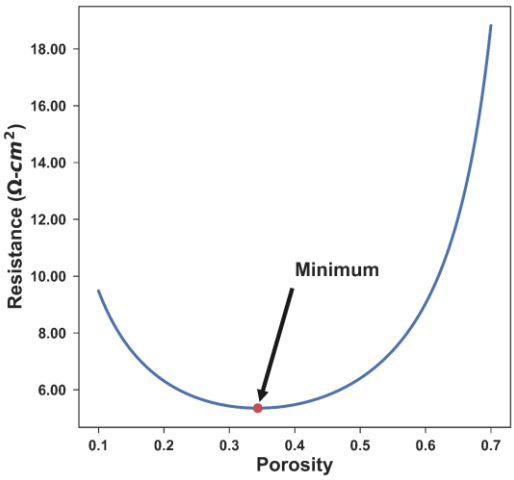

Figure III-1Resistance for cathode as a function of different uniform porosity values. There is a single minimal resistance value in the feasible region of porosity between 0.1 and 0.7, making the optimization problem convex. The minimum is consistent with the optimal porosity of 0.3435 from both the sequential and the simultaneous approaches

Due to the relative simplicity of the electrode model and a small search space, it is straightforward and easy to evaluate the objective function over the feasible region. The result is shown in Fig. 3. From the plot, it can be seen clearly that over the feasible region of [0.1, 0.7] for porosity, the objective function resistance is convex, and the optimal point is consistent with the results from the SOCOLL and CVP methods. It should also be noted that the curve is relatively flat near the optimal point from 0.25 to 0.45, which covers most of the common porosities in commercial cells and in the literature, with around 8.6% difference in resistance in that porosity range.

Since the Bulter-Volmer expression was used instead of the linear kinetics, the optimal porosity depends on the operating condition, the value of i_{app} in this case. The same optimization was carried out with i_{app} =0.2C and 5C (value of 23.12 A/m^2 listed in Table 1 is at 1C), which covers most of the normal operating range for batteries. Optimal porosities of 0.3432 and 0.3480

were achieved, with the minimum resistance of 5.3610 Ω-cm^2 and for 0.2C and 5.1373 Ω-cm^2 for 5C respectively. Compared with the 1C case of 0.3435 being the optimal porosity, the difference in porosity is around 1%, below the controllable error in manufacturing. This is due to the relatively fast electrochemical reaction rate of the system. For the rest of the paper, 1C rate was used for optimization since the influence of C rate is small in this case.

III.3 Graded Electrode Optimization

The idea of using electrode with porosity distribution in model-based electrode design for lithium-ion batteries was first introduced by Ramadesigan et al.[24] Golman and her colleagues[28] also examined the effect of the graded electrode with mechanical properties considered. Recently, Dai et al.[32] carefully looked at the performance improvement by utilizing a full P2D model and recommended the manufacturers not to make the graded electrode due to the additional processes involved and very small improvement achieved. In this paper, we want to quantify the gain in terms of electrode resistance with the two optimization approaches. This is a revisit to Ramadesigan's optimization problem, with nonlinear reaction kinetics instead of the linear kinetics assumption he made in his paper.

The simplest case for the graded electrode is a 2-layer porosity distribution structure. The original cathode can be divided into two regions of equal thickness and within each region, the porosity is a constant, as demonstrated in Fig. 3. For the sequential approach, the original ODE set was doubled with porosity being ε_1 and ε_2 in layer 1 and layer 2 respectively. The values for all

state variables were set to be continuous across the layers. For the simultaneous approach, within each layer at each node point, the polynomial expressions for all the variables were substituted to the original ODE system. A 4.4% reduction in resistance can be obtained from using a graded porosity with 2 layers compared to uniform porosity.

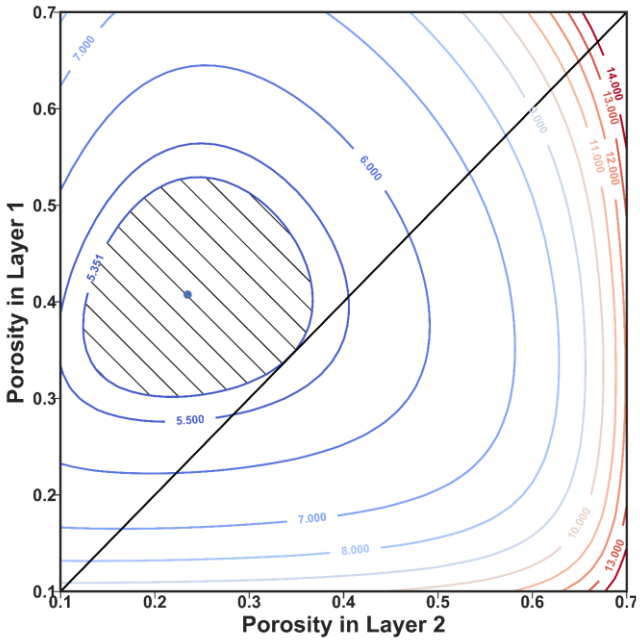

Figure III-2 The contour plot for the resistance of a 2-layer graded.

The blue dot represents the point of minimum resistance (5.1164 Ω-cm2) for the 2-layer graded electrode. The diagonal line of $\varepsilon_1 = \varepsilon_2$ *is equivalent to Fig. 3 for the uniform case with the intersection point with the 5.3510 Ω-cm2. The hatched area inside the contour represents the search space for 2-layer graded electrode design with resistance no bigger than the uniform minimum case. By introducing the second layer of graded electrode, the feasible region changes from a point to a reasonably sized area. With the extra freedom in design, more objectives can be considered without resulting in an electrode with higher resistance.*

Similar to the uniform case, a contour plot of the electrode resistance over the search space can be made to visualize the optimization problem, as shown in Fig. 4. The diagonal line of $\varepsilon_1 = \varepsilon_2$ is equivalent to the uniform electrode case shown in Fig. 3. The area inside the contour of 5.3510 Ω-cm^2 in resistance represents the 2-layer graded electrode designs where resistance is no bigger than the uniform optimal case. Compared with a single point ($\varepsilon = 0.3435$) for the uniform electrode, the design space has been enlarged significantly ($\varepsilon_1 \in (0.31, 0.52)$ and $\varepsilon_2 \in (0.12, 0.36)$) for 2-layer graded electrode, providing greater freedom for other design considerations. It can be

observed that the resistance values get larger for higher porosities, especially for bigger ε_2. The electrode model used only captures the ohmic resistance in the electrolyte and the solid matrix and the charge-transfer resistance associated with the Butler-Volmer kinetics. Since the electronic conductivity in the solid is higher than the ionic conductivity in the electrolyte (see parameters in Table 1), the solid phase is more favorable compared to the electrolyte, thus the optimal porosity (porosities) is smaller than 0.5. The boundary condition at $X = 1$ forces the solid phase to carry all the current, thus lower porosity near the current collector, where the solid phase current is higher, is preferred to reduce the ohmic resistance.

All the results are based on the graded electrode of equally thick sub-layers. Allowing the thickness to vary together with the porosity can further reduce the resistance, but the improvement is not much for this problem. For example, for a 2-layer graded electrode, the minimum resistance with optimal thickness distribution is 5.1019 Ω-cm^2 (62.37% of the total thickness for layer 1 with a porosity of 0.3972 and 37.63% of the total thickness for layer 2 with a porosity of 0.1985). Compared with the minimal resistance of 5.1164 Ω-cm^2 for the equally distributed two sub-layers, the improvement is only 0.3%. Considering that keeping the thickness to be equal in each sublayer would be more practical for manufacturing and to simplify the problem, only the results for equally thick multi-layer graded electrode are shown in this work.

The optimization time for the sequential approach increases dramatically as more layers are used. This is due to the increased number of ODEs required to be solved at each of the porosity combinations. In contrast, the time needed for simultaneous approach did not increase as much, since increasing the number of algebraic equations in the optimization problem does not increase the problem complexity as much, particularly for sparse optimizers. For a graded electrode with

more than 2 layers, Maple's built-in ODE solver "dsolve" does not work properly, so a customized Newton-Raphson solver was used with the collocation approach in x for solving the model.

Comparing the results from the two approaches, the optimal porosity profiles agree very well with each other. As the number of graded layers increases, the disagreement between the two approaches also grows slightly. This probably resulted from the fact that the search space is flat near the optimum, thus there are many combinations of the porosity values that give similar ohmic resistance.

From the perspective of reducing the resistance of the cathode, building graded electrode beyond 2 layers does not help much. Compared with the uniform optimal porosity, the reduction in ohmic resistance for 2-layer, 3-layer, 4-layer, and the 5-layer graded electrode is 4.4%, 5.4%, 5.9%, and 6.1% respectively. The limiting case is a continuously changing porosity distribution, with 5.0034 Ω-cm^2 in resistance, a 6.5% improvement compared with the optimal uniform electrode. Considering the additional processing time and cost for adding layers of different porosities, it is probably not cost-effective to manufacture a graded electrode, especially for more than 2 layers. It is worth pointing out that we did not keep the amount of the active material the same for the graded electrodes in this work. However, the average porosities for 2-layer, 3-layer, 4-layer, and 5-layer graded electrode were 0.3214, 0.3152, 0.3135, and 0.3119 respectively, not far from the uniform optimal porosity 0.3435. With the same active material constraint, the minimal resistances for 2-layer, 3-layer, 4-layer, and 5-layer graded electrode are 5.1300 Ω-cm^2, 5.0976 Ω-cm^2, 5.0823 Ω-cm^2, and 5.0748 Ω-cm^2, which are slightly larger than the previous cases.

If a conclusion was to be made just based on the results so far, it would confirm the conclusion from Dai et al.[32] that graded porosity is not very useful. However, the next section will show the cases where graded design in the electrode is needed.

III.4 Constraints on the State Variables

Uniform Electrode

Apart from the advantage in computational speed, which may not be critical for design since we can afford the time offline, one key advantage of the simultaneous optimization approach is that it allows control of the state variables directly. Owing to the fact that all the variables are discretized before applying the optimizer and that all the discretized numerical values are treated as "control variables", it is easier to give bounds and constraints on the state variables, just as the real control variables. This feature of the simultaneous approach can be very powerful and useful when internal state variables are important. For example, by controlling the overpotential at each internal node points, side reactions can be suppressed, which can be used to improve life performance. In the cases where optimization objective does not improve much compared with the base case (like the graded electrode), we can still use the simultaneous approach to control the state variables for the design.

For this secondary current distribution electrode model, the variable of great interest is the activation overpotential $\eta(X) = \Phi_1(X) - \Phi_2(X)$. $\eta(X)$ is the measure of the interfacial voltage difference above the equilibrium potential, which represents the driving force for lithium intercalation and de-intercalation in the positive electrode. When $\eta(X)$ is larger, the intercalation and the de-intercalation process will be faster according to the Butler-Volmer reaction kinetics, but at the same time, the rate for side reactions also increases. The side reactions are one of the main causes of battery degradation and are strongly dependent on the cell chemistry. For a lithium nickel cobalt oxide cathode, the formation of solid-electrolyte interphase (SEI) layer due to electrolyte oxidation and $LiPF_6$ decomposition accompanied by the evolution of gaseous species are the main concerns.[57] The SEI layer growth in the carbon anode is believed to be responsible

for capacity fade, while the interfacial impedance increase resulted from lithium nickel cobalt oxide cathode expedites power loss, especially at the high end of charge voltages when $\eta(X)$ is large. Generally, a uniform distribution of low $\eta(X)$ values across the electrode is desired to fully utilize the active material while reducing side reactions. To measure the uniformity of $\eta(X)$ values, the standard deviation (SD) was used according to the following equation:

$$s = \sqrt{\frac{\sum_{i=1}^{n} (\eta_i - \bar{\eta})}{n-1}} \qquad \text{(III-5)}$$

where $\bar{\eta}$ is the mean of all the $\eta(X)$ values.

As discussed earlier, to minimize the electrode resistance, an optimal porosity of 0.3435 for uniform electrode was determined. For the optimal uniform electrode, the mean and the standard deviation of η are 6.6834 mV and 2.0914 mV respectively. Thanks to the simultaneous optimization approach, the mean or standard deviation of η can be controlled directly when carrying out the optimization. An example to illustrate the ability to control the standard deviation of the overpotential is given below.

For the uniform electrode, the ohmic resistance of 5.3510 Ω-cm^2 in the optimal case had to increase in order to lower the standard deviation of the overpotential. An inequality constraint on the ohmic resistance

$$\left| \frac{\Phi_1(1) - \Phi_2(0)}{i_{app}} \right| \leq 5.5\ \Omega\text{-}cm^2 \qquad \text{(III-6)}$$

was added to the new optimization formulation to gently relax the constraint on the resistance. The new objective function is

$$\min_{i_1(X),\Phi_1(X),\Phi_2(X),\varepsilon(X)} \varphi = \sqrt{\frac{\sum_{i=1}^{k}(\eta_i - \bar{\eta})}{k-1}} \qquad \text{(III-7)}$$

where k is the number of internal node points (k = 30 was used to ensure convergence). The minimal value of 1.563 mV was achieved where the porosity was 0.4054 and the resistance was at 5.0823 Ω-cm^2. When the constraint on the resistance was completely removed and the only objective was to minimize the standard deviation of the overpotential, the minimal standard deviation of 0.7009 mV could be achieved. In that case, the porosity was 0.5529 and the resistance was 7.4563 Ω-cm^2. The plots for the internal variables of the aforementioned three cases are shown in Fig. 5. Compared with the minimal resistance case, to minimize the overpotential variance, the solid phase current was reduced in absolute value. Since more current was forced through the electrolyte, higher porosity is favored to lower the potential increase in the electrolyte. The slope of the solid phase current was increased in the two cases for overpotential standard deviation minimization. According to the Butler-Volmer equation, as the slope $\frac{-di_1(X)}{dX}$ increases, the overpotential also increases, which corresponds to higher curves in Fig. 5(d) when the standard deviation is smaller.

With this optimization framework, a desired resistance value (greater than the minimal resistance) can be guaranteed while optimizing for other design considerations.

Graded Electrode

From the uniform electrode case, it can be seen that there is a trade-off between the resistance and the overpotential variance. To lower the overpotential variance, a compromise on the resistance has to be made. This is where the graded electrode can come into play. With a greater search space as shown the shaded area in Fig. 4, it is likely that a smaller overpotential variance can be achieved without sacrificing the resistance.

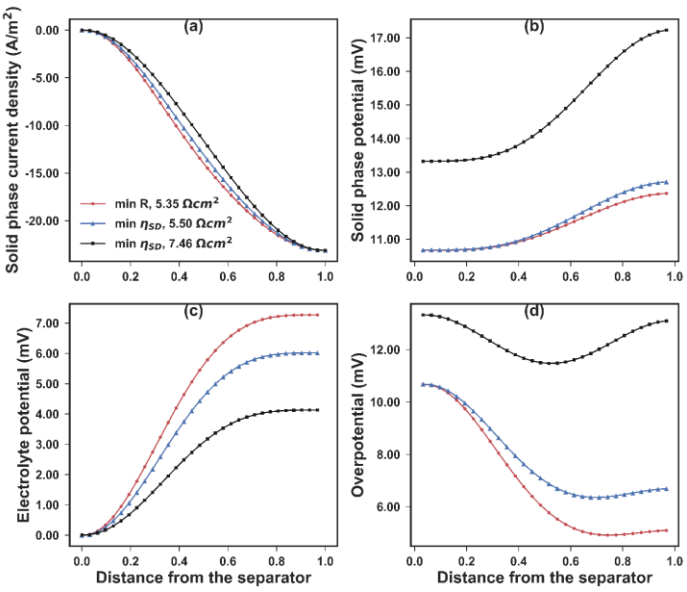

Figure III-3 The internal profiles of (a) the solid phase current density, (b) the solid phase potential, (c) the electrolyte potential, and (d) the activation overpotential for three uniform electrode optimizations.

In case 1 (red dots), the only objective is to minimize the overall resistance, and the minimal resistance is 5.3510 Ω-cm^2. In case 2 (blue triangles), the main objective is to minimize the standard deviation of the overpotential, with a constraint that the overall resistance is no larger than 5.5000 Ω-cm^2. In case 3 (black squares), the only objective is to minimize the standard deviation of the overpotential. The electrode resistance is evaluated at 7.4563 Ω-cm^2 for this case. These optimizations show the ability to control the profile of the internal state variables. off between the electrode resistance and the overpotential variance seem to exist.

The constraint

$$\left|\frac{\Phi_1(1)-\Phi_2(0)}{i_{app}}\right| \le 5.3510\ \Omega cm^2 \qquad \text{(III-8)}$$

was added to the graded electrode optimization problem, where 5.3510 Ω-cm^2 is the minimum resistance for the uniform case. This constraint can ensure that the resistance of the multi-layer graded electrode does not increase compared to the best uniform case. The hypothesis that by employing graded electrode the overpotential variance can be reduced without incrementing the electrode resistance was conformed. The state variables for the optimal cases with 2 to 5 sub-layers are plotted in Fig. 5 together with the optimal uniform case. All 5 cases have the same electrode resistance of 5.3510 Ω-cm^2. Similarly, the most gain of bringing in the graded electrode design can be obtained with 2 sub-layers. In the limiting case of continuously changing porosity (infinite number of sub-layers), the minimal overpotential deviation with the resistance of 5.3510 Ω-cm^2 around 0.9 mV.

III.5 Multi-objective Optimization using an Evolutionary Algorithm

As discussed earlier, there is a trade-off between minimizing the resistance and reducing the overpotential variance. Furthermore, a conflict in minimizing the overpotential variance and the average overpotential can also be observed. For a complicated electrochemical system like lithium-ion batteries, multiple criteria decision making is often encountered, such as the trade-offs between resistance, overpotential variance, and average overpotential in this electrode model.

The thermal voltage $\frac{k_B T}{e}$, where k_B is the Boltzmann constant ($1.381\times10^{-23}\ m^2 kgs^{-2}K^{-1}$), T is the temperature in Kelvin, and e is the elementary charge ($1.602\times10^{-19}\ C$), is 25.5 mV at room temperature (296.15 K). It should be noted that for the parameter set used in this problem (see Table 1), the average overpotential is in the range of 5 to 30 mV, comparable with the thermal

voltage at room temperature, which suggests that the full Butler-Volmer equation should be used, not the linearized version (for $|\eta| << \frac{k_B T}{e}$) or the Tafel form (for $|\eta| >> \frac{k_B T}{e}$). This is consistent with the discussion earlier that the applied current is comparable to the exchange current.

For this problem, no porosity can simultaneously minimize both the average and the standard deviation of the overpotential, thus this is a non-trivial multi-objective optimization problem. For such a problem, instead of a single solution, a number of nondominated solutions, known as the Pareto-optimal solutions, exist. A solution can be called a Pareto-optimal solution when none of its objective functions can be improved without sacrificing another objective function. Without further information, the Pareto optimal solutions are considered to be equally good.

Various optimization algorithms have been proposed to solve multiobjective optimization problems, including the classical scalar approach of converting the problem into a single-objective problem by giving weights to each objective and the evolutionary vector approach of considering all the objectives simultaneously to find multiple Pareto-optimal solutions. In the previous section for applying constraints on the state variables with the simultaneous approach, the ε-constraint method was used .[58] The ε-constraint method is a classical multi-objective optimization method. It converts the original multi-objective optimization problem into a single objective optimization problem with all the other objectives as constraints. In the previous section, the original optimization problem being minimizing resistance and the overpotential variance at the same time and the problem after applying the ε-constraint method is minimizing the overpotential variance while ensuring the resistance is no larger than a certain number (5.5000 Ω-cm^2 for the uniform electrode and 5.3510 Ω-cm^2 for 2-layer graded electrode). The limitation of the ε-constraint method is that the user has to prioritize the objectives and provide the values for the constraints, and only a single solution can be found. Alternatively, the evolutionary algorithms can be used to

keep all the objectives without prioritizing and search for multiple Pareto-optimal solutions. Moreover, evolutionary approaches can provide dense Pareto solutions in single optimization run as opposed to multiple runs required in case of single objective based approaches. Due to the iterative nature of the evolutionary algorithms, they can only be used with the sequential approach.

Considering its fast speed and proven accuracy, the improved nondominated sorting genetic algorithm (NSGA-II), one of the most widely used multi-objective optimization algorithm was chosen for this study.[59] The objective functions were minimizing the average and the standard deviation of the overpotential, while the resistance was reserved as the higher-level information to made the final decision among all the Pareto-optimal solutions. The 100 nondominated Pareto-optimal solutions found for the uniform and 2-layer graded electrode by NSGA-II are plotted in Fig. 6 (objection onto the x-y plane) to form the Pareto front. The area above the Pareto-front is the feasible region for the two objectives. It can be seen that by introducing the 2-layer graded electrode, the Pareto-front has been pushed downwards, resulting in a larger feasible region for the design. The corresponding porosities of the Pareto front range from 0.1401 to 0.5529 for the uniform electrode. For the 2-

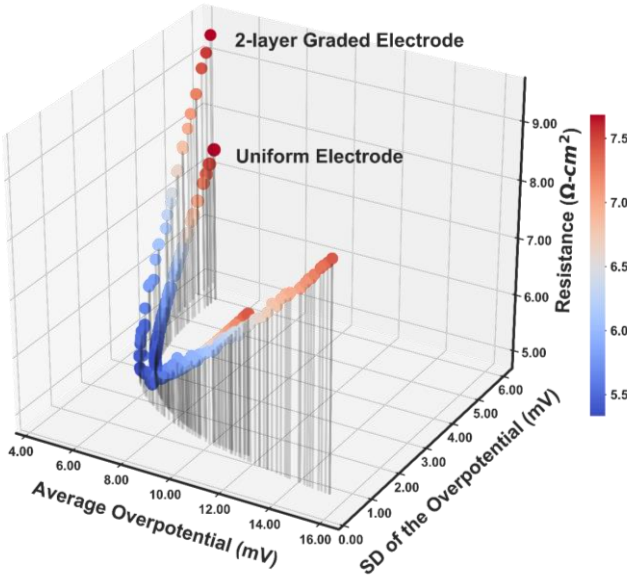

Figure III-4 The corresponding resistance values for the Pareto-optimal solutions from minimizing both the average and the standard deviation of the overpotential.

The resistance is used to help pick the best solution among the Pareto-optimal solutions, which are considered equally good for minimizing both the average and the standard deviation of the overpotential.

layer graded electrode, the porosity of the layer next to the separator varies from 0.1000 to 0.7000, while the porosity of the other layer changes from 0.1120 to 0.5228 for the Pareto-optimal solutions. It is impossible to tell which solutions are better than others when only the average and standard deviation of the overpotential are taken into consideration. Fortunately, in this case, there is a third criterion, resistance, to help with the final decision-making. The ohmic resistance values for the 100 solutions for the uniform and 2-layer graded electrode were computed respectively and are plotted against the average and the standard deviation of the overpotential, shown in Fig. 6. Among the 100 Pareto-optimal solutions, the resistances vary from 5.3345 Ω-cm^2 to 7.6832 Ω-cm^2 for the uniform electrode and 5.2200 Ω-cm^2 to 9.4046 Ω-cm^2 for the 2-layer graded electrode. The solution with the minimum resistance is considered the best among the Pareto-optimal solutions for the balance between the internal resistance, the average and the standard deviation of the overpotential. For the uniform electrode, the optimal porosity obtained is 0.3460, with an average overpotential of 6.6693 mV and a standard deviation of the overpotential of 2.1013 mV. For the 2-layer graded electrode, the optimal porosities are 0.3416 in the layer near the separator and 0.2821 in the layer near the separator. The average overpotential for the 2-layer optimal electrode is 6.074 mV and the standard deviation of the overpotential is 2.046 mV. Compared with the uniform optimal case, all three objectives are smaller for the 2-layer optimal graded electrode due to the extra search space available.

Chapter IV. Expanding to the Pseudo-2-Dimentional Model

IV.1 The P2D Model

Unlike the electrode model in Chapter II, where only the positive electrode is modeled, the Pseudo-2-Dimentional (P2D) model takes the whole cell sandwich into consideration, as shown in Figure IV-1. The *x*-direction is still the direction of interest in this model, where *x=0* is the interface between the current collector and the negative electrode and $x= l_n + l_s + l_p$ being the positive electrode-current collector interface. The first and third assumptions (1-D, no double-layer effects) we made for the electrode model still hold, while the concentration gradients in the system and dependency of electrode equilibrium potential on lithium-ion concentration are included in the P2D model.

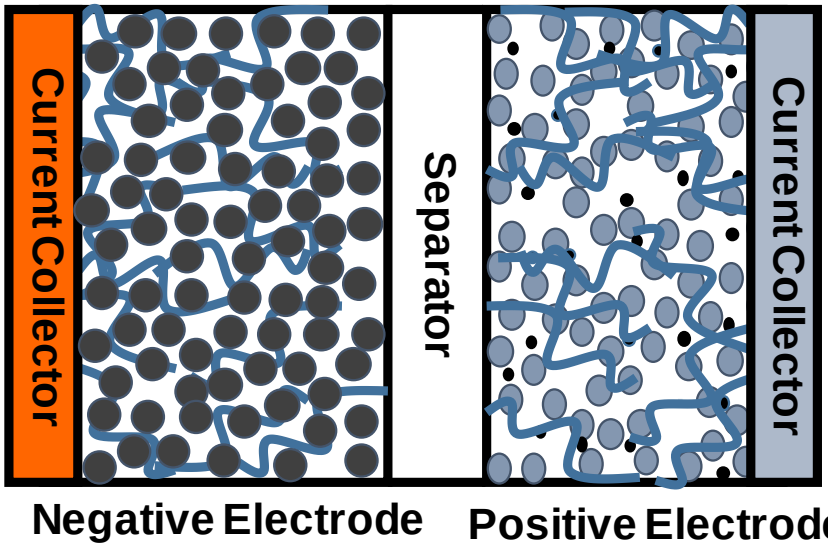

Figure IV-1 Schematic of the lithium-ion battery sandwich being modeled in the P2D model. x=0 (X=0 after nondimensionalization) represents the boundary between the separator and the anode, and x=ln+ls+lp (X=1) refers to the interface between the cathode and the current collector.

The P2D model considers lithium ion concentration, potential, and current in both the solid phase and the electrolyte, which is a more complicated thus more accurate battery model. Applying the simultaneous approach to such a system is extremely challenging. Firstly, since additional

variables like concentration are included in the model, the number of design variables will be increased dramatically. Secondly, the number of governing equations also becomes larger. Furthermore, as a consequence of including the transient behaviors, the time-dependent state variables need to be discretized both in time and in space, which will shoot up the number of final "control variables" for the optimizer thereby making it a huge challenge to solve such problems. The governing equations for such a model is listed in the table below[7].

Table IV-1 Governing Equations of the P2D Model

Governing Equations	Boundary Conditions
Negative Electrode	
$\frac{\partial \varepsilon_n c}{\partial t} = \frac{\partial}{\partial x}\left(D_{eff,n} \frac{\partial c}{\partial x} \right) + a_n \left(1 - t_+\right) j_n$	$-D_{eff,n} \left.\frac{\partial c}{\partial x}\right\|_{x=0} = 0$
	$-D_{eff,n} \left.\frac{\partial c}{\partial x}\right\|_{x=l_n^-} = -D_{eff,s} \left.\frac{\partial c}{\partial x}\right\|_{x=l_n^-}$
$-\sigma_{eff,n} \frac{\partial \Phi_1}{\partial x} - \kappa_{eff,n} \frac{\partial \Phi_2}{\partial x} + \frac{2\kappa_{eff,n} RT}{F}\left(1 - t_+\right) \frac{\partial \ln c}{\partial x} = I_{app}$	$-\kappa_{eff,n} \left.\frac{\partial \Phi_2}{\partial x}\right\|_{x=0} = 0$
	$-\kappa_{eff,n} \left.\frac{\partial \Phi_2}{\partial x}\right\|_{x=l_n^-} = -\kappa_{eff,s} \left.\frac{\partial \Phi_2}{\partial x}\right\|_{x=l_n^+}$
$\frac{\partial}{\partial x}\left(\sigma_{eff,n} \frac{\partial}{\partial x} \Phi_1 \right) = a_n F j_n$	$\Phi_1\|_{x=0} = 0$
	$-\sigma_{eff,n} \left.\frac{\partial \Phi_1}{\partial x}\right\|_{x=l_n^-} = 0$
$\frac{\partial}{\partial t} c_n^s = \frac{1}{r^2} \frac{\partial}{\partial r}\left(D_n^s r^2 \frac{\partial c_n^s}{\partial r} \right)$	$-D_n^s \left.\frac{\partial c_n^s}{\partial r}\right\|_{r=0} = 0$
	$-D_n^s \left.\frac{\partial c_n^s}{\partial r}\right\|_{r=R_n} = j_n$
Separator	
$\frac{\partial \varepsilon_s c}{\partial t} = \frac{\partial}{\partial x}\left(D_{eff,s} \frac{\partial c}{\partial x} \right)$	$c\|_{x=l_n^-} = c\|_{x=l_n^+}$
	$c\|_{x=l_n+l_s^-} = c\|_{x=l_n+l_s^+}$
$-\kappa_{eff,s} \frac{\partial \Phi_2}{\partial x} + \frac{2\kappa_{eff,s} RT}{F}\left(1 - t_+\right) \frac{\partial \ln c}{\partial x} = I_{app}$	$\Phi_2\|_{x=l_n^-} = \Phi_2\|_{x=l_n^+}$
	$\Phi_2\|_{x=l_n+l_s^-} = \Phi_2\|_{x=l_n+l_s^+}$
Positive Electrode	

$$\frac{\partial \varepsilon_p c}{\partial t} = \frac{\partial}{\partial x}\left(D_{eff,p} \frac{\partial c}{\partial x} \right) + a_p (1 - t_+) j_p$$

$$-D_{eff,s} \left.\frac{\partial c}{\partial x}\right|_{x=l_n+l_s^-} = -D_{eff,p} \left.\frac{\partial c}{\partial x}\right|_{x=l_n+l_s^+}$$

$$-D_{eff,p} \left.\frac{\partial c}{\partial x}\right|_{x=l_n+l_s+l_p} = 0$$

$$-\sigma_{eff,p} \frac{\partial \Phi_1}{\partial x} - \kappa_{eff,p} \frac{\partial \Phi_2}{\partial x} + \frac{2\kappa_{eff,p} RT}{F}(1 - t_+) \frac{\partial \ln c}{\partial x} = I_{app}$$

$$-\kappa_{eff,s} \left.\frac{\partial \Phi_2}{\partial x}\right|_{x=1_n+1_s^-} = -\kappa_{eff,p} \left.\frac{\partial \Phi_2}{\partial x}\right|_{x=1_n+1_s^+}$$

$$-\kappa_{eff,p} \left.\frac{\partial \Phi_2}{\partial x}\right|_{x=1_n+1_s+1_p} = 0$$

$$\frac{\partial}{\partial x}\left(\sigma_{eff,p} \frac{\partial \Phi_1}{\partial x} \right) = a_p F j_p$$

$$\left.\frac{\partial \Phi_1}{\partial x}\right|_{x=l_n+l_s^-} = 0$$

$$-\sigma_{eff,n} \left.\frac{\partial \Phi_1}{\partial x}\right|_{x=l_p+l_s+l_n} = I_{app}$$

$$\frac{\partial c_p^s}{\partial t} = \frac{1}{r^2} \frac{\partial}{\partial r}\left(D_p^s r^2 \frac{\partial c_p^s}{\partial r} \right)$$

$$-D_p^s \left.\frac{\partial c_p^s}{\partial r}\right|_{r=0} = 0$$

$$-D_p^s \left.\frac{\partial c_p^s}{\partial r}\right|_{r=R_p} = j_p$$

Additional Expressions

$$U_n = f(\theta_n),\ U_p = f(\theta_p);\ \theta_n = \frac{c_n^s|_{r=R_n}}{c_{n,\max}^s},\ \theta_p = \frac{c_p^s|_{r=R_p}}{c_{p,\max}^s}$$

$$j_p = k_p c^{0.5} \left(c_p^s|_{r=R_p} \right)^{0.5} \left(c_{p,\max}^s - c_p^s|_{r=R_p} \right)^{0.5} \left[\exp\left(\frac{\alpha_a F(\Phi_1 - \Phi_2 - U_p)}{RT} \right) - \exp\left(\frac{\alpha_c F(\Phi_1 - \Phi_2 - U_p)}{RT} \right) \right]$$

$$j_n = k_n c^{0.5} \left(c_n^s|_{r=Rn} \right)^{0.5} \left(c_{n,\max}^s - c_n^s|_{r=R_n} \right)^{0.5} \left[\exp\left(\frac{\alpha_a F(\Phi_1 - \Phi_2 - U_n)}{RT} \right) - \exp\left(\frac{\alpha_c F(\Phi_1 - \Phi_2 - U_n)}{RT} \right) \right]$$

$$\kappa_{eff,i} = \varepsilon_i^{brugg_i} f(c),\ i = n, s, p$$

$$D_{eff,i} = D \cdot \varepsilon_i^{brugg_i},\ i = n, s, p$$

$$\sigma_{eff,i} = \sigma_i \left(1 - \varepsilon_i - \varepsilon_{f,i} \right)^{\alpha_i},\ i = n, p$$

$$a_i = \frac{3}{R_i}(1 - \varepsilon_i - \varepsilon_{f,i}),\ i = n, s, p$$

Nomenclature

Symbol	Variables	Units

c	Concentration of lithium ion in the electrolyte	mol/m^3
c_i^s	Concentration of lithium ion in solid	mol/m^3
Φ_1	Solid phase potential	V
Φ_2	Electrolyte potential	V
$c^{s,surf}$	Solid phase concentration at surface	mol/m^3
$c^{s,ave}$	Average solid phase concentration	mol/m^3
I	Applied current density	A/m^2
U_i	Open circuit potential at positive $(i = p)$ and negative $(i = n)$	V
j_i	Pore wall flux at positive $(i = p)$ and negative $(i = n)$	mol/m^2/s
$\kappa_{eff,i}$	Liquid phase conductivity at positive $(i = p)$, separator $(i = s)$, and negative $(i = n)$	S/m
$D_{eff,i}$	Effective diffusion coefficient conductivity at positive $(i = p)$, separator $(i = s)$, and negative $(i = n)$	m^2/s
$\sigma_{eff,i}$	Effective solid phase conductivity at positive $(i = p)$ and negative $(i = n)$	S/m
θ_i	State of charge at positive $(i = p)$ and negative $(i = n)$	-
j_{SEI}	Flux associated with SEI layer growth	mol/m^2/s
c_{sol}	Concentration of solvent at anode surface	mol/m^3
c_{Li^+}	Concentration of electrolyte at anode surface	mol/m^3
δ	SEI layer thickness	m

Building on the reformulated P2D model developed by the Subramanian group[30], a model adapted for electrode design has been developed. The effect of electrode thickness has been studied on the full cell level as a trial of simulating different design parameters using the P2D model.

As can be seen from Figure IV-2, when the thickness of the positive electrode doubled from 66μm to 132μm, the discharge time was increased from 3637s to 5241s under the same constant current discharge conditions, suggesting 44% of increase in capacity. One of the drawbacks of thick electrode is longer mass transport passage, and the graded electrode design can help improve the mass transport. To conduct design optimization of graded electrode, the first step is to do simulation of batteries with multi-layer electrodes.

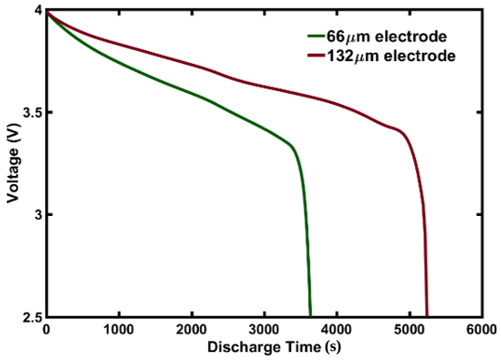

Figure IV-2 Discharge profiles of battery cells with thick (red) or regular (green) cathode

IV.2 Multi-layer Graded Electrode Simulation using the P2D Model

Similarly to the multi-layer graded electrode design with the electrode model, the way to model a multi-layer graded electrode structure with the P2D model is to model each layer as an additional positive electrode. For each layer, the equations for the positive electrode in Table IV-1 will be repeated, with continuity of the value and flux for lithium-ion concentration, solid-phase potential, and electrolyte potential across layers as additional boundary conditions. To test out the feasibility of multi-layer graded electrode simulation with the P2D model, 2-layer graded electrode simulation was performed using the in-built DAE solver, doslve in Maple. Preliminary comparison between the uniform and the graded electrode of normal thicknesses are shown in Figure IV-3. The blue line represents the discharge performance of uniform cathode of 80 microns with the porosity of 0.385,

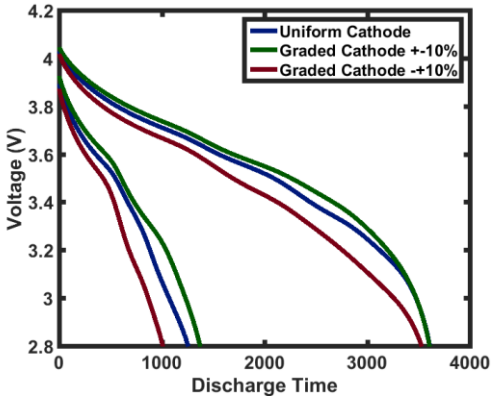

Figure IV-3 Discharge performance at 1C for uniform (0.385) and 2-layer graded electrode (+- / -+10%)

while the green and red curves represent the same cathode with porosities of +- and -+10% of 0.385. From the simulation, it can be observed that graded electrode design can improve energy performance of a lithium-ion battery. A higher porosity near the separator and lower porosity near the current collector is favored for higher cell energy. This preliminary result shows that there is some benefit for conducting the graded electrode design, which encouraged us to further explore the idea.

IV.3 Collocation in Time for the P2D Model

Compared to the electrode model discussed in Chapter II, the P2D model is a more complicated model because it considers the time dependency of the variables in addition to the space dependency. Since this is a dynamic model, dynamic optimization is required to solve for the optimal porosity profiles. A general dynamic optimization can be expressed mathematically as follows:

$$\min_{\mathbf{z}(t),\mathbf{y}(t),\mathbf{u}(t),\mathbf{p}} \varphi(z(t_f))$$

$$s.t.\ DAE\ problem$$

$$\frac{dz(t)}{dt} = F(\mathbf{z}(t),\mathbf{y}(t),\mathbf{u}(t),t,\mathbf{p}),$$

$$G(\mathbf{z}(t),\mathbf{y}(t),\mathbf{u}(t),t,\mathbf{p}) = 0$$

with initial conditions: $\mathbf{z}(t_0) = \mathbf{z}_0$

subject to bounds:

$$\mathbf{z}^L \le \mathbf{z}(t) \le \mathbf{z}^U,\ \mathbf{y}^L \le \mathbf{y}(t) \le \mathbf{y}^U,\ \mathbf{u}^L \le \mathbf{u}(t) \le \mathbf{u}^U,\ \mathbf{p}^L \le \mathbf{p} \le \mathbf{p}^U$$

where

ϕ	Objective function
F	Differential equation constraints
G	Algebraic equation constraints
z	Vector of differential state variables
y	Vector of algebraic state variables
u	Vector of control variables
p	constant parameters

To solve a dynamic optimization problem expressed by a system of differential algebraic equations (DAEs), different methods and approaches can be used, as shown in Figure IV-4[60,61]. Due to the ease of control over path constraints and the ability to avoid infeasible intermediate solutions, we focused on the simultaneous approach for this work.

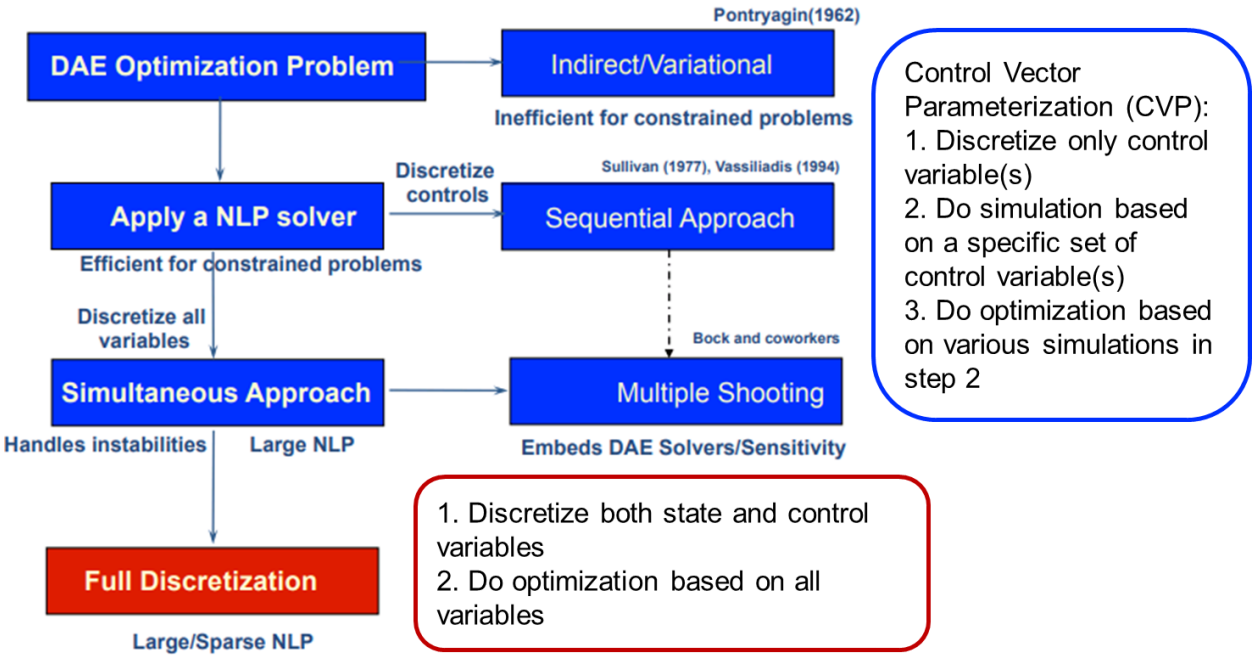

Figure IV-4 Different approaches for dynamic optimization problems expressed by DAEs

In order to apply the SOCOLL method introduced in Chapter III, an effective discretization scheme in time is required in addition to space. Inspired by the collocation method in space demonstrated in Chapter III, we explored applying a similar orthogonal collocation on finite elements method (OCFE) based on orthogonal polynomials to time for battery modeling applications. This method allows the solver to evaluate variables at specified times. OCFE divides the whole time horizon into finite elements, then set the equation residuals to zero at each collocation points within every element as demonstrated in

. Commonly used polynomials include Lagrange polynomials[56], Legendre polynomials, Chebyshev polynomials, and Jacobi polynomials. The collocation points can be determined by Gaussian quadrature, Lobatto quadrature, Radau collocation, and so on.[62]

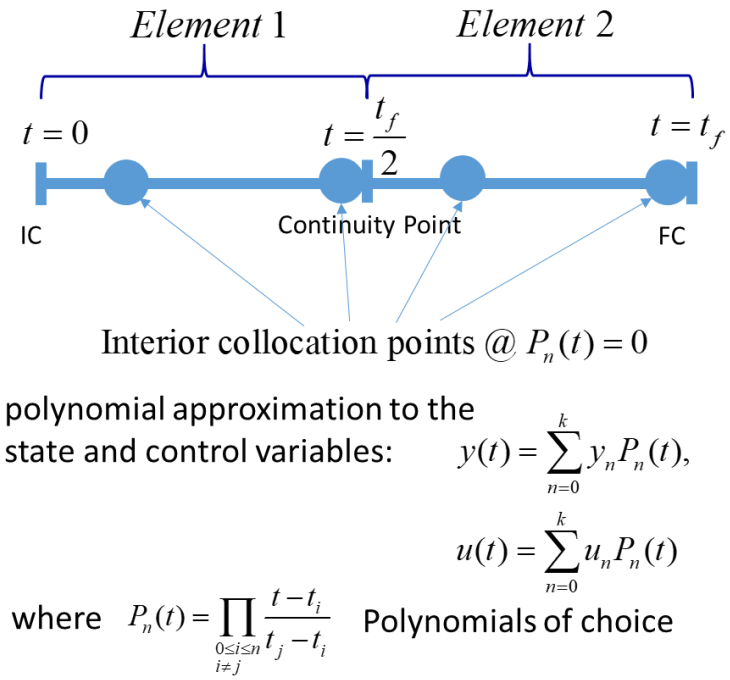

Figure IV-5 Schematic of the orthogonal collocation on finite element discretization scheme

We tried Gauss collocation, Radau collocation, and Chebyshev polynomials, and found that Radau collocation works best for the P2D model because it includes the end value of each element as a collocation point, which helps to stabilize the system more efficiently, especially for high index DAEs[61].

The differential variables are approximated by monomial basis representation:

$$z(t) = z_{i-1} + h_i \sum_{q=1}^{K} \Omega_q \left(\frac{t - t_{i-1}}{h_i} \right) \frac{dz}{dt_{i,q}} \qquad \text{(IV-1)}$$

Where z_{i-1} is the value at the beginning of the i^{th} element, h_i is the duration of the i^{th} element, q is the numbering of the collocation points, and Ω_q is a polynomial of order K (eg. Lagrange

polynomials), where $\begin{cases}\Omega_q(0)=0 \quad for\ q=1,...,K \\ \Omega_q^{'}(\rho_r)=\delta_{q,r} \quad for\ q,r=1,...,K\end{cases}$, ρ_r is the r^{th} collocation point with each element. Continuity between the elements can be set as $z_i = z_{i-1} + h_i \sum_{q=1}^{K} \Omega_q(1) \frac{dz}{dt_{i,q}}$.

The algebraic variables can be written with the Lagrange polynomials as:

$$y(t) = \sum_{q=1}^{K} \psi_q \left(\frac{t - t_{i-1}}{h_i}\right) y_{i,q} \qquad \text{(IV-2)}$$

for the q^{th} collocation point in the i^{th} element, where ψ_q is the Lagrange polynomial of degree K satisfying $\psi_q(\rho_r) = \delta_{q,r} \quad for\ q,r = 1,...,K$.

Convergence test in space

For discretization in space, coordinate transformation was used with and model reformulation following the previous work published by our group.[30] OCFE was used with Gauss collocation points. In order to determine how many elements are needed for 2nd order Gauss collocation, simulation with different number of elements in all three regions (anode, separator, cathode) was performed. To benchmark the converngence performance in space, the standard ordinary differential equation solver "dsolve" in Maple was used in time. The simulation results for model variables electrolyte concentration, electrolyte potential, electrode potential, and interfacial overpotential at the end of discharge and at the cathode-current collector interface are shown in Figure IV-6-9. From these plots, it can be observed that concentration profiles are harder to capture compared to the potential profiles and 3 elements with 2^{nd} order polynomial in each region is enough to get the majority of the variable profiles. For the following study, 3 elements with 2^{nd} order polynomial was used in spatial discretization.

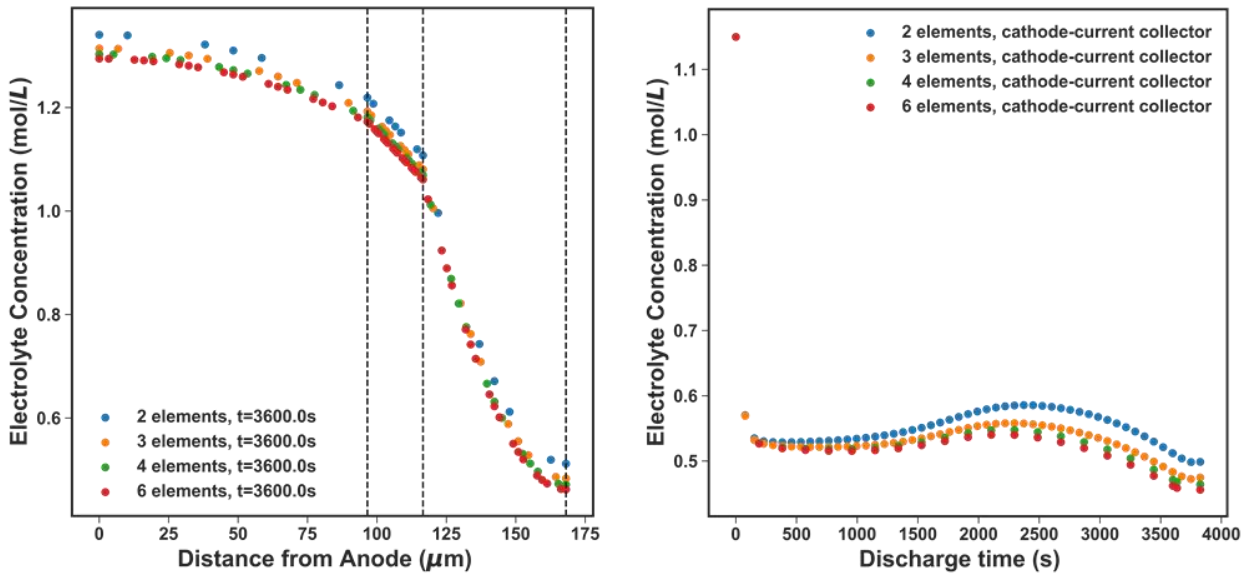

Figure IV-6 Convergence plots for electrolyte concentration using 2-6 elements in each region

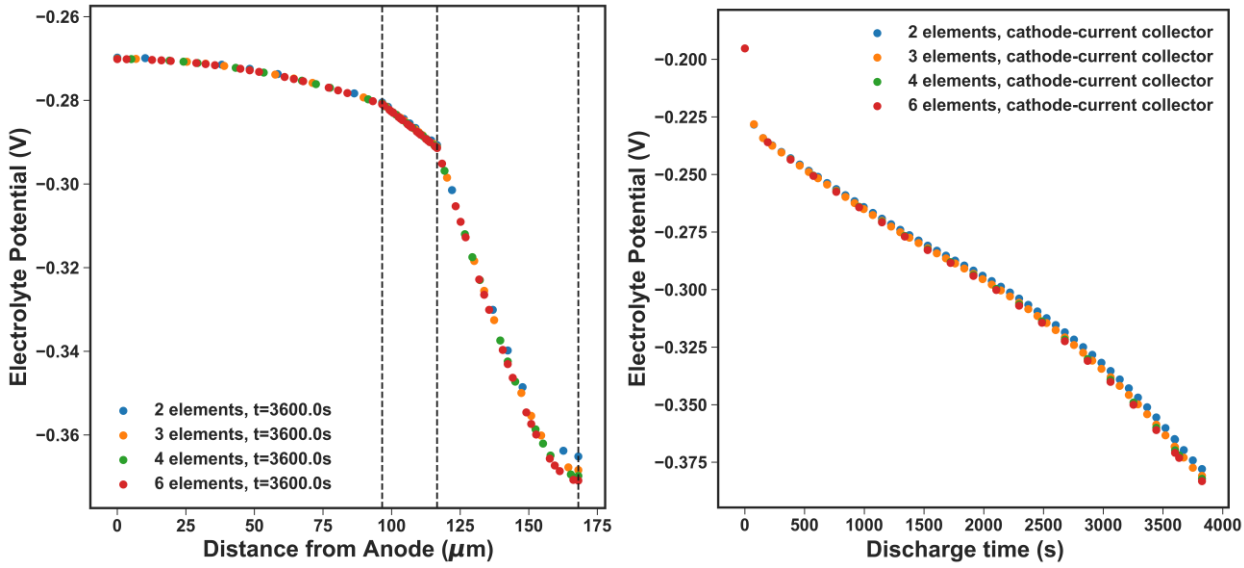

Figure IV-7 Convergence plots for electrolyte potential using 2-6 elements in each region

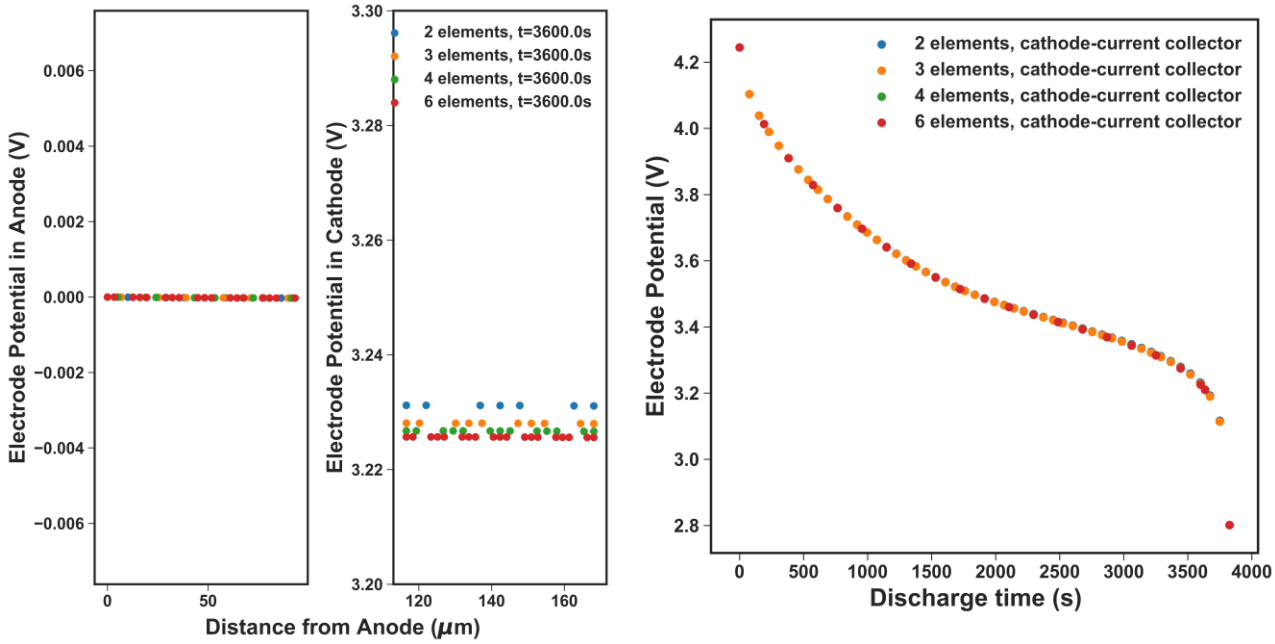

Figure IV-8 Convergence plots for electrode potential using 2-6 elements in each region

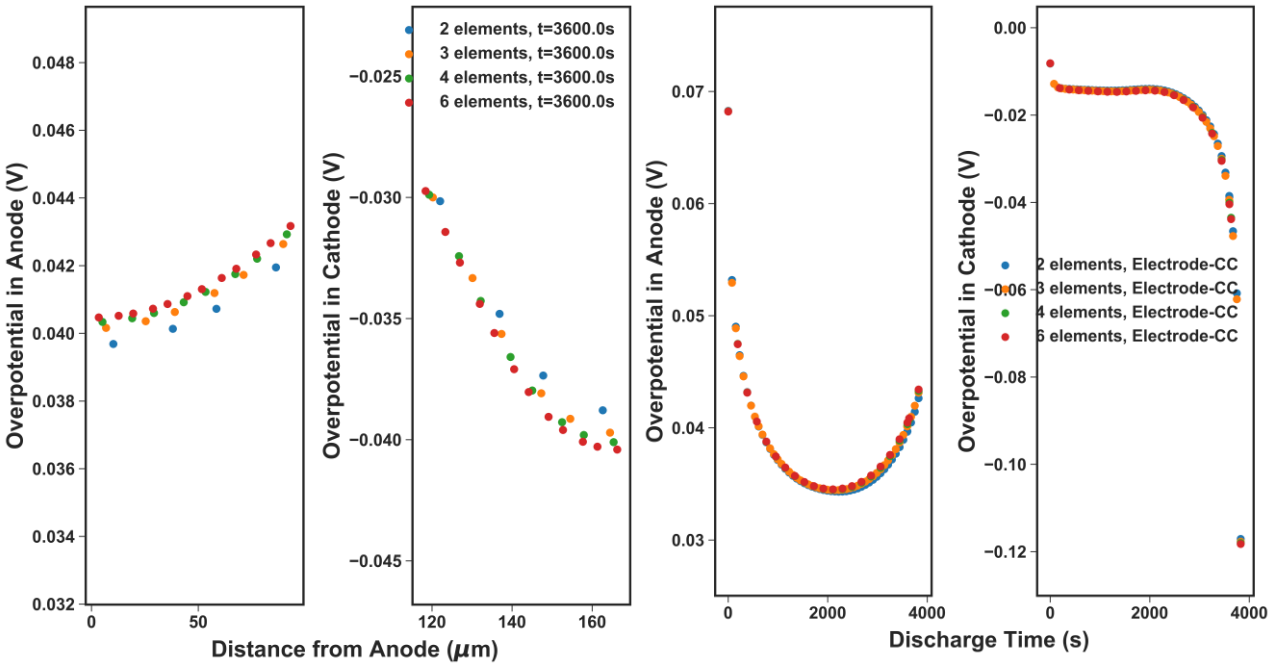

Figure IV-9 Convergence plots for electrode overpotential using 2-6 elements in each region

Convergence test in time

To test the convergence in time, different number of elements and different element placement was tested with 3 elements in space as determined previously. The different element placement was tested because for a typical lithium-ion battery, the concentration and voltage profiles change more drastically at the beginning and end of a charge/discharge, thus using more elements there can effectively improve the simulation efficiency. Therefore, we separated the time horizon into three parts: beginning, middle and end phases of the charge/discharge, and allocated different number of elements in each phase. As a base case, we tried dividing the time horizon into ¼, ½, and ¼ of the total discharge time. The discharge profiles are plotted in Figure IV-10 (first three dotted lines), where the first three numbers in the legend represent the number of elements. The discharge profile simulated with dsolve, the standard ODE solver in Maple is plotted as a benchmark (solid line). We also experimented with different length of the three phases. The following dotted lines in Figure IV-10 have two more numbers in the legend after the underscore, representing the location of the start of a new phase. For example, "412_88" means we used 4, 1, and 2 elements at 1/8, ¾, and 1/8 of the total discharge process. We can observe from the discharge curve that it is not very sensitive to how many elements and where they are allocated; a small number of elements is good enough to capture the shape and trend of the discharge curve. If we only care about the discharge energy or capacity, then only a small number of elements is required when using OCFE.

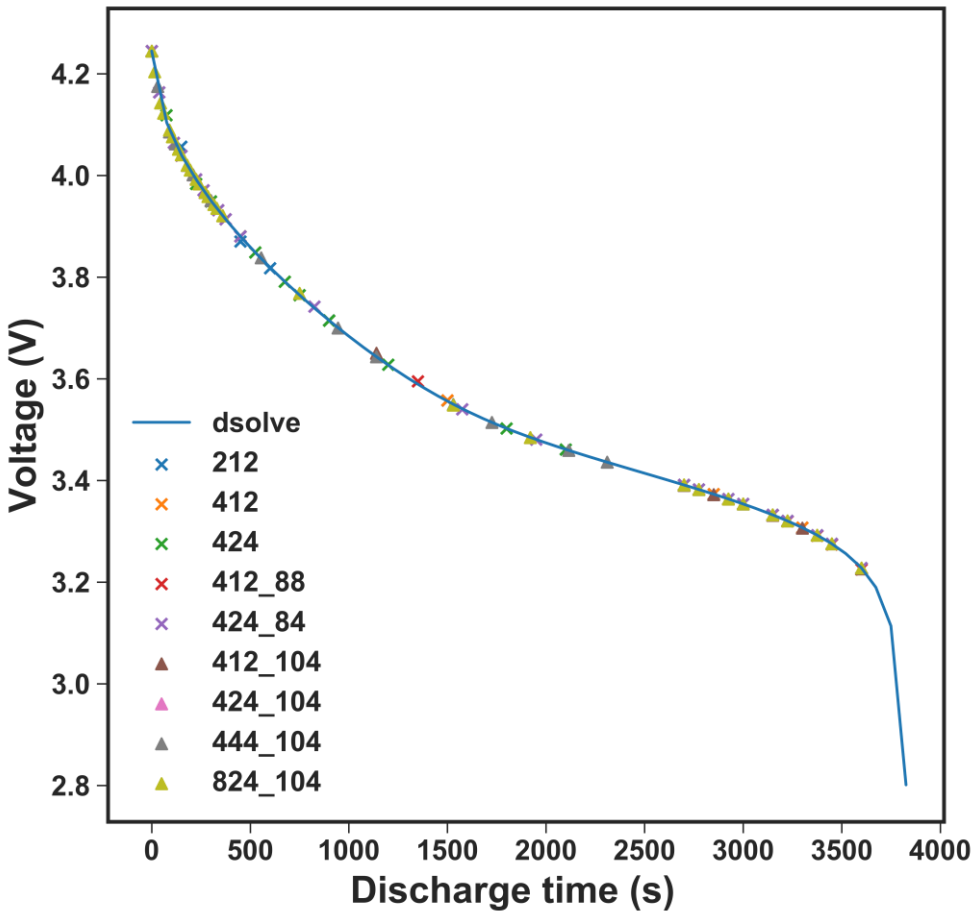

Figure IV-10 Discharge curve with varying number of collocation points in time

We then looked at other variables in the system, and see how sensitive they are to the number of time elements and their locations. The results are shown in the following plots. Figure IV-11 shows the end of discharge concentration profile. Similar to the convergence test performed on spatial variables, concentration profile is the most sensitive one about how many elements we put in the time horizon, so the concentration profile is shown here to represent all the variable profiles at the end of discharge. From the plot, it can be observed that the end of discharge profile can be well represented by using a small number of elements in time. If we only care about the end of discharge properties, then using a reasonable number of elements to improve computation efficiency is sufficient.

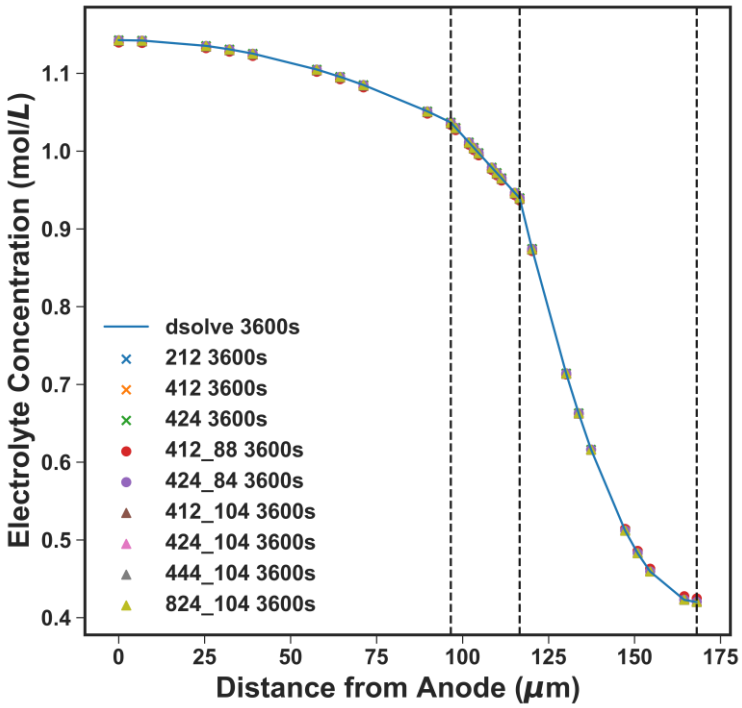

Figure IV-11 End of discharge electrolyte concentration profile with varying time collocation points

We then looked at the variable profiles over time as shown below. For concentration profiles in Figure IV-12, it can be seen clearly that the start of discharge concentration in short time is the most difficult to capture. Shorten the start of discharge phase to 1/8 or even 1/10 of the total discharge time (one hour) helps with the convergence. Another variable that requires a certain number of elements to converge is the overpotential deviation, plotted in Figure IV-13. Because this is a secondary variable derived from the overpotential distribution and because of its small value, overpotential deviation requires a large number of elements throughout the discharge process to be captured precisely. This is not a good variable to design around with the OCFE simultaneous optimization approach.

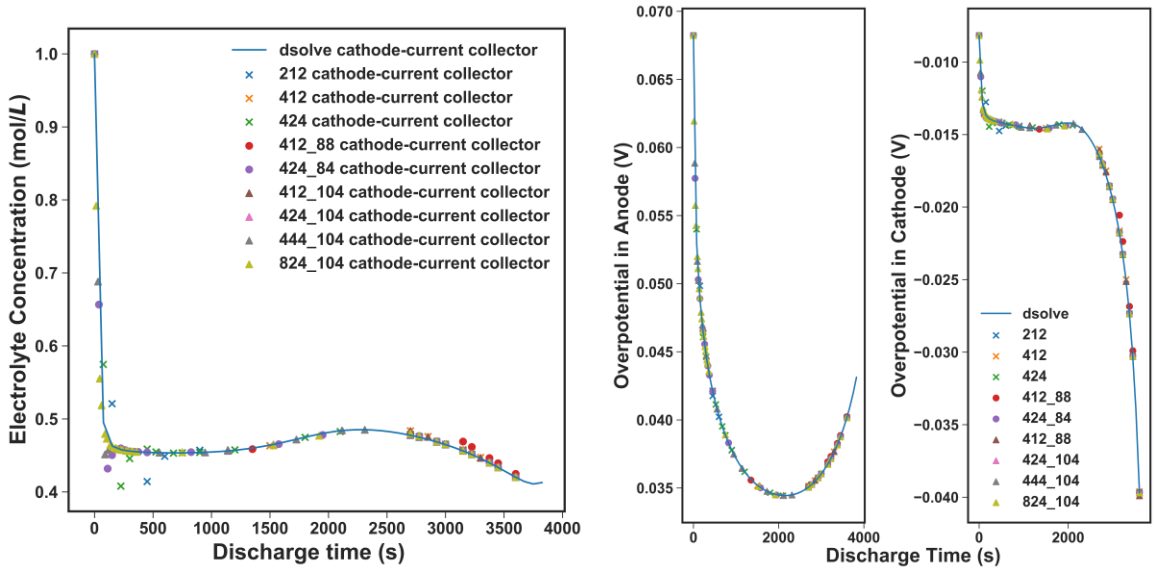

Figure IV-12 Electrolyte concentration and electrode ovrpotential change over discharge time

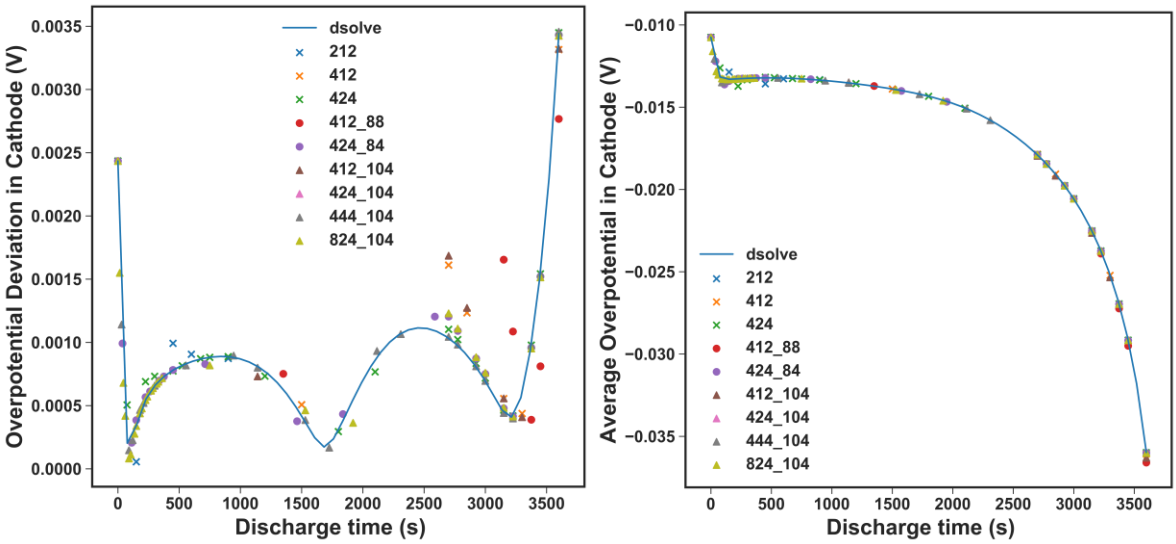

Figure IV-13 Average and distribution of overpotential in the positive electrode over time

IV.4 Design Optimization with the P2D Model

After successfully validated the OCFE approach in time, we then attempted to apply OCFE to both spatial and temporal variables to perform simultaneous optimization on graded electrode design. The objective is to maximize the total discharge energy for a fixed amount of active material by changing the porosity thus active material distribution in the cathode. The approach is as such:

1. Pick the values for values for cathode thickness, discharge time, anode/cathode ratio, and other model parameters based on literature, excluding cathode porosity, anode thickness, and applied current
2. Conduct uniform electrode optimization to determine the cathode porosity (thus determine the total amount of active material in cathode), anode thickness (determined by anode/cathode ratio), and applied current (determined by discharge time)
3. Run multi-layer electrode optimization with determined average porosity, anode thickness, and applied current from step 2

One additional advantage of using the simultaneous approach for battery modeling is that it eliminates the need to check the discharge time requirement. Figure IV-14 is taken from Dai et. al[32]. and represents a typical work flow for battery design using the sequential approach. There are two nested loops. The inner loop is used to determine the applied current needed to meet the discharge time requirement for a specific set of design parameters. The outer loop is then used to find the optimal set of parameters that optimizes the design objective. On the contrary, simultaneous approach with OCFE has the discharge time constraint built-in and includes the applied current as a control variable, therefore completely eliminate the need to do the inner and loop. Due to the

nature of simultaneous approach, all variables are discretized and the integration only happens once at the optimum, which further improves the optimization efficiency by eliminating the outer loop.

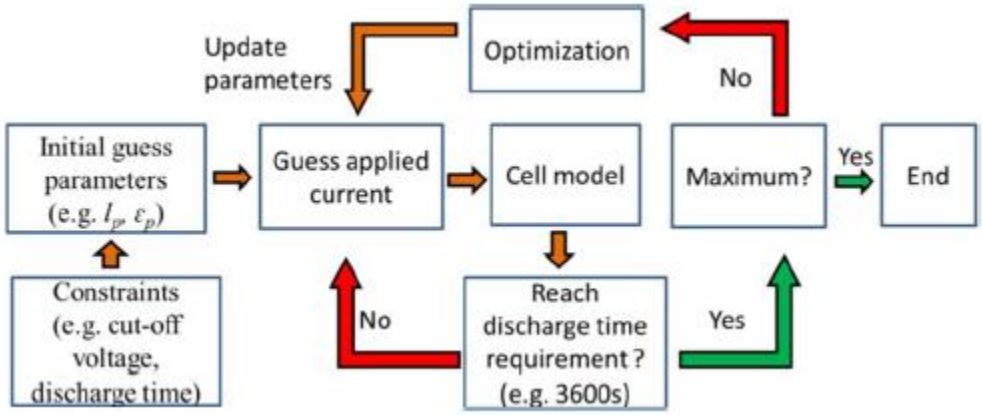

Figure IV-14 Flow chart of discharge optimization using sequential approach

The optimization results for a uniform electrode and a 2-layer and a 3-layer graded cathode are plotted in Figure IV-15 and Figure IV-16. From these two plots, it can be seen that by changing the active material distribution in cathode, the internal variable profiles can be modified. From the concentration profile, it can be observed clearly that graded electrode design with multiple layers can facilitate the mass transfer in the electrode and increase the electrolyte concentration in the cathode. Similar to the results that we have seen earlier in Chapter III, the biggest improvement can be achieved by dividing the whole electrode into two layers. The graded electrode design also has an effect on the overpotential profile in the two electrodes as shown in Figure IV-16. The overpotentials in both electrodes are increased when using graded electrode compared to the uniform electrode. For the anode where the overpotential is positive, an increased overpotential suggests a faster reaction rate based on the Butler-Volmer kinetics and it is more likely for other oxidation reactions to happen. Whereas for the cathode where the overpotential is negative, an increased overpotential means a decreased overpotential value in absolute number. This suggests

that it is less likely for other reduction reactions to happen thus could help with side-reaction-related degradation mitigation. Note that this is a discharge process and most of the electrochemical-related side reactions like lithium plating and solid-electrolyte interface growth happen on the anode during charging.[63]

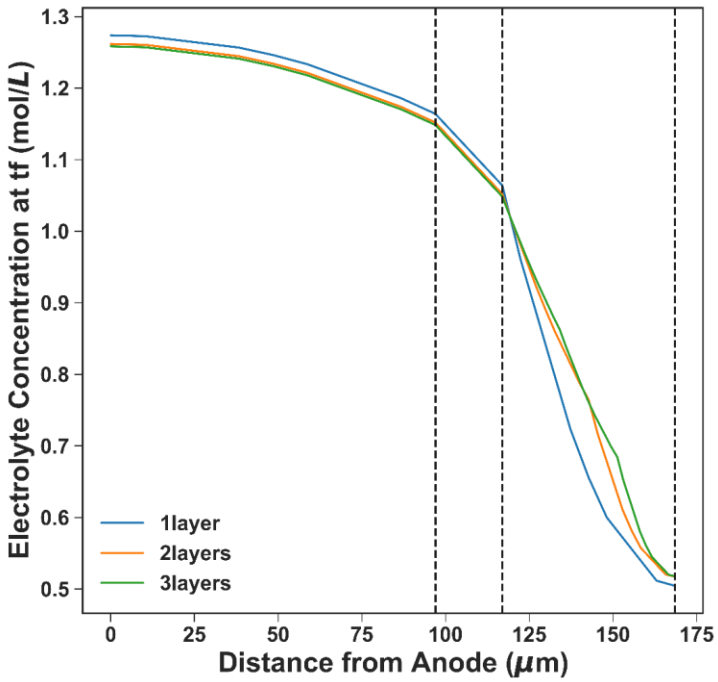

Figure IV-15 End of discharge electrolyte concentration profile for optimal graded electrode design of different layers

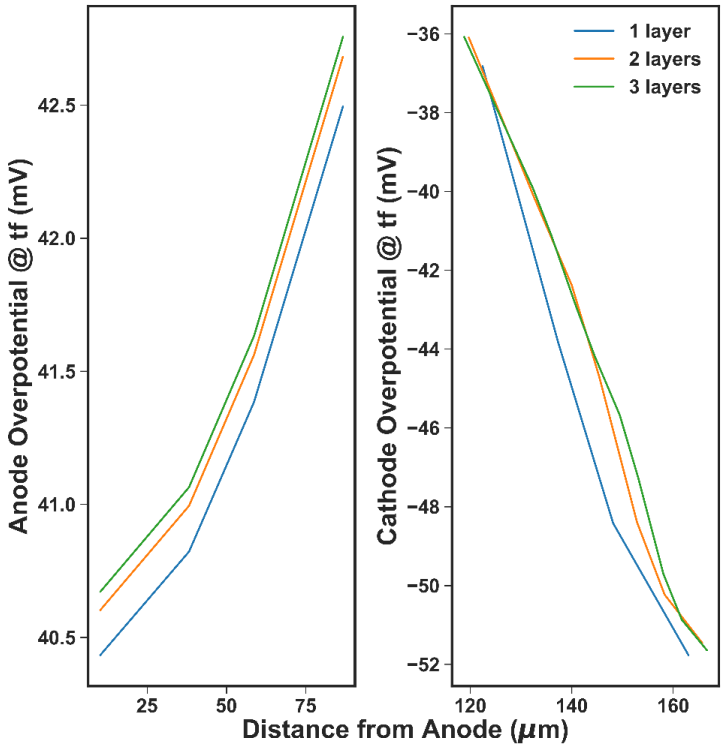

Figure IV-16 Overpotential distribution in the electrodes for optimal graded electrode design of different layers

Table IV-2 Optimization results for maximizing discharge energy

	Rate	ln (um)	# of layers	specific E (Wh/kg)	Applied current (A/m^2)	% improvement	Porosities		
NMC	1/3C	104.22	1	195.16	35.15		0.106		
			2	195.21	35.13	0.03%	0.111	0.100	
			3	195.19	35.12	0.01%	0.117	0.100	0.100
	1C	96.97	1	158.21	27.80		0.155		
			2	158.54	27.80	0.21%	0.185	0.126	
			3	158.66	27.81	0.29%	0.196	0.165	0.104
	3C	85.81	1	107.47	17.89		0.232		
			2	107.60	17.89	0.12%	0.271	0.192	
			3	107.65	17.89	0.17%	0.284	0.246	0.164
LCO	1/3C	71.20	1	168.07	21.15		0.263		
			2	168.63	21.03	0.34%	0.308	0.217	
			3	168.88	21.01	0.48%	0.328	0.276	0.184
	1C	64.20	1	152.48	18.29		0.333		
			2	152.96	18.19	0.31%	0.394	0.271	
			3	153.17	18.18	0.45%	0.416	0.350	0.233
	3C	46.82	1	117.21	11.92		0.507		
			2	117.37	11.91	0.13%	0.581	0.433	
			3	117.42	11.91	0.17%	0.602	0.528	0.389

The improvement in total discharge energy is listed in Table IV-2 above. The cathode thickness is set as 51.5μm and the anod/cathode capacity ratio is set to 1.1. Difference rates is determined by the discharge time, 1/3 C means the discharge time is 3 hours and 3C is 20min. Optimization was performed on two different chemistries with parameter values from the literature.[38,42] When the discharge time is longer, the specific energy is higher, and the optimal porosity is lower, as expected. The porosity near the separator is higher than the porosity near the current collector to facilitate the mass transport process in the electrodes. Overall, the increase of total energy for a specific amount of active material is negligible, consistent with the previous report in literature.[32]

Chapter V. What's Next?

V.1 Design with Aging Effects

Aging is an important factor in battery operation and design. Most of the previous design work only focused on the fresh cell performance, which may not necessarily be the best design criteria.

Recently, Liu et al.[63] has shown decrease of 8.3% in capacity fade over 50 cycles for a battery with $LiNi_{0.5}Mn_{1.5}O_4$ (LNMO) cathode experimentally. They also observed improved conductivity and diffusivity of the 2-layer graded cathode design. We have seen from our model that graded electrode can change the overpotential distribution in the electrode. Once we have a reasonable degradation model, then conducting optimal design over many cycles would be an attractive approach to explore.

Another model that can help with tracking battery degradation is the impedance model. A fast and robust impedance code has been developed by the Subramanian group.[64] The change of impedance data over cycling can be a good indicator of the battery health, and a suitable objective function for fade based electrode design. Right now the impedance model does not include any fade mechanism. A validated impedance model with aging factor needs to be developed first, and then an optimization framework needs to be built around that model.

V.2 Design with User-profiles

Design for specific use case is another promising research direction. Right now most of the design simulation and optimization attempts are based on constant current charge/discharge. When using dynamic profiles for specific applications, graded electrode design may offer additional benefit.

As an example, for electric vehicle applications, United States Advanced Battery Consortium has published a battery test manual that includes dynamic charging protocol.[65] One challenge for

electric vehicle is the balance between energy and power performance, thus the longer time scale and shorter time-scale performance, which may benefit from the graded electrode design.

V.3 Design with Techno-economic Considerations

All aforementioned optimal design problems considered only the battery performance. For real-life production decision making, cost versus improvement would be the determining factor. To make a 2-layer graded electrode, additional processing time is required (variable cost) and the production line may need to be updated (additional fixed cost). The performance improvement may enable battery manufacturers to charge a surplus or sell more to customers. If the increase in revenue can offset the increase in cost, then graded electrode design is favorable to the manufactures. To estimate the pack-level production cost, BatPaC developed by Argonne National Laboratory would be a valuable resource.

Bibliography

1. Society, G. B.-J. of T. E. & 2017, undefined. The development and future of lithium ion batteries. *jes.ecsdl.org*
2. Ceder, G., Doyle, M., Arora, P. & Fuentes, Y. Computational Modeling and Simulation for Rechargeable Batteries. *MRS Bull.* **27**, 619–623 (2002).
3. Nejad, S., Gladwin, D. T. & Stone, D. A. A systematic review of lumped-parameter equivalent circuit models for real-time estimation of lithium-ion battery states. *J. Power Sources* **316**, 183–196 (2016).
4. Mousavi G., S. M. & Nikdel, M. Various battery models for various simulation studies and applications. *Renew. Sustain. Energy Rev.* **32**, 477–485 (2014).
5. Ramadesigan, V. *et al.* Modeling and Simulation of Lithium-Ion Batteries from a Systems Engineering Perspective. *J. Electrochem. Soc.* **159**, R31 (2012).
6. Zhang, D., Popov, B. N. & White, R. E. Modeling Lithium Intercalation of a Single Spinel Particle under Potentiodynamic Control. *J. Electrochem. Soc.* **147**, 831 (2000).
7. Doyle, M. Modeling of Galvanostatic Charge and Discharge of the Lithium/Polymer/Insertion Cell. *J. Electrochem. Soc.* **140**, 1526 (1993).
8. Guo, M., Sikha, G. & White, R. E. Single-Particle Model for a Lithium-Ion Cell: Thermal Behavior. *J. Electrochem. Soc.* **158**, A122 (2011).
9. Baba, N., Yoshida, H., Nagaoka, M., Okuda, C. & Kawauchi, S. Numerical simulation of thermal behavior of lithium-ion secondary batteries using the enhanced single particle model. *J. Power Sources* **252**, 214–228 (2014).
10. Wu, B. *et al.* Coupled thermal–electrochemical modelling of uneven heat generation in lithium-ion battery packs. *J. Power Sources* **243**, 544–554 (2013).
11. Ye, Y., Shi, Y., Cai, N., Lee, J. & He, X. Electro-thermal modeling and experimental validation for lithium ion battery. *J. Power Sources* **199**, 227–238 (2012).
12. Vetter, J. *et al.* Ageing mechanisms in lithium-ion batteries. *J. Power Sources* **147**, 269–281 (2005).
13. Golmon, S., Maute, K. & Dunn, M. L. Numerical modeling of electrochemical-mechanical interactions in lithium polymer batteries. *Comput. Struct.* **87**, 1567–1579 (2009).
14. Arora, P., White, R. E. & Doyle, M. Capacity Fade Mechanisms and Side Reactions in Lithium-Ion Batteries. *J. Electrochem. Soc.* **145**, 3647–3667 (1998).
15. Spotnitz, R. Simulation of capacity fade in lithium-ion batteries. *J. Power Sources* **113**, 72–80 (2003).
16. Ramadass, P., Haran, B., Gomadam, P. M., White, R. & Popov, B. N. Development of First Principles Capacity Fade Model for Li-Ion Cells. *J. Electrochem. Soc.* **151**, A196 (2004).

17. Ning, G., White, R. E. & Popov, B. N. A generalized cycle life model of rechargeable Li-ion batteries. *Electrochim. Acta* **51**, 2012–2022 (2006).
18. Safari, M., Morcrette, M., Teyssot, a. & Delacourt, C. Multimodal Physics-Based Aging Model for Life Prediction of Li-Ion Batteries. *J. Electrochem. Soc.* **156**, A145 (2009).
19. Pinson, M. B. & Bazant, M. Z. Theory of SEI Formation in Rechargeable Batteries: Capacity Fade, Accelerated Aging and Lifetime Prediction. *J. Electrochem. Soc.* **160**, A243–A250 (2013).
20. Lin, X. *et al.* A Comprehensive Capacity Fade Model and Analysis for Li-Ion Batteries. *J. Electrochem. Soc.* **160**, A1701–A1710 (2013).
21. Tiedemann, W. & Newman, J. Maximum Effective Capacity in an Ohmically Limited Porous Electrode. *J. Electrochem. Soc.* **122**, 1482–1485 (1975).
22. Newman, J. Optimization of Porosity and Thickness of a Battery Electrode by Means of a Reaction-Zone Model. *J. Electrochem. Soc.* **142**, 97 (1995).
23. Srinivasan, V. & Newman, J. Design and Optimization of a Natural Graphite/Iron Phosphate Lithium-Ion Cell. *J. Electrochem. Soc.* **151**, A1530 (2004).
24. Ramadesigan, V., Methekar, R. N., Latinwo, F., Braatz, R. D. & Subramanian, V. R. Optimal Porosity Distribution for Minimized Ohmic Drop across a Porous Electrode. *J. Electrochem. Soc.* **157**, A1328 (2010).
25. Du, W., Gupta, A., Zhang, X., Sastry, A. M. & Shyy, W. Effect of cycling rate, particle size and transport properties on lithium-ion cathode performance. *Int. J. Heat Mass Transf.* **53**, 3552–3561 (2010).
26. Du, W., Xue, N., Sastry, a. M., Martins, J. R. R. a. & Shyy, W. Energy Density Comparison of Li-ion Cathode Materials Using Dimensional Analysis. *J. Electrochem. Soc.* **160**, A1187–A1193 (2013).
27. Golmon, S., Maute, K. & Dunn, M. L. Multiscale design optimization of lithium ion batteries using adjoint sensitivity analysis. *Int. J. Numer. Methods Eng.* **92**, 475–494 (2012).
28. Golmon, S., Maute, K. & Dunn, M. L. A design optimization methodology for Li+ batteries. *J. Power Sources* **253**, 239–250 (2014).
29. De, S., Northrop, P. W. C., Ramadesigan, V. & Subramanian, V. R. Model-based simultaneous optimization of multiple design parameters for lithium-ion batteries for maximization of energy density. *J. Power Sources* **227**, 161–170 (2013).
30. Northrop, P. W. C., Ramadesigan, V., De, S. & Subramanian, V. R. Coordinate Transformation, Orthogonal Collocation, Model Reformulation and Simulation of Electrochemical-Thermal Behavior of Lithium-Ion Battery Stacks. *J. Electrochem. Soc.* **158**, A1461 (2011).
31. Xue, N. *et al.* Optimization of a Single Lithium-Ion Battery Cell with a Gradient-Based Algorithm.

J. Electrochem. Soc. **160**, A1071–A1078 (2013).

32. Dai, Y. & Srinivasan, V. On Graded Electrode Porosity as a Design Tool for Improving the Energy Density of Batteries. *J. Electrochem. Soc.* **163**, A406–A416 (2015).
33. Du, D. L., Wood, C. & Daniel, S. Z. Kalnaus and J. *Li J. Appl. Electrochem. 47* **405**,
34. Liu, C., Society, L. L.-J. of T. E. & 2017, undefined. Optimal design of Li-ion batteries through multi-physics modeling and multi-objective optimization. *jes.ecsdl.org*
35. J. S. Newman and C. *W Tobias J. Electrochem. Soc. 109* **1183**,
36. Qi, Y., Jang, T., Ramadesigan, V., … D. S.-J. of T. & 2017, undefined. Is There a Benefit in Employing Graded Electrodes for Lithium-Ion Batteries? *jes.ecsdl.org*
37. Yu, S., Kim, S., Kim, T. Y., Nam, J. H. & Cho, W. Il. Model Prediction and Experiments for the Electrode Design Optimization of LiFePO 4 /Graphite Electrodes in High Capacity Lithium-ion Batteries. *Bull. Korean Chem. Soc.* **34**, 79–88 (2013).
38. Subramanian, V. R., Boovaragavan, V. & Diwakar, V. D. Toward Real-Time Simulation of Physics Based Lithium-Ion Battery Models. *Electrochem. Solid-State Lett.* **10**, A255 (2007).
39. Arora, P., Doyle, M., Gozdz, A. S., White, R. E. & Newman, J. Comparison between computer simulations and experimental data for high-rate discharges of plastic lithium-ion batteries. *J. Power Sources* **88**, 219–231 (2000).
40. Dai, Y., Cai, L. & White, R. E. Simulation and analysis of stress in a Li-ion battery with a blended LiMn2O4 and LiNi0.8Co0.15Al0.05O2 cathode. *J. Power Sources* **247**, 365–376 (2014).
41. Albertus, P., Christensen, J. & Newman, J. Experiments on and Modeling of Positive Electrodes with Multiple Active Materials for Lithium-Ion Batteries. *J. Electrochem. Soc.* **156**, A606 (2009).
42. Appiah, W. A. *et al.* Design optimization of LiNi0.6Co0.2Mn0.2O2/graphite lithium-ion cells based on simulation and experimental data. *J. Power Sources* **319**, 147–158 (2016).
43. Murata, K., Izuchi, S. & Yoshihisa, Y. An overview of the research and development of solid polymer electrolyte batteries. *Electrochim. Acta* **45**, 1501–1508 (2000).
44. Fleischer, C., Waag, W., Heyn, H. & Sauer, D. On-line adaptive battery impedance parameter and state estimation considering physical principles in reduced order equivalent circuit battery models: Part 1. *J. Power Sources* (2014).
45. Santhanagopalan, S., Guo, Q. & White, R. E. Parameter Estimation and Model Discrimination for a Lithium-Ion Cell. *J. Electrochem. Soc.* **154**, A198 (2007).
46. Ramadesigan, V. *et al.* Parameter Estimation and Capacity Fade Analysis of Lithium-Ion Batteries Using Reformulated Models. *J. Electrochem. Soc.* **158**, A1048 (2011).
47. Forman, J. C., Moura, S. J., Stein, J. L. & Fathy, H. K. Genetic identification and fisher identifiability analysis of the Doyle-Fuller-Newman model from experimental cycling of a LiFePO 4 cell. *J. Power*

Sources **210**, 263–275 (2012).

48. Zhang, L. *et al.* Multi-objective optimization of lithium-ion battery model using genetic algorithm approach. *J. Power Sources* **270**, 367–378 (2014).
49. Li, J. *et al.* Parameter Identification of Lithium-Ion Batteries Model to Predict Discharge Behaviors Using Heuristic Algorithm. *J. Electrochem. Soc.* **163**, A1646–A1652 (2016).
50. Guo, Q. & White, R. Cubic spline regression for the open-circuit potential curves of a lithium-ion battery. *J. Electrochem. Soc.* (2005).
51. Appiah, W., Park, J., Song, S., Byun, S. & Ryou, M. Design optimization of LiNi 0.6 Co 0.2 Mn 0.2 O 2/graphite lithium-ion cells based on simulation and experimental data. *J. Power* (2016).
52. Lee, S., Kim, J., Lee, J. & Cho, B. State-of-charge and capacity estimation of lithium-ion battery using a new open-circuit voltage versus state-of-charge. *J. Power Sources* (2008).
53. Pontryagin, V., Boltyanskii, R. & NY, ,. L. Gamkrelidze and E. *Mishchenko Sch.* (1962).
54. L. T. Biegler and I. *E Grossmann Comput. Chem. Eng. 28* **1169**,
55. D. W. Marquardt, Journal of the society for Industrial and Applied Mathematics, 11, . **431**,
56. Biegler, L. T. Solution of dynamic optimization problems by successive quadratic programming and orthogonal collocation. *Comput. Chem. Eng.* **8**, 243–247 (1984).
57. Vetter, J., Nov, P., Wagner, M. R. & Veit, C. Ageing mechanisms in lithium-ion batteries ☪. **147**, 269–281 (2005).
58. Hartikainen, M., Miettinen, K. & Wiecek, M. M. PAINT: Pareto front interpolation for nonlinear multiobjective optimization. *Comput. Optim. Appl.* **52**, 845–867 (2012).
59. Deb, K., Pratap, A., Agarwal, S. & Meyarivan, T. A fast and elitist multiobjective genetic algorithm: NSGA-II. *IEEE Trans. Evol. Comput.* **6**, 182–197 (2002).
60. Biegler, L. T. *Optimization of Differential-Algebraic Equation Systems Case Studies-Software Demonstration DAE Optimization Outline*.
61. Biegler, L. T., Cervantes, A. M. & Wächter, A. Advances in simultaneous strategies for dynamic process optimization. *Chem. Eng. Sci.* **57**, 575–593 (2002).
62. Hedengren, J. D., Shishavan, R. A., Powell, K. M. & Edgar, T. F. Nonlinear modeling, estimation and predictive control in APMonitor. *Comput. Chem. Eng.* **70**, 133–148 (2014).
63. Kabir, M. M. & Demirocak, D. E. Degradation mechanisms in Li-ion batteries: a state-of-the-art review. *International Journal of Energy Research* **41**, 1963–1986 (2017).
64. Pathak, M. *et al.* Fast impedance simulation of lithium-ion batteries with pseudo-two dimensional electrochemical models. *J. Electrochem. Soc.* **165**, A1324–A1337 (2018).
65. Christopherson, J. P. *Battery Test Manual For Electric Vehicles*. (2015).

Appendices

The secondary current distribution model

As there is no diffusion or convection in the system, all the current is carried entirely by migration. Therefore, the current density i_2, where the subscript 2 indicates the liquid phase (electrolyte), can be directly related to the migration flux: $\vec{i}_2 = F\sum_i z_i \overrightarrow{N_i}$, where $\overrightarrow{N_i} = -z_i u_i F \varepsilon c_i \nabla \Phi_2$, and z_i is the charge number of species i, u_i is the electrochemical potential of species i, F is the Faraday's constant (96,487C/mol), ε is the porosity, c_i is the concentration of species i, and Φ_2 is the potential in the liquid phase. Substituting the expression of $\overrightarrow{N_i}$ into that of $\vec{i}_2$, we can arrive at the equation for the electrolyte conductivity

$$\vec{i}_2 = -\kappa \nabla \Phi_2 \tag{IV-3}$$

where the electrolyte conductivity $\kappa = F^2 \varepsilon \sum_i z_i^2 u_i c_i$.

Similarly, for the solid matrix, we have the equation for solid conductivity, where the subscript 1 represents the solid phase and σ is the solid matrix conductivity.

$$\vec{i}_1 = -\sigma \nabla \Phi_1 \tag{IV-4}$$

The total current density for the whole system is the sum of the current densities in the solid and liquid phases.

$$\vec{i}_{app} = \vec{i}_1 + \vec{i}_2 \tag{IV-5}$$

From the material balance, the change in concentration of lithium ion in the electrolyte is equal to the amount of ions transferred through the solid electrolyte interface:

$$-\nabla \cdot \vec{N}_i + a j_{in} = 0 \tag{IV-6}$$

where the active surface area (*a*, defined as surface area per unit volume) times the normal pore wall flux density of species *i* averaged over the surface area (j_{in}) gives the total flux of the species *i* transferred from the electrolyte to the solid phase.

From electroneutrality, the divergence of the total current density is zero, therefore $\nabla \cdot \vec{i}_1 + \nabla \cdot \vec{i}_2 = 0$. An average transfer current density i_n for the system is defined as $i_n = F \sum_i z_i j_{in}$. Substituting it into Eqn. (18), we got

$$\nabla \cdot \vec{i}_2 = -\nabla \cdot \vec{i}_1 = a i_n \tag{IV-7}$$

The average transfer current density (i_n) is determined by reaction kinetics. Previously, linear kinetics was often used to simplify the problem:

$$\nabla \cdot \vec{i}_2 = -\nabla \cdot \vec{i}_1 = a i_n = a i_0 \frac{F}{RT}(\Phi_1 - \Phi_2 - U) \tag{IV-8}$$

where U stands for the equilibrium potential of the system. In this work, we have explored the influence of **nonlinear kinetics** on the electrode performance and its design, in which the equation above will be replaced by Eqn. (21).

$$-\nabla \cdot \vec{i}_1 = a i_0 \{\exp[\frac{\alpha_a nF}{RT}(\Phi_1 - \Phi_2 - U)] - \exp[\frac{-\alpha_c nF}{RT}(\Phi_1 - \Phi_2 - U)]\} \tag{IV-9}$$

where *n* is 1 for lithium ion, $\alpha_a + \alpha_c = 1$ for lithium ion reaction; if we take $U=0$ (assuming it is evaluated with a reference electrode of the same kind as the working electrode), then the equation for kinetics in the *x*-direction becomes

$$-\frac{di_1(x)}{dx} = a(x) i_0 \{\exp[\frac{\alpha_a F}{RT}(\Phi_1(x) - \Phi_2(x))] - \exp[\frac{-\alpha_c F}{RT}(\Phi_1(x) - \Phi_2(x))]\} \tag{IV-10}$$

The final set of equations for the 1-D porous electrode electrode model consists of the following four equations:

$$\begin{cases} i_1(x) = -\sigma(x)\dfrac{d\Phi_1(x)}{dx} \\ i_2(x) = -\kappa(x)\dfrac{d\Phi_2(x)}{dx} \\ i_1(x) + i_2(x) = i_{app} \\ -\dfrac{di_1(x)}{dx} = a(x)i_0\{\exp\{\dfrac{\alpha_a F}{RT}[\Phi_1(x) - \Phi_2(x)]\} - \exp\{\dfrac{-\alpha_c F}{RT}[\Phi_1(x) - \Phi_2(x)]\}\} \end{cases} \quad \text{(IV-11)}$$

One of the most important design parameters of the battery electrode is its porosity $\varepsilon(x)$. The electrode porosity comes into effect through its influence on the material properties, such as the active surface area (for spherical particles), the solid phase and the electrolyte conductivities[21]:

$$\begin{cases} a(x) = \dfrac{3\left(1-\varepsilon_{f+p}-\varepsilon(x)\right)}{R_p} \\ \sigma(x) = \sigma_0\left(1-\varepsilon_{f+p}-\varepsilon(x)\right)^{1.5} \\ \kappa(x) = \kappa_0\varepsilon(x)^{1.5} \end{cases} \quad \text{(IV-12)}$$

where ε_{f+p} is the volume fraction of the electrode filler and the polymer binder.

The boundary conditions are:

$$\begin{cases} i_1(0) = 0 \qquad i_1(l_p) = i_{app} \\ i_2(0) = i_{app} \quad i_2(l_p) = 0 \\ \Phi_2(0) = 0 \end{cases} \quad \text{(IV-13)}$$

This DAE system can be further simplified to cut down the computational cost. In this case, the simplified DAE system becomes an ODE system without algebraic constraints.

The algebraic equation and $i_2(x)$ can be eliminated by substituting $i_2(x) = i_{app} - i_1(x)$ into the equation set (9). To facilitate the numerical simulation, nondimensionalization was conducted on x ($X = \dfrac{x}{l_p}$), so that dimensionless distance X varies from 0 to 1. For lithium intercalation/de-intercalation reaction, it is reasonable to assume symmetry by taking $\alpha_a = \alpha_c = 0.5$.

VITA

Education

Aug/19 **Ph.D. in Chemical Engineering (3.76/4.00)** **University of Washington**
Prof.s Daniel T. Schwartz and Venkat R. Subramanian group
- Battery Modeling, Simulation, & Optimization (4 publications; 7 presentations)
- Data Science Option (Machine Learning, Visualization, Software Engineering)
- Technology Entrepreneurship Certificate (5 MBA classes, 20 credits)

Dec/13 **M.S. in Chemical Engineering (3.88/4.00)** **Columbia University**
Prof. Alan C. West group: Electro- and electroless metal deposition (2 articles)

Jun/12 **B.S. in Chemistry (3.42/4.00)** **Fudan University, China**
Biosensor (1 publication); Outstanding Student (1/100); National Scholarships

Research Experience

Dec/14-Now **Research Assistant** **University of Washington**
Prof.s Daniel T. Schwartz and Venkat R. Subramanian group
- Optimization of Li-ion battery design using physics-based models
- Parameter estimation of battery systems for real-time monitoring and control
- Modeling and analysis of battery impedance

Oct/12-Dec/13 **Research Assistant** **Columbia University**
Prof. Alan C. West group
- QCM for electroless copper deposition
- Ni and ceramic nano-/micron-particle co-deposition

Mar/10-Jun/12 **Student Researcher** **Fudan University, China**
The National Basic Research Program of China (973 Program); Fudan's Undergraduate Research Opportunities Program; Prof. Baohong Liu group
- Microfluidic devices and bio-sensors
- Selected by the National Innovation Plan for University Students

Work Experience

Dec/15-Sep/16 **CTO and Founding Member** **Coulomb Sea, Seattle, WA**
- Led 4 undergrads for technology and business development with the GAANN Fellowship (1/50) and won the Lawrence Award for Entrepreneurship (1/100)
- Led the company to final rounds in 3 innovation competitions and won the Best Consumer Product Award in the Business Plan Competition (1/93)
- Raised $6,800 in grant and prize money for initial prototyping and marketing

Jun/13-Sep/13 **R&D Intern** **Atotech R&D Damascene group, Albany, NY**
- Established a protocol to screen electrolyte additives 2x faster than manual experiments using a previously nonfunctional millifluidics device
- Standardized and documented the operation procedure

Oct/11-Jan/12 **Research Intern** **Philips Research Asia-Shanghai, China**
Customer Lifestyle I&D
- Designed and conducted pesticide residues experiments
- Conducted market research and analyzed competitive products

Jul/11-Sep/11 **Research Intern** **Medical School of Newcastle University, UK**
Prof. Jeremy H. Lakey group
- Acquired experimental skills in bio-medical studies faster than most students
- Finished a grad-level antibody-antigen interaction project as an undergrad

Leadership Experience

Jun/17-Jun/18 **VP of Relations** **UW Science & Engineering Business Association**
- Built and maintained relationship with 50+ external and internal partners
- Raised $2300 in prize money and arranged 15 judges for the Sci&Tech Showcase

Jan/16-Sep/17 **VP of PR & founding member** **Electrochemical Society UW Student Chapter**
- Raised public awareness and attracted 60+ members through online marketing (built FB group and website)
- Received 2017 chapters of excellence from ECS

Oct/08-Dec/10 **Deputy Director** **Sci & Tech Innovation Service Center, Fudan University**
- Connected 1000+ students with 20+ academic and industrial resources

Oct/08-Jun/10 **VP & co-founder** **Girls Up, Fudan University**
- Co-founded Fudan's 1st student association promoting the overall development of female students
- Organized 10+ events including the Miss Fudan Competition; raised $1000+

Honors & Awards

Nov/18 Graduate Student Teaching Award **University of Washington**
Feb/18 Best Student Poster Award **Battery500 Consortium, DOE**
Sep/16 Clean Energy Institute & Data Science Fellowship **University of Washington**
Feb/16 Customer Development Funding **NSF I-Corps Program**
Jun/16 Lawrence Award for Innovation and Entrepreneurship **University of Washington**
Sep/15 Chemical Engineering Innovation Program Fellowship **University of Washington**

Volunteer Experience

Since 2016 Clean Energy Ambassador (5+ K-12 outreach) **University of Washington**
Since 2015 UW Engineering Discovery Days Presenter **University of Washington**
May/10 Entrance and Information Volunteer (team lead) **EXPO 2010 Shanghai**
Jul/09 Teaching Volunteer for Wenchuan Earthquake Post Disaster Relief, China

Publications

1. Qi, Y., Jang, T., Schwartz, D. T, Subramanian, V. R., Model-based Graded Electrode Design with Time Collocation Method, in preparation (2019).

2. Qi, Y., Kolluri, S., Subramanian, V. and Chen, S.Y., University of Washington. Systems and methods for direct estimation of battery parameters using only charge/discharge curves. U.S. Patent Application 15/725,192 (2018).

3. Qi, Y., Jang, T., Ramadesigan, V., Schwartz, D. T, Subramanian, V. R., Is there a Benefit in Employing Graded Electrodes for Lithium-ion Batteries?, JES, 164 (13), A3196-A3207 (2017)

4. Qi, Y., Kolluri, S., Schwartz, D. T., Subramanian, V. R., Estimating and Identifying Parameters from Charge-Discharge Curves of Lithium-ion Batteries. ECS Trans., 75(20): 121-137 (2017).

5. Pathak, M., Murbach, M., Pathak, C., Jang T., Qi, Y., Schwartz, D. T., Subramanian, V. R., Fast Impedance Simulation of Lithium-ion Batteries with Pseudo-two Dimensional Electrochemical Models, JES, 165(5) A1-A14 (2018)

Presentations

1. Qi, Y., Jang, T., Ramadesigan, V., Schwartz, D. T., Subramanian, V. R., Multi-Parameter Graded Electrode Design of Lithium-Ion Batteries Using Simultaneous Optimization Approach, AiMES 2018, Interface 2, Oct 3 2018 4:20PM

2. Qi, Y., Jang, T., Ramadesigan, V., Schwartz, D. T., Subramanian, V. R., Optimal Graded Electrode Design of Lithium-ion Batteries with Simultaneous Optimization Approach, 233rd ECS, Multiscale Modeling 1, May 16 2018 9:20AM

3. Qi, Y., Chen, J., Kolluri, S., Pathak, M., Schwartz, D. T., Subramanian, V. R., Simultaneous Optimization Approach for Optimal Electrode Design of Lithium-Ion Batteries, 232nd ECS, Continuum Modeling 2, Oct 3 2017 2:40PM

4. Qi, Y., Chen, J., Pathak, C., Schwartz, D. T., Subramanian, V. R., The Effect of Kinetic Nonlinearity on Battery Electrode Design: A Closer Look at Electrode Processes, 231st ECS, Fundamental Studies 2, May 29 2017 3:20PM

5. Qi, Y., Kolluri, S., Schwartz, D. T., Subramanian, V. R., Estimating and Identifying Parameters from Charge-Discharge Curves of Lithium-Ion Batteries, ECS PRiME, Lithium-ion Batteries - Modeling 2 Oct 5 2016 5:40PM

6. Qi, Y.,The Commercial Potential of Battery Modeling, UW Science and Technology Showcase Jan 19 2016 5:00PM

7. Qi, Y., Schwartz, D. T., Subramanian, V. R., Design of Graded Porous Electrodes Based on Inverse Optimization of Li-ion Battery Models, 228th ECS, Meso-scale Modeling and Systems Design II Oct 13 2015 2:00PM